INFORMATION TO USERS

This manuscript has been reproduced from the microfilm master. UMI films the text directly from the original or copy submitted. Thus, some thesis and dissertation copies are in typewriter face, while others may be from any type of computer printer.

The quality of this reproduction is dependent upon the quality of the copy submitted. Broken or indistinct print, colored or poor quality illustrations and photographs, print bleedthrough, substandard margins, and improper alignment can adversely affect reproduction.

In the unlikely event that the author did not send UMI a complete manuscript and there are missing pages, these will be noted. Also, if unauthorized copyright material had to be removed, a note will indicate the deletion.

Oversize materials (e.g., maps, drawings, charts) are reproduced by sectioning the original, beginning at the upper left-hand corner and continuing from left to right in equal sections with small overlaps.

Photographs included in the original manuscript have been reproduced xerographically in this copy. Higher quality 6" x 9" black and white photographic prints are available for any photographs or illustrations appearing in this copy for an additional charge. Contact UMI directly to order.

Bell & Howell Information and Learning
300 North Zeeb Road, Ann Arbor, MI 48106-1346 USA
800-521-0600

IONIC STABILITY OF OXIDE PARTICLES IN POLAR ORGANIC MEDIA

By

GONGHOU WANG, B. Eng., M. Sc.

A Thesis

Submitted to the School of Graduate Studies

in Partial Fulfilment of the Requirements

for the Degree

Doctor of Philosophy

McMaster University

IONIC STABILITY OF OXIDE PARTICLES IN POLAR ORGANIC MEDIA

DOCTOR OF PHILOSOPHY (1998)
(Materials Science and Engineering)

McMaster University
Hamilton, Ontario

TITLE: Ionic Stability of Oxide Particles in Polar Organic Media

AUTHER: Gonghou Wang
B. Eng. (Metallurgy)
(Beijing University of Iron and Steel Technology, China)
M. Sc. (Metallurgy)
(University of Science and Technology Beijing, China)

SUPERVISOR: Professor Patrick S. Nicholson

NUMBER OF PAGES: xxi, 191

ABSTRACT

The ionic stability of oxide particles in polar non-aqueous media is studied. Surface chemistry and interparticle forces are manipulated by controlling the acidity and ionic strength of the suspensions without dispersants.

The acidity of ethanolic solution is determined using ion transfer functions, wherein the relationships between acidity, oxide particle-surface-charge, zeta-potential, stability and suspension rheological behaviour are established. The ionic stability of oxide particles in ethanol can be controlled by combination of potential determining ions and indifferent electrolyte to optimize the values of repulsive potential and repulsive force. It is shown oxide particles can be charge-stabilized, as in aqueous suspensions. The viscosity and flow curves for oxide/ethanol suspensions are acidity dependent. The flow curves of the suspensions follow the Casson model and the Casson yield value is used to evaluate their stability. Positive isoelectric point shifts were observed for alumina and magnesia in ethanol on increasing the solid concentration. However both dilute and concentrated aqueous suspensions of alumina give the same isoelectric point. Silica/ethanol suspensions are stable near the IEP. This result suggests the colloidal stability of silica in ethanol can not be explained exclusively by the ionic stability mechanism of DLVO theory. The discrepancy is believed due to a steric barrier consisting of a silicic acid gel network.

The surface chemistry and rheological properties of alumina suspensions in EtOH and DMSO are strongly influenced by the ionic strength of the suspensions. Rheological measurements show the viscosity of the suspensions decreases with increasing salt concentration due to suppression of the second electroviscous effect. Solvent is found to have a marked influence on suspension rheology.

The heterocoagulation behaviour of oxide-mixture/ethanol suspension systems is examined, elucidating the general principles underlying structure formation in mixed dispersions. It is demonstrated that the architecture of composites can be controlled by manipulation of the relative colloidal stability of the constituent primary particles.

ACKNOWLEDGEMENT

The author wishes to express his gratitude to Dr. P. S. Nicholson for his guidance and encouragement during the course of this study. Grateful acknowledgements are also due to Dr. W-K Lu and Dr. D. R. Woods for their fruitful suggestions and discussions.

Thanks are also due to my fellow lab members in the Ceramic Research Group.

I would specially like to thank Dr. Partho Sarkar, Dr. C-K Kuo and Mrs. Ena Nicholson for their help throughout the study.

Special thanks to my wife, Wen, for her support and encouragement.

TABLE OF CONTENTS

TABLE OF CONTENTS (continued)

TABLE OF CONTENTS (continued)

TABLE OF CONTENTS (continued)

LIST OF FIGURES

LIST OF FIGURES (continued)

LIST OF FIGURES (continued)

LIST OF FIGURES (continued)

LIST OF FIGURES (continued)

LIST OF FIGURES (continued)

LIST OF FIGURES FOR APPENDIX

LIST OF TABLES

LIST OF TABLES (continued)

LIST OF SYMBOLS

A	surface area, Hamaker constant
a	particle radius, activity
C	electrolyte concentration, capacitance
c	sound velocity
D	particle diameter, shear rate
E	electric field
e	elementary charge
F	interparticle force, Faraday constant
f	frictional coefficient
H	surface to surface distance between two particles
h	Planck constant
K_D	electrolyte dissociation constant
k	specific conductivity, Boltzmann constant
N	Avagadro number
n	index of refraction
$n_{\pm}$	number concentration of ions in double layer
$n^{o}_{\pm}$	number concentration of ions in bulk solution
p	pressure
Q	total particle surface charge

LIST OF SYMBLES (continued)

R	resistance, gas constant
T	temperature
t	time
U	mobility
u	velocity
V	interparticle potential, voltage
v	volume
W	stability ratio
Z	impedance
z	valence of ions
Λ	equivalent conductivity
Λ_O	limiting equivalent conductivity
ε	dielectric constant
φ	solid volume fraction in suspension
γ	activity coefficient
η	viscosity
κ	Debye-Huckel parameter
λ	wavelength
μ	partial molar free energy
ν	kinematic viscosity

LIST OF SYMBLES (continued)

ρ	density
σ	surface charge density
τ	shear stress, turbidity
ω	frequency
ψ	electric potential
ψ_o	surface potential
ζ	zeta potential

CHAPTER I

INTRODUCTION

The fabrication of ceramic materials involves powder processing, shaping, and firing. The reliability of ceramic products depends on the uniformity of their microstructure. The latter can be accomplished most effectively by processing colloidal suspensions. Reproducible and optimised colloidal processing depends on control of the stability of colloidal suspensions. Agglomerates are one of the main causes of inhomogeneities since they cause an uneven distribution of pores, yielding uneven pore collapse during subsequent consolidation procedures (Dynys and Halloran, 1983). The preparation of well-dispersed, stable suspensions helps alleviate the problems caused by agglomeration and leads to the formation of a uniform green body and consequently results in improved consolidation results.

Among many ceramic colloidal processing techniques, electrophoretic deposition (EPD) is an inexpensive, controllable method. It has been used to fabricate ceramic-ceramic microlaminates (Sarkar et al., 1992, 1993, 1994) and functionally-graded materials (Sarkar et al., 1997).

The traditional medium for ceramic powder dispersion is water. However, electrophoretic deposition from aqueous suspensions has the disadvantage of electrolysis of water. The formation of hydrogen at the cathode prevents deposition of a uniform adhering layer. Also, because electrolysis occurs in parallel with the powder deposition, the current efficiency is low. Recently organic media have been used for electrophoretic deposition.

Particles may be stable in suspension due to their charge and consequent repulsion (ionic stabilization) or due to the presence of adsorbed polymer layers (steric stabilization). Ionic stabilization is most effective in high-dielectric-constant media, i.e. water. However, it also plays a part in non-aqueous solvents. The extent of ionic stabilization in non-aqueous media is extremely sensitive to the dielectric constant of the solvent, particularly affecting stability through the degree of dissociation of the electrolyte. Low dielectric constant, non-aqueous media have a low degree of electrolyte dissociation and thus a low ionic concentration. As a result, the Debye-Huckel parameter, κ, is small. It is usually assumed that, for systems with such low ionic strengths (lower than 10^{-6} M), the repulsive pressure will be small i.e. not of sufficient magnitude to stabilize the colloids (Napper, 1983; Walbridge, 1975; Feat and Levine, 1976). Steric stabilization must be used for such suspensions and various dispersants have been used (Lee and Rives, 1991; Moloney et al., 1995; Chou and Lee, 1989; Chou and Senna, 1987). However, dispersants are transient additives that must be eliminated from ceramic components prior to densification without introducing residual strength-limiting

defects (e.g., large voids, cracks) and can be difficult to remove from a green body during binder burn-out, particularly if submicrometer-size particles are involved.

A number of workers (Lyklema, 1968; Parfitt and Peacock, 1978; Kitahara, 1984; Van der Hoeven and Lyklema, 1992) kept the ionic stabilization option open and Fowkes (Fowkes et al. 1982; Fowkes and Push, 1984) fulminated against the "wide-spread scepticism concerning the importance of electrostatics in organic media" and warned against its negligence.

If a certain degree of electrolyte dissociation can be obtained in a medium of low dielectric constant and a high surface potential be created, significant repulsive forces should be possible. This is feasible in polar organic media of moderate dielectric constant. However, most previous work has focused on the two extreme cases of ionic stabilization in aqueous and non-polar organic solvents, while its role in polar organic media has received little attention. There have been few studies of ceramic suspensions in polar organic solvents thus they are poorly understood. The most potent tool for modifying oxide suspension stability is the acidity. However, no systematic study has reported the effect of acidity on the surface charge and ionic stability of oxide particles in pure polar organic solvents.

The present work systematically studied the ionic stabilization of suspensions of oxide particles in polar organic media. The acidity of ethanolic solution was determined using an ion-transfer function wherein the relationships between acidity, oxide particle-surface-charge, zeta-potential, stability and suspension rheological behaviour have been established. The influence of

indifferent electrolyte and ionic strength on alumina particle surface chemistry and suspension rheology in polar organic media have been determined. The heterocoagulation behaviour of oxide-mixture/ethanol suspension systems has also been examined, elucidating the general principles underlying structure formation in mixed dispersions. Using simple, well-characterized model systems, it is demonstrated that the architecture of composite aggregates, produced in suspension, can be controlled by useful manipulation of the relative colloidal stability of the constituent primary particles.

CHAPTER II

LITERATURE REVIEW

II-1 Colloidal Dispersions

Particle suspensions are considered colloidal when the particle dimensions are 1 nm < x < 1 μm. If the dispersed phase (particles) does not coagulate but remains as discrete, single particles for a long time, the dispersion is said to be stable. This stability is achieved when a strong enough, long range repulsive force exists between the particles, preventing approach inducing a van der Waals attractive force field. The latter extends ~ 5 - 10 nm from the particle surface (Napper, 1983).

The two recognized forces that stabilize colloids are known as ionic (electrostatic) and steric forces. The theory which models interparticle interactions between charged (ionic) colloidal particles was first derived by Derjaguin and Landau (1941) and Verwey and Overbeek (1948) (this model is referred to as the DLVO theory). In this theory, the interparticle (spherical particles assumed) interactions are modeled as the total pair interaction potential, V_T, as a function of the interparticle distance. V_T is described by an

electrostatic (entropic) repulsive force originating from the formation of a net charge on the surface and an attractive force (i.e., the van der Waals forces) which results from fluctuating dipoles within the solid. Colloidal stability is achieved when the particles are separated by repulsion which originates from the overlap of the electrical double layers surrounding the charged particles.

The second recognized stabilizing force is steric hindrance which originates from the interaction between macromolecules adsorbed on the particle surfaces (i.e., steric stabilization) (Napper, 1983). In this case the repulsion results from overlap of the polymer segments which pushes them apart. This repulsion is caused by the increase of osmotic pressure at close interparticle distances in the region where the polymer segments overlap. The present work will be concerned with non-aqueous suspensions which do not contain polymers so steric stabilization is not considered hereafter.

II-2 Electrical Interactions

II-2.1 Electrical Double Layers

II-2.1.1 General

Unless it can be proven otherwise, it is assumed all surfaces are charged (Woods, 1983). The distribution of ions around a charged particle, in an electrolyte

solution, is not uniform and gives rise to an electrical "double-layer". The simplest model of such a system is attributed to Helmholtz who considered both charge layers to be fixed as parallel planes to form an ionic condenser. His parallel-plate condenser model predicts constant capacitance but this is contradicted by experimental results.

Gouy (1910, 1917) and Chapman (1913) proposed the double-layer is diffuse to account for the thermal motion of the counterions in the solution phase. Counterions are attracted to the particle surface charge by coulombic forces but are randomized by thermal motion. Thus a layer with an equilibrium distribution of counterions is established.

The electric potential (ψ) in the diffuse layer is analyzed in terms of two basic equations i.e. the Poisson equation:

$$\nabla^2 \psi = -\frac{\rho}{\varepsilon} \qquad (2.1)$$

where ε is the permittivity of the dielectric medium and ρ is the volume density of charge; and the Boltzmann equation which describes the ionic population of the diffuse layer;

$$n_i = n_i^o \exp(-z_i e\psi / kT) \qquad (2.2)$$

where n_i is the number concentration of ion i in the diffuse layer, n_i^o that in the bulk solution, z_i the valence of the ions, e the elementary charge, k the Boltzmann constant and T the absolute temperature.

The volume charge density in the neighbourhood of the surface is:

$$\rho = \sum n_i z_i e \qquad (2.3)$$

the summation operating over all species of ion present.

A widely accepted model for the double layer is due to Stern (1924), later modified by Graham (1947), in which part of the counterion charge is located close to the particle surface (the Stern layer) and the remainder distributed broadly in the diffuse layer.

The interaction between charged particles is governed predominantly by overlap of the diffuse layers, so the potential most relevant to the interaction is that at the boundary between the Stern and diffuse layers (the Stern potential, ψ_δ), rather than the potential at the particle surface. This boundary (the Stern plane) is generally considered to be at ~ 0.3 to 0.5 nm from the particle surface. There is no direct experimental method for determining the Stern potential, but there is good reason to believe (Lyklema, 1977) that the electrokinetic or zeta potential, ξ, is an adequate substitute, although there is some doubt on this point (Barough and Matijevic, 1987). The electrokinetic potential is that at the plane of shear between a particle and a fluid, when there is relative motion therebetween. The technique of particle electrophoresis is the most common method of determining the zeta potential and is widely used in fundamental studies of colloid stability.

The two major influences on electrical interaction between particles are the magnitude of the effective "surface potential" (generally assumed to be ψ_δ or ξ) and the extent of the diffuse layer since the latter governs the range of the interaction.

The extent of the diffuse layer is dependent on the ionic strength of the suspension and is best determined via the variation of potential as a function of distance from the Stern plane. The Poisson-Boltzmann approach is commonly employed to estimate this thickness.

II-2.1.2 Flat Plate Double Layers

The complete Poisson-Boltzmann equation for a flat double layer is:

$$\nabla^2\psi = \frac{d^2\psi}{dx^2} = -\frac{1}{4\pi\varepsilon_o}\cdot\frac{4\pi}{\varepsilon_r}\sum n_i^o z_i e \exp(-z_i e\psi/kT) \qquad (2.4)$$

where Ψ is the potential at distance x from the surface, ε_o the dielectric permittivity of vacuum and ε_r the relative dielectric constant ($\varepsilon_r=\varepsilon/\varepsilon_o$).

This is a second-order, nonlinear differential equation which can be solved exactly but, before doing so, it is useful to examine a valuable approximation.

If the electrical energy is small compared with the thermal energy of the ions ($|z_i e\psi| < kT$) it is possible to expand the exponential in Eq.2.4 ($e^{-x} = 1 - x + x^2/2! \ldots$), neglecting all but the first two terms, to give:

$$\frac{d^2\psi}{dx^2} = -\frac{1}{\varepsilon}(\sum z_i e n_i^o - \sum z_i^2 e^2 n_i^o \psi/kT) \qquad (2.5)$$

The first summation term must be zero to preserve electroneutrality in the bulk solution, so

$$\nabla^2 \psi = \frac{d^2\psi}{dx^2} = \kappa^2 \psi \qquad (2.6)$$

where

$$\kappa = \left(\frac{e^2 \sum n_i^o z_i^2}{\varepsilon kT}\right)^{1/2} \qquad (2.7)$$

This simplification of assuming ψ small is called the Debye-Huckel (linear) approximation. The parameter, κ, is referred to as the Debye-Huckel parameter. It is of great importance in colloid stability and depends on the electrolyte concentration (n_i^o).

Eq.2.6 can be solved by integrating with respect to x, from some point in the bulk solution up to a point in the double layer, to give:

$$\frac{d\psi}{dx} = -\kappa\psi \qquad (2.8)$$

under the boundary conditions of dΨ/dx = 0 and Ψ = 0 in the bulk solution (where x = ∞). The negative sign on the right side is chosen so that dΨ/dx is always negative for Ψ > 0 and positive for Ψ < 0. This ensures that $|\psi|$ always decreases going into the bulk solution becoming zero far from the surface.

A second integration of Eq.2.8 using $\Psi = \Psi_o$ at the plate (where x=0) gives:

$$\psi = \psi_o e^{-\kappa x} \qquad (2.9)$$

This solution gives the approximate potential distribution near the surface, where Ψ_o is referred to as the surface potential. Increasing the ionic strength causes an increase in κ as a result of which the potential falls off more rapidly with distance.

The Debye-Huckel parameter has the dimensions of reciprocal length and $1/\kappa$ (Debye length) is referred to as the "thickness" of the double layer, i.e.; the extent of the diffuse layer.

Unfortunately, the assumption that $|z_i e\Psi| < kT$, i.e.; $|z\Psi_o| < 25.7$ mV at 25°C is not valid for many situations of interest in colloid science. Under such conditions the complete Poisson-Boltzmann equation must be solved.

To simplify the algebra, $z_i = z_+ = -z_- = z$ and $n_i^\circ = n_+^\circ = n_-^\circ = n^\circ$ is set, so the analysis is limited to symmetrical z:z valence electrolytes. It turns out this is not a serious restriction because, in most situations of interest, the behaviour is determined overwhelmingly by the ions of sign opposite to that of the surface. So it is possible to treat most electrolytes as symmetric, with valence z, equal to the valence of the counterions. In this case, Eq.2.4 can be written:

$$\frac{d^2\psi}{dx^2} = \frac{2n^\circ ze}{\varepsilon}\sinh\frac{ze\psi}{kT} \qquad (2.10)$$

The same integration procedure gives the exact solution of the complete Poisson-Boltzmann equation for the case of a flat double layer, i.e.;

$$\tanh(ze\psi/4kT) = \tanh(ze\psi_o/4kT)\exp(-\kappa x) \qquad (2.11)$$

The surface charge per unit area, σ, must balance that in the adjacent solution:

$$\sigma = -\int_0^\infty \rho dx \qquad (2.12)$$

and, substituting for ρ from Eq.2.1;

$$\sigma = \varepsilon \int_0^\infty \frac{d^2\psi}{dx^2} dx = -\varepsilon \left(\frac{d\psi}{dx} \right)_{x=0} \qquad (2.13)$$

For small potentials, Eq.2.8 yields:

$$\sigma = \varepsilon \kappa \psi_o \qquad (2.14)$$

II-2.1.3 The Double Layer around a Sphere

In the case of particles of radius a, κa is a measure of their flatness. For κa > 10, the flat double layer model is a good approximation. For κa < 10, the spherical double layer model is more appropriate.

The Poisson-Boltzmann equation remains valid for the potential distribution around a sphere but the coordinates must be converted to spherical ones. The Laplacian operator for a radially symmetric potential is used, i.e.;

$$\nabla^2 \psi = \frac{1}{r^2} \frac{d}{dr} \left(r^2 \frac{d\psi}{dr} \right) = -\frac{1}{\varepsilon} \sum n_i^o z_i e \exp(-z_i e \psi / kT) \qquad (2.15)$$

This equation cannot be solved analytically and the Debye-Huckel approximation, valid for low potentials, must be used. Expanding the exponential to the linear term again gives (cf. Eq.2.5);

$$\frac{1}{r^2} \frac{d}{dr} \left(r^2 \frac{d\psi}{dr} \right) = \kappa^2 \psi \qquad (2.16)$$

for which the general solution is:

$$\psi = \frac{Ae^{\kappa r}}{r} + \frac{Be^{-\kappa r}}{r} \qquad (2.17)$$

The constant A must be zero since $\Psi=0$ at $r=\infty$ and, if the particle has radius 'a' and the potential on its surface is Ψ_o, then:

$$\psi_o = \frac{Be^{-\kappa a}}{a} \qquad (2.18)$$

Substituting for B in Eq.2.17 gives:

$$\psi = \psi_o \frac{a}{r} \exp[-\kappa(r-a)] \qquad (2.19)$$

where Ψ is now the potential at a distance r from the particle centre.

The charge on the particle must balance that in the double layer so that;

$$Q = -\int_a^\infty 4\pi r^2 \rho dr \qquad (2.20)$$

where Q is the total surface charge of a particle. Substituting for ρ from Eqs 2.1 and 2.16:

$$Q = 4\pi\varepsilon_o\varepsilon_r\kappa^2\int_a^\infty r^2\psi dr \qquad (2.21)$$

Using the value of Ψ from Eq.2.19 and, integrating by parts, yields:

$$Q = 4\pi a\varepsilon(1+\kappa a)\psi_o \qquad (2.22)$$

II-2.2 Double Layer Interactions

II-2.2.1 General

When two charged particles come in the vicinity of each other in an electrolyte solution, their diffuse layers overlap and entropic repulsion is experienced.

One distinction recognized early in colloid stability theory (Verwey and Overbeek, 1948) is that interactions at constant-surface-potential are different from those at constant-surface-charge. The constant-potential boundary assumption is valid if the surface charge is generated by potential-determining ions and an adsorption equilibrium is maintained by the potential-determining ions (Frens and Overbeek, 1972, Overbeek, 1986, Rajagopalan and Kim, 1986). If these conditions are not met, constant-charge boundary conditions might exist or both boundary assumptions may not be constant (Overbeek, 1986). Gregory (1975) comments that, for most real systems, neither constant charge nor constant potential likely exists. Other solutions for interparticle repulsion (Barouch et al, 1978) require elaborate calculation schemes and there is controversy as to their accuracy (Barouch and Matijevic, 1985, Chan, 1983, Overbeek, 1988).

The overlap involves only the outermost parts of the double layers and stability calculations are not sensitive to whether the constant charge or constant

potential approach is used (Parfitt and Peacock, 1978). Therefore, in the present study, stability calculations will be based on the constant potential assumption.

II-2.2.2 Ionic Repulsion between Flat Double Layers

Consider the pressure of interaction between two flat double layers separated by distance H (Figure 2.1). The dashed line in Figure 2.1 represents the electric potential that a single double layer would have in the absence of interaction.

Two pressures operate between two surfaces with overlapping double layers: one is "osmotic" (entropic in origin) P_{Osm} and one of electrostatic origin (resulting from the energy change), P_{El}. P_{Osm} results from differences between the ionic concentrations in the double layer and the bulk of the solution;

$$P_{Osm} = (n_+ + n_-)kT - 2n^\circ kT \qquad (2.23)$$

where $n_{+(-)}$ is the number concentration of cations (anions) and n° that in the bulk solution ($n_+^\circ = n_-^\circ = n^\circ$).

P_{El} stems from the electric field energy of the double layers;

$$P_{El} = -\frac{\varepsilon}{2}\left(\frac{d\psi}{dx}\right)^2 \qquad (2.24)$$

P_{El} is attractive as the "pushing" of the counterions between the charged surfaces decreases their Coulombic energy because the average distance between the positive and negative charges is decreased. P_{Osm}, on the other hand,

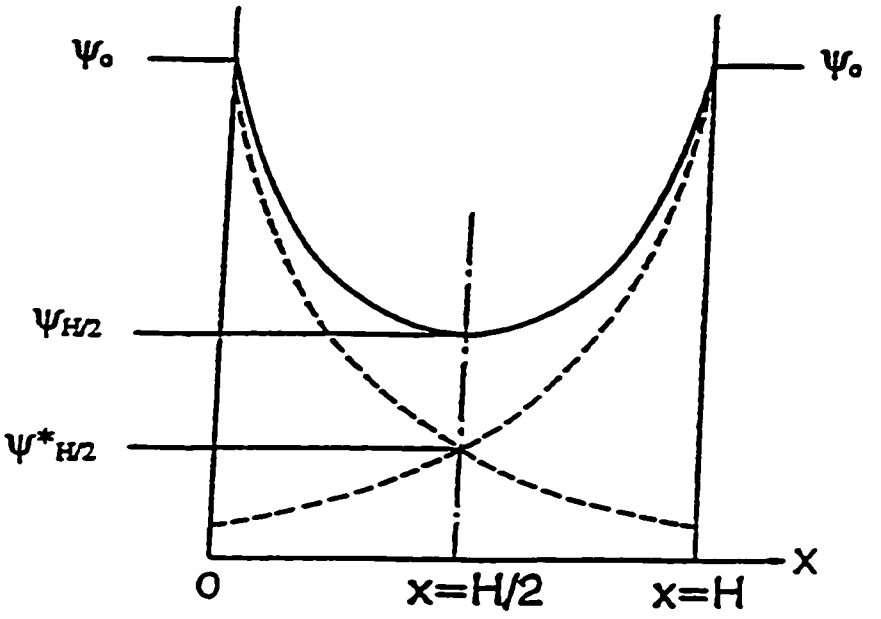

Figure 2.1 Schematic representation of the electric potential between flat double layers

is repulsive because the associated counterions in the intervening solution experience restriction of movement, i.e., their configurational entropy is decreased.

This is a very important concept. A common misapprehension is that the repulsion is "electrostatic." In fact, the electrostatic force is attractive. The repulsion is due to the osmotic pressure originating from the ionic concentration difference between the overlapping double layers and the bulk of the solution. A more appropriate term should be ionic repulsion (as used in this thesis).

The Poisson-Boltzmann equation, Eq.2.4, integrates to yield;

$$(\frac{d\psi}{dx})^2 = \frac{2n^\circ kT}{\varepsilon}(2\cosh\frac{ze\psi}{kT} + C) \qquad (2.25)$$

thus P_{El} is calculated. C is the integration constant determined from the boundary condition that $d\Psi/dx = 0$ at $x = H/2$; thus;

$$C = -2\cosh\frac{ze\psi_{H/2}}{kT} \qquad (2.26)$$

where $\Psi_{H/2}$ is the electric potential half-way between the plates. By combining Eqs.2.24, 2.25, and 2.26, P_{El} is obtained.

$$P_{El} = -n^\circ kT(2\cosh\frac{ze\psi}{kT} - 2\cosh\frac{ze\psi_{H/2}}{kT}) \qquad (2.27)$$

P_{Osm} is obtained by combining the Boltzmann equation (Eq.2.2) and Eq.2.23,

$$P_{Osm} = 2n^\circ kT(\cosh\frac{ze\psi}{kT} - 1) \qquad (2.28)$$

P_{El} and P_{Osm} vary with Ψ, but, for equilibrium at any point between the two particles, the total pressure, $P_R = P_{El} + P_{Osm}$, i.e. the sum of the electrostatic and the osmotic contributions, is independent of position. P_{Osm} at x = H/2 is required to calculate P_R, i.e. at $d\Psi/dx = 0$ and $P_{El} = 0$. Then;

$$P_R = P_{Osm(x=H/2)} = 2n^o kT(\cosh\frac{ze\Psi_{H/2}}{kT} - 1) \qquad (2.29)$$

Although rigorous, Eq.2.29 is not practically useful because $\Psi_{H/2}$ is not experimentally accessible. Thus a replacement must be identified that is tenable.

For weak interactions, $\Psi_{H/2}$ is considered relatively small (see Figure 2.1), and Eq.2.29 then reduces to;

$$P_R = n^o kT(\frac{ze\Psi_{H/2}}{kT})^2 \qquad (2.30)$$

For small $\Psi_{H/2}$ it can be further assumed that;

$$\Psi_{H/2} = 2\Psi^{\cdot}_{H/2} \qquad (2.31)$$

where $\Psi^{\cdot}_{H/2}$ is the value of Ψ at x=H/2 for a single particle double layer in the absence of interaction. Using Eq. 2.11 and the Debye-Huckel approximation for small potentials and assuming far out in the double layer, tanh p ≈ p, the following relation between Ψ_o and $\Psi^{\cdot}_{H/2}$ can be written

$$\psi^{\cdot}_{H/2} = \frac{4kT}{ze}(\tanh\frac{ze\psi_o}{4kT})\exp(-\frac{\kappa H}{2}) \qquad (2.32)$$

By combining Eqs. 2.30, 2.31, and 2.32, Eq.2.29 finally becomes;

$$P_R = 64n^{\circ}kT(\tanh\frac{ze\Psi_o}{4kT})^2\exp(-\kappa H) \qquad (2.33)$$

Eq.2.33 allows calculation of an approximate value of the repulsive pressure in terms of Ψ_o, ε and n° only.

The potential energy of repulsive interaction, V_R, is:

$$V_R = -\int_{\infty}^{H} P_R dH \qquad (2.34)$$

Which leads to;

$$V_R(flat) = 64n^{\circ}kT(\tanh\frac{ze\Psi_o}{4kT})^2\frac{1}{\kappa}\exp(-\kappa H) \qquad (2.35)$$

For a low surface potential, Eq.2.35 reduces to;

$$V_R(flat) = 2\varepsilon_o\varepsilon_r\psi_o^2\kappa\exp(-\kappa H) \qquad (2.36)$$

Although Eq.2.35 has been derived for the case of weak interaction, this approximation is widely used for practical purposes.

II-2.2.3 Ionic Repulsion between Spherical Double Layers

The potential energy of interaction between two spherical double layers can be calculated using Derjaguin's integration method (Usui and Hachisu, 1984), which is based on the repulsive energy between flat double layers.

If the particles are separated by a short distance, H (Figure 2.2), and it is assumed the spherical double-layer interaction, V_R (sphere), is an accumulation of the interaction of infinitesimal parallel rings that make up the sphere, then;

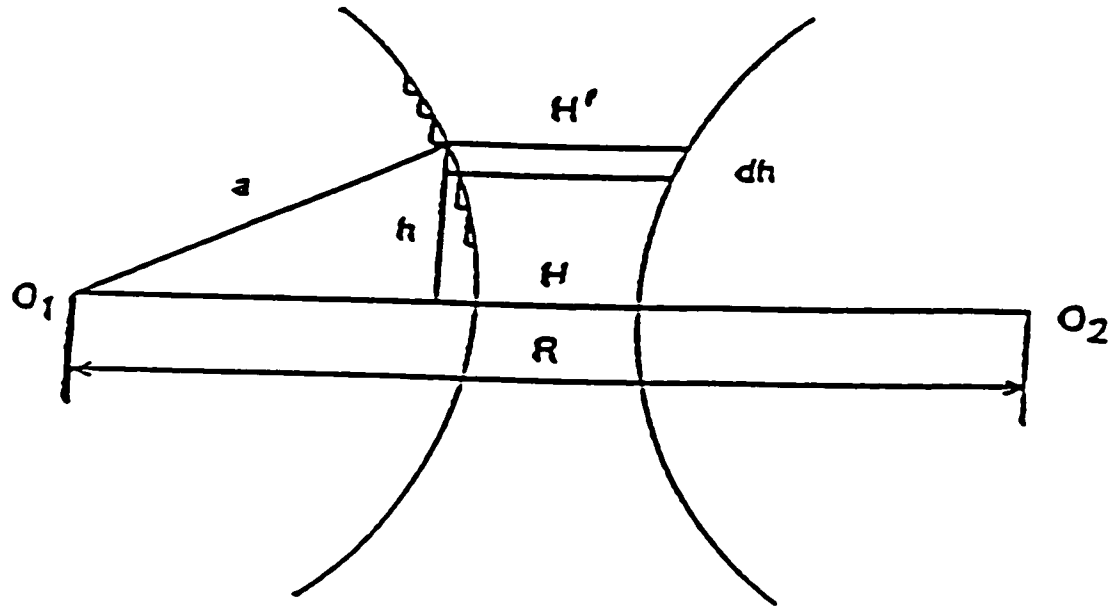

Figure 2.2 Interaction of spherical double layers

$$V_R(sphere) = 2\pi \int_0^\infty h[2G(H') - 2G(\infty)]dh$$

where 2G is the Gibbs energy per unit of surface between parallel plates (at distance H' and at infinite distance respectively) and h is the distance from the axis of symmetry of a ring under consideration. This equation is valid when the range of interaction is much smaller than the particle radius. This condition is satisfied when $\kappa a >> 1$.

For spherical particles with a large radius, 'a' and small values of h; (H'- H)/2 = $a - (a^2 - h^2)^{1/2}$ and $2h\,dh = a\,dH'(1 - h^2/a^2)^{1/2} \approx a\,dH'$. The repulsive Gibbs energy for two interacting spheres, V_R(sphere), can then be written as;

$$V_R(sphere) = 2\pi a \int_H^\infty [G(H') - G(\infty)]dH' \qquad (2.37)$$

The potential energy of interaction, V_R, for two flat double layers is the free-energy change involved to bring them from infinity to distance H' thus;

$$V_R(flat) = 2[G_R(H') - G_R(\infty)] \qquad (2.38)$$

Combining Eq.2.37 and Eq.2.38;

$$V_R(sphere) = \pi a \int_H^\infty V_R(flat)\,dH' \qquad (2.39)$$

The approximation for small $\Psi_{H/2}$ is obtained after substitution of Eq.2.35 into Eq.2.39 and integration between the limits H and ∞;

$$V_R(sphere) = \pi a 64 n^o kT (\tanh \frac{ze\Psi_o}{4kT})^2 \frac{1}{\kappa^2} \exp(-\kappa H) \qquad (2.40)$$

If $\Psi_{H/2}$ and Ψ_o are both small, then from Eq.2.36 and Eq.2.39, after integration between H and ∞, it follows that;

$$V_R(sphere) = 2\pi a\, \varepsilon_o \varepsilon_r \Psi_o^2 \ln[1 + \exp(-\kappa H)] \qquad (2.41)$$

The repulsive force between two interacting spherical particles, F_R (sphere), is defined as;

$$F_R = -\frac{dV_R(sphere)}{dH}$$

An approximate equation for small $\Psi_{H/2}$ can thus be obtained;

$$F_R(sphere) = \pi a 64 n^\circ kT \left(\tanh\frac{ze\Psi_o}{4kT}\right)^2 \frac{1}{\kappa}\exp(-\kappa H) \qquad (2.42)$$

Van der Hoeven and Lyklema (1992) defined an 'effective' surface area, A(eff.), of repulsion

$$A(eff.) = \frac{\pi a}{\kappa}$$

analogous to an 'effective' surface area of attraction of 2πaH for two interacting spheres as defined by Israelachvili (1985). So the repulsive pressure between two spheres can be calculated from the repulsive force therebetween.

These approximate equations (e.g., Eq.2.40 and Eq.2.42), however, are not valid for strong overlap of the double layers. In this case, numerical solutions of Poisson-Boltzmann equation are required. Chan et al. (1980) have given a fast numerical procedure of high precision capable of computing the ionic interaction for a symmetric electrolyte.

II-3 Van der Waals Attractive Interactions

II-3.1 Macroscopic Approach

The universal attractive forces between atoms and molecules, known as van der Waals forces, also operate between macroscopic objects and play an important role in the interaction of colloidal particles.

The interaction between macroscopic bodies arises from spontaneous electric and magnetic polarization, which results in a fluctuating electromagnetic field within the particles and within the gap between them. In order to calculate the force, the variation in electromagnetic wave energy with separation distance has to be determined. Lifshitz (1956) derived an expression for the force between two semi-infinite particles separated by a plane-parallel gap and his treatment was later extended by Dzyaloshinskii et al. (1960) to deal with the case of two bodies separated by a third medium. Direct measurements of the van der Waals forces between mica sheets (Israelachvili and Tabor, 1972) have confirmed the correctness of the Lifshitz macroscopic approach. Proper application of this approach requires detailed knowledge of the dielectric responses of the interacting particles over a wide frequency range. Certain simplifications may be possible and the procedures are clearly described by Hough and White (1980). Nevertheless, considerable computation is needed

and, for many systems of practical interest, the required dielectric data are not available.

II-3.2 The Hamaker Expressions

An older approach due mainly to Hamaker (1937) is still widely used because of difficulties with the macroscopic theory. The Hamaker analysis involves assumption of the pairwise additivity of intermolecular forces.

The van der Waals energy of attraction at a distance r, for a pair of macrobodies consisting of many identical molecules, can be approximated by the summation (or integration) over all interacting atom and/or molecular pairs, i.e.;

$$V_A = -\Sigma\frac{\beta}{r^6} = -\int_{v_1}\int_{v_2}\frac{\beta q^2}{r^6}dv_1 dv_2 \qquad (2.43)$$

where β is a positive constant related to the nature of the atoms and molecules and r is the distance between the centres of the atoms. v_1 and v_2 are the volume of particles 1 and 2, and q the number of atoms per unit volume of the particle.

Hamaker (1937) solved the integral of Eq.2.43 for various geometries. For two macrobodies of type 1 in vacuum, all solutions have the same general form:

$$V_A = -A_{11}f(G)$$

In this expression f(G) is an arbitrary but known function of geometry related to the shape and distance of the macrobodies involved in the interaction. The proportionality constant A_{11} is the Hamaker constant which reflects the material

contribution to the attractive London-van der Waals energy between the two macrobodies.

The van der Waals energy of attraction, for a pair of equal spheres of radius a, with particle centre-to-centre distance D and distance of closest approach between the spherical surface H(=D-2a) (defining s=D/a), is given by;

$$V_A = - A_{11} \frac{1}{6} \left(\frac{2}{s^2 - 4} + \frac{2}{s^2} + \ln \frac{s^2 - 4}{s^2} \right) \qquad (2.44)$$

For short distances of approach, i.e. H << a, Eq.2.44 can be approximated by;

$$V_A = - A_{11} \frac{1}{12} \frac{a}{H}$$

showing, that for short distances, V_A (spheres) is proportional to a/H. This means that, at given H, the V_A (spheres) is larger when the particle size is larger. Hence, it takes more energy to separate large particles than small ones or, for that matter, the energy gain obtained on approach is larger for big than for small particles.

The force of attraction, F_A, between two macrobodies can be obtained from (the negative value of) the first derivative with respect to the distance of the energy of attraction;

$$F_A = - \frac{dV_A}{dH}$$

For spherical particles, the following analytical solution was given by van Mil, et al. (1984)

$$F_A = -A_{11}\frac{32}{3}\frac{1}{as^3(s^2-4)^2} \qquad (2.45)$$

The equations above apply to the interaction of particles across a vacuum. The same expressions can be used for interactions through a liquid, but a modified Hamaker constant, for particles 1 and 2 separated by medium 3, is written:

$$A_{132} = A_{12} + A_{33} - A_{13} - A_{23} \qquad (2.46)$$

where A_{12} is the Hamaker constant for materials 1 and 2, etc.

A useful approximation for Hamaker constants of different materials is the geometric mean assumption, i.e.;

$$A_{12} \approx (A_{11}A_{22})^{1/2}$$

With this and the corresponding expressions for A_{13} and A_{23}, Eq.2.46 becomes:

$$A_{132} \approx (A_{11}^{1/2} - A_{33}^{1/2})(A_{22}^{1/2} - A_{33}^{1/2}) \qquad (2.47)$$

For similar materials, 1 and 1 interacting across a medium 3:

$$A_{131} \approx (A_{11}^{1/2} - A_{33}^{1/2})^2 \qquad (2.48)$$

Eq.2.48 led Hamaker to the conclusion that the van der Waals interaction between similar materials in a liquid would always be attractive (positive Hamaker constant), whatever the values of A_{11} and A_{33}. However, the possibility of negative Hamaker constants, for different materials, gives van der Waals repulsion, i.e.; when $A_{11} > A_{33} > A_{22}$.

Israelachvili (1985) has derived an alternative expression from the macroscopic Lifshitz theory, i.e.;

$$A_{131} = \frac{3}{4}kT\left(\frac{\varepsilon_{r1} - \varepsilon_{r3}}{\varepsilon_{r1} + \varepsilon_{r3}}\right)^2 + \frac{3h\nu_e}{16\sqrt{2}}\frac{\left(n_1^2 - n_3^2\right)^2}{\left(n_1^2 + n_3^2\right)^{3/2}} \qquad (2.49)$$

where n is the index of refraction, h Planck's constant and ν_e is the characteristic adsorption frequency in the UV range (typically ~ 3 X 10^{15} s^{-1}).

There are recent studies on the Hamaker constants of inorganic materials by Bergstrom and coworkers (1996,1997). These allow more precise estimation of the van der Waals energy for these systems.

II-3.3 Retardation

Because dispersion forces are electromagnetic in character, they are subject to a retardation effect. The finite time of propagation causes a reduced correlation between oscillations in the interacting bodies and a smaller interaction. Retardation is implicitly included in the full Lifshitz treatment but it is easy to modify the simple Hamaker approach to take this effect into account (Gregory, 1981).

It is convenient to think of a "characteristic wavelength" of the interaction, λ, which has a value around 100 nm. It is assumed retardation only becomes significant when the separation distance between particles is of the same order as the characteristic wavelength.

II-4 Combined Interactions – Ionic Stability

II-4.1 General

The Derjaguin-Landau-Verwey-Overbeek (DLVO) theory (Derjaguin and Landau, 1941; Verwey and Overbeek, 1948) makes it possible to quantify the ionic stability of lyophobic colloids. According to the DLVO theory, the sum of the repulsion (V_R) and van der Waals attraction (V_A) between particle pairs, reflects the total energy of interaction between particle pairs in suspension.

In Figure 2.3, the total-interaction and repulsion and attraction energies are plotted against separation distance. The case shown is for repulsion > attraction over the important range of separation. The plots show the potential energy barrier that ensures colloidal stability. Two colliding particles must possess sufficient energy to overcome this barrier to aggregate. The average kinetic energy is (3/2)kT for particles undergoing Brownian diffusion. So, for a barrier height of 15 kT units, very few collisions will successfully produce aggregates. The particles are held in a deep primary minimum once the barrier has been overcome and escape therefrom is unlikely.

Another important feature of Figure 2.3 is the secondary minimum in the potential-energy curve. This is a mathematical consequence of the different distance dependencies of the ionic and van der Waals interactions. The former decays exponentially and the latter via a power law. The latter gives a slower

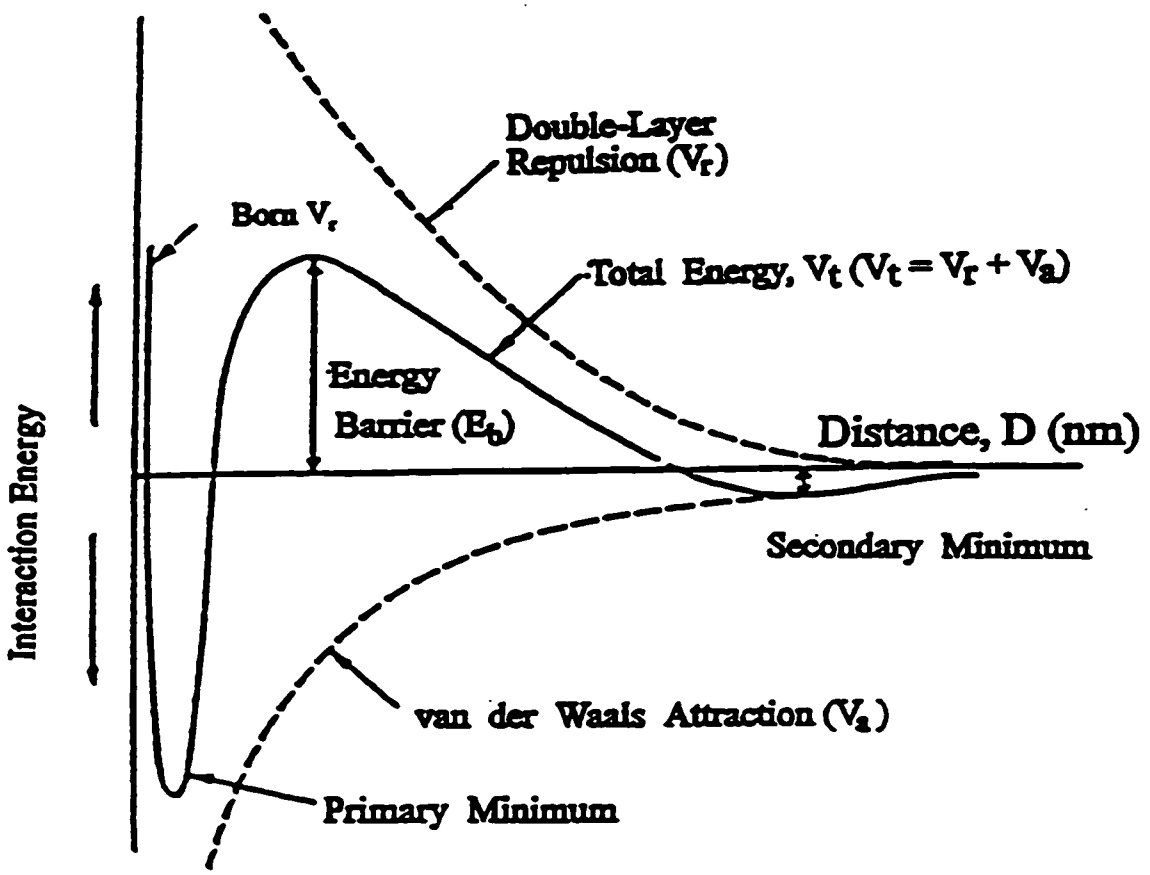

Figure 2.3 Schematic of the interaction energy as a function of separation between two particles

decrease at large distances. The attraction will outweigh the repulsion at some separation distance, but at low ionic strengths (e.g., in non-aqueous suspensions), the double-layer entropic repulsion may act over too great a distance for the attraction to be significant, thus the secondary minimum may not occur in the potential energy curve.

The repulsive barrier height can be reduced by increasing the ionic strength of the medium. As salt is added, there comes a point, the critical coagulation concentration (CCC), at which the barrier disappears. At this point, the following conditions apply:

$$dv_T/dH = 0, \text{ and } V_T = 0$$

Increasing the suspension solid volume fraction, φ, causes changes in the suspending-medium ionic strength due to the increase of concentration of ions required to balance the particle charge and the concomitant reduction of the fluid volume. The screening parameter in concentrated systems is determined, in part, by the concentration of added electrolyte and, in part, by the counterions accompanying the particles ('self-screening'). Ionic interactions between particles at finite concentrations dictate that, either the surface potential or the surface charge density, must deviate from the value measured at infinite dilution and be determined by the ionic environment at the finite concentration. Russel and Benzing (1981) developed a model facilitating determination of the average ion concentration in the fluid phase of a suspension based on ordered monodisperse latices system. This formulation provides the basis for constructing a modified

pairwise additive, or mean-field, description of the interactions between particles in concentrated dispersions. The pair-potential remains as per the conventional DLVO theory except for the volume-fraction-dependent Debye length and the corresponding variation in either the surface charge or potential.

II-4.2 Stability Ratios

When particles have been fully destabilized by the addition of sufficient salt, coagulation occurs at a rate which depends on their collision frequency. This is known as rapid coagulation. With lower salt concentration (i.e., below CCC), slow coagulation occurs at a rate which depends on the height of the potential energy barrier.

The Stability Ratio (W) is a measure of the rate at which the coagulation is retarded and is defined as the ratio of the rapid-coagulation-rate vs. the slow-coagulation-rate, i.e.;

$$W = J_R / J_S = 2a \int_{2a}^{\infty} \exp[V(H)/kT] H^{-2} dH \qquad (2.50)$$

Here, V(H) is the total potential energy of interaction between two approaching particles at distance H and a is their radius. The stability ratio can be considered a delay factor to rapid coagulation or the reciprocal of the coagulation efficiency due to the presence of a potential energy barrier that opposes coagulation.

II-5. Heterocoagulation

Most work on colloidal dispersions has treated single component systems, i.e., sols consisting of one type of particle. Interactions in dispersed systems containing particles of more than one kind have been studied theoretically (Derjaguin, 1954, Devereux and De Bruyn, 1963, Hogg et al., 1966, Barouch et al., 1978) and experimentally (Harding, 1972, Healy et al., 1973, Matijevic and Kitazawa, 1983) in recent years. This topic is receiving increased attention because composite systems are of interest in many applications such as ceramic composites (the addition of reinforcements and processing additives, e.g., sintering aids, stabilizers, to ceramic systems etc.). Uniformity between composite constituents is important since it governs the microstructure of the final sintered bodies. However, the properties of these systems are poorly understood compared with those of suspensions containing a single particle type.

When a colloidal dispersion contains oxide particles of more than one kind, it is likely that the various oxide species will have different surface charges for a given solution condition (e.g., pH). Under certain circumstances it is possible these charges will be opposite in sign. Under these conditions, mutual coagulation can take place, i.e., coagulation due to the interaction of opposite charges. Knowledge of the heterocoagulation conditions of suspensions has been applied to the deposition and adhesion of material coatings (Elimelech, 1991, Tamura et al, 1983).

Heterocoagulation is also governed by the double-layer and van der Waals interactions between particles. This is also the case for homocoagulation but the problem of interactions between unlike particles is considerably more complex, although substantial progress has been made in understanding the phenomena involved.

In the mid-1960s, Hogg, Healy and Fuerstanau (1966) built a theory of quantitative kinetic stability of nonidentical particles to develop a model applicable to actual systems. The Hogg-Healy-Fuerstanau (HHF) theory uses the same approach to describe the total potential energy of interaction as does the DLVO theory. However, HHF uses an expanded attraction and repulsion force equation which takes account of the differences between the particle types. The linear form of the Debye-Huckel approximation of the Poisson-Boltzmann equation is used (as in DLVO theory) to develop an equation to calculate the repulsive energy of interaction between dissimilar double layers. Hogg et al. show that the approximation is valid for Ψ_i and Ψ_j values of less than 50-60 mV as opposed to the 25 mV assumed in DLVO theory. According to the HHF model, the energy of repulsion between two spherical particles is;

$$V_R = \frac{\pi\varepsilon_o\varepsilon_r a_1 a_2(\psi_1^2+\psi_2^2)}{(a_1+a_2)}\{\frac{2\psi_1\psi_2}{\psi_1^2+\psi_2^2}\ln\frac{1+\exp(-\kappa H)}{1-\exp(-\kappa H)}+\ln[1-\exp(-2\kappa H)]\} \qquad (2.51)$$

where, a_1, a_2 and Ψ_1,Ψ_2 are the radii and surface potentials of the respective dissimilar particles.

Van der Waals attraction without retardation for two different interacting particles of radii a_1 and a_2 separated by distance H can be represented by (Hamaker, 1937)

$$V_A = -\frac{A_{132}}{12}\left[\frac{y}{x^2+xy+x} + \frac{y}{x^2+xy+x+y} + 2\ln\left(\frac{x^2+xy+x}{x^2+xy+x+y}\right)\right] \qquad (2.52)$$

where $x = H/(a_1+a_2)$, $y = a_1/a_2$.

Barouch et al. (1978) developed a complex interaction potential for nonidentical particles that uses an approximate solution of the Poisson-Boltzmann equation in its two-dimensional form with boundary conditions of constant potential. Barouch et al. note there is only one axis of symmetry for spherical particles and conclude that a two-dimensional solution yields more accurate results. The results of their solution for the interaction potential are comparable with those of the Hogg-Healy-Fuerstanau (HHF) model (Eq.2.51). The two models agree fairly well for unlike particles with potentials of opposite sign and different magnitudes. For particles with the same sign and different magnitudes, the HHF equation overestimates the interparticle repulsion as calculated by Barouch and Matijevic (1985). However, the model developed by Barouch-Matijevic-Ring-Finlan (BMRF) is mathematically complex and its solution complicated. There is also some question as to the accuracy of their method (Chan, 1983).

II-6 Ionic Stability of Suspensions in Non-aqueous Solvents

The extent of ionic stabilization of particles in non-aqueous media is theoretically extremely sensitive to the dielectric constant of the liquid. The dielectric constant is an important parameter because it affects particle interaction in two ways: (a) indirectly through its effect on the electrolyte dissociation and (b) directly via the screening of charges by the solvent.

The dielectric constant is also important in determining the potential gradient across the diffuse double layer. The latter is important because it determines the ionic force between particles. To obtain a sufficiently strong ionic repulsive force in media of low dielectric constant, a high surface potential is not enough. A sufficiently large potential gradient must also exist. The repulsive force between interacting particles is too low if this condition is not satisfied (Albers and Overbeek, 1959). The major effect of a low dielectric constant is to restrict the dissociation of ionizable substances, thereby decreasing the ionic concentration in the non-aqueous medium. The resulting Debye-Huckel parameter, κ, is small. For a symmetrical electrolyte ($n_+^o = n_-^o = n^o$, $z_+ = z_- = z$), from Eq.2.7,

$$\kappa = \left(\frac{e^2 \sum n_i^o z_i^2}{\varepsilon kT}\right)^{1/2} \qquad (2.7)$$

and Eq.2.9,

$$\psi = \psi_o e^{-\kappa x} \qquad (2.9)$$

yielding

$$-d\ln\psi/dx = \kappa = (\frac{2e^2z^2n^o}{\varepsilon kT})^{1/2}$$

thus, the low ionic concentrations of low-dielectric-constant liquids reduce the potential gradient. The latter has discouraged some investigators from utilising ionic stabilization in non-aqueous media. Feat and Levine (1976) concluded, that for systems involving a non-polar solvent with dielectric constant < 5, the repulsive pressure is insufficient to stabilize colloids.

A number of workers (Lyklema, 1968; Parfitt and Peacock, 1978; Kitahara, 1984) kept the ionic option open. Recently, van der Hoeven and Lyklema (1992) confirmed that ionic stabilization is possible for low-polar organic media (dielectric constant between 5 and 11) provided some dissociated electrolyte is present. They used dodecyl-benzene sulphonic acid (HDBS) as a stabilizer. The HDBS created the zeta potential and enhanced the dielectric constant and the ionic strength of the solvent.

The stability of dispersion in polar organic media, such as the lower alcohols, is not necessarily similar to that in aqueous, non-polar ($\varepsilon_r < 5$) or low-polar ($5 < \varepsilon_r < 11$) organic media. There are however, few studies on the stability of powders in polar organic media and thus they are poorly understood. Lyklema and co-workers (1978) investigated the stability of silver halides in a water/ ethylene-glycol mixture. This system is considered a bridge between aqueous and non-aqueous systems. de Rooy et al. (1980) carried this work a step further by

preparing electrostatically stabilized sols of Ag, AgI and α-FeOOH in the following polar organic media: methanol, ethanol, ethanol-water mixtures, 2-propanol and acetone. They investigated the effect of electrolytes on dispersion stability. They discovered coagulation by monovalent counterions is due to double layer compression.

It is clear that three conditions must be fulfilled to ionically protect colloids against coagulation:

(i) the particles should carry sufficient surface charge and potential,

(ii) there should be enough ions to develop a sufficiently strong ionic repulsive force, but not so large as to compress the double layer, and

(iii) the van der Waals attraction between particles should be less than the ionic repulsion at satisfactory particle separation.

According to Eq.2.22;

$$Q = 4\pi a\varepsilon(1+\kappa a)\psi_o \qquad (2.22)$$

which shows that, for particles of given electrostatic potential and radius, the charge is proportional to the dielectric constant. Thus, the charge required to produce a given potential in ethanol (ε_r=24.3) is ~ 25% that observed in water (ε_r=78). So it is possible to obtain high enough surface potentials in polar organic media to ensure ionic stabilization.

If a certain degree of dissociation of an electrolyte can be obtained in a medium of low dielectric constant and, at the same time, a high surface potential is created, it should be possible to create a steep potential gradient and significant

repulsive force. This approach should be feasible in polar organic media of dielectric constant > 11. The intriguing conclusion is that, in such media, there is a range of electrolyte concentration wherein addition of ions improves colloidal stability.

From the above considerations, it seems the option of ionic dispersion stabilization is available to polar organic media. Jang and Moon (1990) claimed it is extremely difficult to produce uniform and kinetically stable Al_2O_3 dispersions in anhydrous alcohol (ethanol) due to lack of ionic stabilization. This observation seems erroneous, but Fowkes and Push (1984) suggested "..... be wary of any claims of steric stabilization unless the ionic contribution has been measured".

Solid oxide particles in aqueous suspension have pH-dependent electrical charge (Parks, 1965). The surface-potential or charge-density of an oxide particle is sensitive to pH. Significant pH effects on aqueous oxide suspension rheology have been reported for zirconia (Leong et al., 1991) and α-Al_2O_3 (Nikumbh et al. 1990). Nikumbh et al. (1990) also reported the rheological behaviour of slips of Al_2O_3 in ethanol at different pH values with and without deflocculant. They did not study the influence of pH on surface potential or charge density.

Magnesia is not stable in water as it forms hydroxide which dissolves easily. This makes it necessary to consider solvents such as alcohols or ketones. Stability studies of MgO in non-aqueous media, in terms of zeta potential, are scarce in the literature. Brown and Salt (1965) reported the zeta potential of MgO in methanol, ethanol, acetone and 1-nitropropane without electrolyte.

There are many publications dealing with the surface chemistry and colloidal stability of silica in water (Iler, 1979). Aqueous silica sols are colloidally stable in the isoelectric region (Iler, 1979). The stability of silica sols at the IEP has been explained via repulsive hydration forces at the silica-water interface (Sasaki and Maeda, 1994). Several groups have recently shown that the forces between silica surfaces deviate from classic DLVO theory (Grabbe and Horn, 1993, Meagher, 1992, Ducker et al., 1991). An additional non-DLVO short-range monotonic repulsive force has been measured at surface separations, 1-5 nm. This behaviour has been explained by the presence of a structured layer of water (10 to 20 molecular layers thick) at the silica interface. This gives rise to a short-range, repulsive, hydration force. On the basis of adhesion, friction, contact-angle and surface-force measurements, Vigil et al. (1994) proposed the additional short range repulsion was due to a short-range steric repulsive force originating from a surface gel layer of oligomeric silicic acid groups. The work of Vigil et al. (1994) supports the original gel layer model proposed by Tadros and Lyklema (1968).

Despite the interest in silica, few studies have attempted to understand its colloidal stability in organic media. Recently Ketelson et al. (1996) investigated the colloidal stability of Stober silica in acetone using electrophoresis and coagulation experiments with NaI, $CaCl_2$, and Bu_4NI. They found that the experimental coagulation concentrations for NaI and Bu_4NI did not agree with simple DLVO theory. They used the thin steric barrier, originally proposed by

Vigil et al. (1994) to explain their results. Kosmulski and Matijevic (1992) investigated the pH-zeta-potential relationships for silica in a water-alcohol mixture.

In summary of this section; to our knowledge, no systematic study has been undertaken on the effect of pH on the surface charge and ionic stability of oxide particles in pure organic solvents.

II-7 Correlation between pH Scales in Different Solvents

The most potent tool for modifying oxide suspension stability is to change the pH. The latter is, however, an aqueous concept and, to apply the same approach to non-aqueous suspensions, a correlation must be identified.

The fundamental aspects of pH scales for different solvents are documented by Bates (1973). Acidity in aqueous media is defined by the pH scale which relates acidity to hydrogen ion activity;

$$pa_H = -\log a_H \qquad (2.53a)$$

$${}_w\mu_H = {}_w\mu_H^{\circ} + RT\ln a_H \qquad (2.53b)$$

This definition can be extended to non-aqueous media using ion-transfer functions (Popovych and Tomkins, 1981), ie;

$$pa_H^{\cdot} = -\log a_H^{\cdot} \qquad (2.54a)$$

$${}_s\mu_H = {}_s\mu_H^{\circ} + RT\ln a_H^{\cdot} \qquad (2.54b)$$

Subscripts w and s indicate the partial molar free energy (μ) is referred to the standard state in water and non-aqueous solvent, respectively. The non-aqueous

activity is labelled with an asterisk. The activities and molalities in the above equations are related as usual, i.e.;

$$a_H = m_H \, {}_w\gamma_H \qquad (2.53c)$$

$$a^*_H = m_H \, {}_s\gamma_H \qquad (2.54c)$$

where the activity coefficients ${}_w\gamma_H$ and ${}_s\gamma_H$ become unity at infinite dilution in water and non-aqueous solvents, respectively.

In general, the quantity required to correlate the free energy properties of species i in two solvents, is the difference between the partial molar free energies of the solute in its aqueous and non-aqueous standard states, i.e.;

$$\Delta\mu^o_t(i) = {}_s\mu^o_i - {}_w\mu^o_i = RT \ln {}_m\gamma_i \qquad (2.55)$$

and,

$${}_w\gamma_i = {}_s\gamma_i \, {}_m\gamma_i \qquad (2.56)$$

This difference is known as the standard free energy of transfer for solute i from water to the given non-aqueous solvent. The corresponding activity coefficient ${}_m\gamma_i$ is known as the transfer activity coefficient, or medium effect of solute i between the two solvents. It can be used as a conversion factor from a non-aqueous to an aqueous activity scale. Thus, in the case of hydrogen-ion activity;

$$a_H = a^*_H \, {}_m\gamma_H \qquad (2.57)$$

and,

$$p\,a_H = p\,a^*_H - \log {}_m\gamma_H \qquad (2.58)$$

to correlate the pa_H scales in water and media other than water.

The common pH meter determines the so-called "operational pH values." In any medium, the operational pH differs from pa_H by the residual liquid-junction potential, ΔE_j:

$$pH - pa_H = \frac{\Delta E_j}{(RT \ln 10)/F} \qquad (2.59)$$

or;

$$pH - pa_H = \frac{\Delta E_j}{0.05916} \quad at\ 25^\circ C \qquad (2.60)$$

where F is the Faraday constant, R the gas constant per mole, pH the pH meter reading, and ΔE_j the difference between the liquid-junction potentials encountered in the standardization and testing step. When both the buffer and the unknown solution in a pH measurement are aqueous, ΔE_j is small, but when the buffer is aqueous and the unknown non-aqueous, ΔE_j is appreciable, perhaps of the same order of magnitude as the pH itself. There is evidence (Bates et al., 1963) however that the ΔE_j values between aqueous KCl bridges and dilute non-aqueous solutions are primarily a function of the solvent and the quantity $[(\Delta E_j/0.05916) - \log {}_m\gamma_H] = \delta$ is approximately constant for a given solvent medium, independent of the acidity of solution.

Equation 2.60 can be rewritten as;

$$P a_H = pH - \delta - \log_m \gamma_H = pH - \frac{\Delta E_j}{0.05916} \quad at\ 25^\circ C \qquad (2.61)$$

Thus, when both δ and log $_m\gamma_H$ are known for a given solvent, the pa_H of its solutions, referred to the aqueous standard state, can be evaluated directly from the operational pH readings in the non-aqueous medium.

II-8. Specific Conductivity and Calculation of the Ionic Concentration

There must be certain levels of ion in the suspension to ensure sufficient force of repulsion. The ionic-strength of non-aqueous media can be determined via conductivity measurements (Kitahara et al. 1967; Kitahara, 1973).

The specific conductivity (k) is related to the ionic concentration by:

$$k = \sum n_i^o U_i z_i e \qquad (2.62)$$

where n_i^o, U_i and z_i are the ionic concentration (number of ions per cm^3), ionic mobility and the number of charges on the i-th ion, respectively.

For symmetrical monovalent electrolytes, Eq. 2.62 reduces to:

$$k = n^o e(U_+ + U_-) \qquad (2.63)$$

and, since $U_+ + U_- = \Lambda_o/F$,

$$k = n^o e\Lambda_o/F \qquad (2.64)$$

where Λ_o is the limiting equivalent conductivity and F the Faraday constant. The limiting equivalent conductivity can be attributed to cations and anions independently, i.e.:

$$\Lambda_o = \Lambda_{+,o} + \Lambda_{-,o} \qquad (2.65)$$

Walden's law is used to obtain the value of Λ_o in non-aqueous solution, i.e.;

$$\Lambda_{\alpha(aq)}\eta_{(aq)} = \Lambda_{\alpha(nonaq)}\eta_{(nonaq)} \qquad (2.66)$$

The conductivity data can be analyzed using the Ostwald dilution law which relates the equivalent conductivity of a solution to the equivalent conductivity at infinite dilution and the dissociation constant (Bockris and Reedy, 1970), i.e.;

$$\frac{1}{\Lambda} = \frac{1}{\Lambda_o} + \frac{C_o \Lambda \gamma_{\pm}^2}{K_D \Lambda_o^2} \qquad (2.67)$$

where Λ is the equivalent conductivity, Λ_o the equivalent conductivity extrapolated to infinite dilution, C_o the concentration of salt added, $\gamma_{\pm}$ the activity coefficient and K_D the dissociation constant. A plot of $1/\Lambda$ vs. $C_o\Lambda$ should give a straight line of slope $\gamma_{\pm}^2/K_D\Lambda_o^2$ and intercept, $1/\Lambda_o$. This law is valid for solvents of low dielectric constant where the largest change in conductivity is due to ion-pair formation and there is a negligible change in ionic mobility.

CHAPTER III

EVALUATION OF DISPERSION STABILITY

III-1 Introduction

To be able to fully control the stability, proper evaluation of suspension stability is very important (Pugh, 1994, Lange, 1989). Ceramists have used several tools to assess colloidal stability. Approaches that measure macroscopic properties include sedimentation and rheology. Sedimentation approaches (Parish et al., 1985) examine the rate at which particles settle and their resultant packing density. While this approach closely reflects some types of forming processes used in the ceramic industry (e.g., slip casting), such experiments utilizing submicrometer particles span lengthy times where the state of the suspension at the onset does not reflect that at the end of the experiment. Thus, sedimentation cannot be used to characterize the suspension state on an instantaneous basis but rather is used to assess long-term stability.

The relation between rheology and dispersion stability has been extensively reviewed (Bell and Crowl, 1973; Tadros, 1980; Russel et al., 1989). Colloidal suspension rheology is influenced by the surface chemistry, content, size and

shape of the suspended particles, as well as the chemical nature of the solvents. The rheological properties of suspensions depend strongly on the range and magnitude of interparticle interactions and the resulting structures they form. The rheology of a suspension can be used to assess the particle interactions, while control of suspension stability will in turn lead to well dispersed systems with the low viscosity needed for the colloidal processing of ceramics.

Apparent-viscosity measurement at fixed shear rates is widely used to assess stability. Its limitations are, however, obvious for concentrated systems (Bergstrom, 1994). A rheological flow curve can be used instead. The latter can provide information that relates to the interactions between the particles and the media. Furthermore, the strength of the interactions can be estimated via information at various shear-rates (Darby, 1986). In particular, if the data can be represented by an appropriate model, evaluation may become more convenient and effective (Hiemenz, 1986). Several models have been developed for non-Newtonian systems. These include the Bingham plastic model, the Ostwald-de Waele power law, the Casson model and the Herschel-Buckley model (Darby, 1986). These models have been widely and successfully used to explain, characterize and predict the flow behaviour of various systems; nevertheless, little has been reported on the study of ceramic suspensions via these models.

Approaches that measure microscopic properties include electrokinetic and (particle size)-(particle density) dependent effects. Particle sizing approaches directly determine the degree of colloidal stability regardless of the dispersion

mechanism. Turbidity measurements reflect both particle size and particle density and have been used classically to determine stability ratios (Wiese and Healy, 1975). X-ray photosedimentation and other particle-sizing approaches have been used in the ceramic industry to infer stability by correlating particle-size-distribution with the concentration of processing additives (Sacks and Khadilkar, 1983). In this case, improvements of stability are determined by decreases in both mean-particle-size and particle-size-distribution breadth. Such approaches only allow observation of the relative improvements of dispersion stability without knowledge of the intrinsic particle size distribution (a distribution free of agglomeration). Light scattering approaches have the same limitation (dynamic (Barringer et al., 1984) and static (Muly and Frock, 1980)).

Electrokinetic methods on the other hand, reveal the sign and magnitude of the electrical charge residing near the solid particle-liquid interface and thus give insight into the degree of ionic stabilization. The measurement of the electrophoretic mobility is well established and easily applicable.

III-2 Electrophoretic Mobility Measurement

When a particle suspended in a liquid is subjected to an applied dc electric field, the particle accelerates towards the oppositely-charged electrode, until it reaches a terminal velocity. At this point the resistance to the particle's motion

through the liquid equals the force of the electric field acting on the particle. The electrophoretic mobility of the particle is thus defined as;

$$U_E = u/E \qquad (3.1)$$

where: u = terminal velocity (μm/s), and E = applied electric field (V/cm).

Electrophoresis is the most widely used of electrokinetic procedures for measuring electrophoretic mobilities. Doppler-electrophoretic-light-scattering is a new technique (Ware, 1974). The velocity of particles migrating in a suspension in an electric field is determined by measuring the Doppler shift of laser light scattered thereby. The major drawback of the electrophoresis-based techniques is the necessary low concentration of particulates in suspension.

The electroacoustic technique, based on the physical effects described by Debye (1933), is also relatively new (since the mid-1980's). Electroacoustic phenomena arise via the interaction between electric fields and sound waves in a suspension of charged particles. As sound travels through a suspension, particles will oscillate relative to the suspending medium as a consequence of the difference in the densities between the particle and medium phases. This relative motion is termed acoustophoresis. Acoustophoresis induces a macroscopic colloid vibration potential (CVP) as the ionic atmospheres of the suspended particles relax. Marlow et al. (1988) described a commercial instrument for applying the CVP technique to the electrokinetic properties of colloids.

A second type of electroacoustic effect occurs when an alternating electric field is applied to a suspension of charged particles. The particles move back and

forth in the liquid due to the force of the electric field creating tiny pressure disturbances. If there is a density difference between the particles and the liquid, a macroscopic acoustic wave is developed at the boundary of the suspension (the electrodes). This effect has been termed the Electrokinetic Sonic Amplitude (ESA) and it was discovered at Matec (Oja et al., 1985) in 1982. Matec Applied Sciences markets the ESA-8000 system which can be configured to measure either the ESA or CVP and thus characterize the electrokinetic properties of colloidal suspensions.

O'Brien (1988) developed a theory for the ESA effect. He showed it is linked to the CVP via a reciprocal relation. More significantly, he showed that the ESA and CVP effects are related to a fundamental property of the particles known as dynamic mobility. The dynamic mobility, U_d, is defined as the particle velocity, u, divided by the electric field, E, acting on the particle for a charged particle moving under the force of a sinusoidal electric field with angular frequency, ω.

The dynamic mobility of the particle is a complex quantity, i.e., it has both magnitude and argument (or phase angle). The magnitude of U_d is u_o/E_o, the amplitude of the particle velocity divided by the amplitude of the electric field. The argument of U_d relative to the electric field is $\omega(\Delta t)$. The argument of U_d gives the time-delay or phase-lag between the particle motion and the applied field. The dynamic mobility of a colloidal particle is a function of the zeta potential, the particle radius, the double layer thickness and the frequency of the applied field. The dynamic mobility reduces to the familiar electrophoretic mobility defined by a dc electric field as the frequency of the ac electric field approaches zero. When the

frequency of the electric field is increased, the particle velocity will lag the field and the velocity amplitude will drop because of inertial forces which are proportional to the particle size.

The ESA signal is directly proportional to the dynamic or high frequency electrophoretic mobility of the colloid for moderately concentrated suspensions (up to 10 vol%) (O'Brien et al., 1990), i.e.;

$$ESA = c\,\Delta\rho\,\phi\,U(\omega) \qquad (3.2)$$

where c is sound velocity, $\Delta\rho$ the difference in density between the solid and liquid phase, ϕ the solid volume fraction and $U(\omega)$ the dynamic mobility.

The principle advantage of electroacoustics is that it can be used for concentrated systems. Such are opaque to light and most other methods cannot be used unless the sample is diluted a thousand times or more. Such dilution often changes the surface properties and makes measurements unreliable.

III-3 Calculation of the Zeta Potential from the Electrophoretic Mobility

The conversion of the electrophoretic mobilities to zeta potentials is not straightforward (Hunter, 1981).

There are two resistances to the movement of particles by electrophoresis (Dukhin and Derjaguin, 1974). The first is electrophoretic retardation (k_1), i.e; the action of the electric field on the double layer ions. This will cause the liquid to move in the opposite direction and thus reduce the velocity of the migrating particles. It

will depend on the effective value of the slipping velocity of the diffuse layer relative to the particle, u_{ef}. The second is the Stoke's frictional resistance of the medium (k_2) which depends on the rate of motion of the particle, u, relative to the medium. The two velocities are of approximately the same order, i.e, $u \sim u_{ef}$, while the two forces are proportional to the gradients of the velocities. For viscous resistance, the characteristic linear dimension is of the order of the radius of the particle, i.e, $k_2 \sim u/a$, whereas for the electrophoretic retardation force, it is of the order of the double-layer thickness, i.e., $k_1 \sim u_{ef}/\kappa^{-1}$. From this, an important approximation is obtained:

$$\frac{k_1}{k_2} \approx \kappa a \qquad (3.3)$$

This means the ratio of the retardation force (k_1) to the viscous resistance (k_2) is ~ κa.

Thus for small values of κa, although the retardation force acts across the whole double layer, very little is transmitted to the particle and the main retarding force thereon is the frictional resistance of the medium. The Huckel equation can be used in this case;

$$\kappa a < 0.1 \quad U_E = \frac{2\varepsilon\zeta}{3\eta} \qquad (3.4)$$

where U_E is the electrophoretic mobility of the particle, ε and η are the permittivity of the dielectric and viscosity of the solvent respectively.

For $\kappa a >> 1$, the forces imparted to the liquid by the applied electric field are transmitted to the particle as the liquid flows along its surface. Electrophoretic

retardation is now the dominant force and the particle motion is equal and opposite to that of the liquid. The Smoluchowski equation can be used in this extreme situation;

$$\kappa a > 100 \quad U_E = \frac{\varepsilon \zeta}{\eta} \qquad (3.5)$$

Henry (1931) showed the two equations could be reconciled if account is taken of the effect of the particle shape and size on the electric field. When an external field is superimposed on the local field around the particle, the mobility can be written:

$$U_E = (4\pi \varepsilon_o).\frac{\varepsilon_r \zeta}{6\pi\eta}.f_1(\kappa a) = \frac{2\varepsilon\zeta}{3\eta}.f_1(\kappa a) \qquad (3.6)$$

The function $f_1(\kappa a)$ is a correction factor for the retardation effects of the double layer and depends on the particle shape. For spheres, it is given by:

$$f_1(\kappa a) = 1 + \frac{(\kappa a)^2}{16} - \frac{5(\kappa a)^3}{48} - \frac{(\kappa a)^4}{96} + \frac{(\kappa a)^5}{96}$$
$$- \left[\frac{(\kappa a)^4}{8} - \frac{(\kappa a)^6}{96}\right] e^{\kappa a} \int_{\infty}^{\kappa a} \frac{e^{-t}}{t} dt \qquad (for \quad \kappa a < 1) \qquad (3.7)$$

and

$$f_1(\kappa a) = \frac{3}{2} - \frac{9}{2\kappa a} + \frac{75}{2(\kappa a)^2} - \frac{330}{(\kappa a)^3} \qquad (for \quad \kappa a > 1) \qquad (3.8)$$

Values of the function $f_1(\kappa a)$ are given by Abramson et al. (1966). Note that $f_1(\kappa a)$ approaches 1 for small κa, and 3/2 for large κa.

Henry's calculations were based on the assumption that the external field could be superimposed on the field due to the particle and that the latter could be

described by the linearized version of the Poisson-Boltzmann equation. The treatment is therefore only valid for particles with low potential (ζ < 25 mV). As the zeta potential rises, the problem becomes more complicated. It also fails to account for the distortion of the field induced by the movement of the particle - the relaxation effect. As the particle moves, the surrounding atmosphere must re-form by suitable double-layer-ion motion. The extent to which the atmosphere symmetry is destroyed by movement of the particle depends on the mobility and charge of the counter ions.

It is necessary to account for the geometrical effect considered by Henry and the relaxation and retardation effects, to obtain a mobility expression valid for all κa and zeta potentials. This involves simultaneously solving several differential equations.

Any theoretical treatment of electrokinetics must start from the fundamental equations describing (i) the electrostatic potential, (ii) the ion concentration and (iii) the fluid flow.

Firstly the total electric potential, ψ, which includes the external dc field, around the particle, must satisfy the Poisson equation:

$$\nabla^2\psi = -\frac{\rho}{\varepsilon} \qquad (2.1)$$

where $\rho = e(n_+ z_+ - n_- z_-)$ as usual. (Note that in this formulation the valency z_- is to be used as a positive number). It is essential that n_+ and n_- are the ion

concentrations in the distorted atmosphere; introduction of these quantities enters the relaxation effect into the differential equations.

Inside the particle, the potential, ψ_i, satisfies Laplace's equation ($\nabla^2\psi_i = 0$) since there is no space charge within the particle.

The unknown concentrations n_+ and n_- are determined by the balance between the electrical and diffusional forces and the bulk fluid transport. They must satisfy a generalized form of the Poisson-Boltzmann equation of the Nernst-Planck type;

$$div[\mp(n_{\pm}z_{\pm}e)grad\,\psi - kT\,grad\,n_{\pm} + n_{\pm}f_{\pm}u] = 0 \qquad (3.9)$$

where $f_\pm$ are the frictional coefficients of the ions and u is the velocity of the liquid with respect to the particle. The first term in the brackets represents the migration of ions in the electric field, the second is a diffusion term and the last recognises the flow of the liquid gives an extra velocity to the ions. The sum of these three contributions gives the total flow of ions. For a coordinate system based on the particle, the divergence of the ion flow is zero because, at steady state, the ion distribution around a moving particle remains constant.

The fluid motion is described by the time-independent form of the Navier-Stokes equation for an incompressible fluid:

$$\eta\,curl\,curl\,u + grad\,p + \rho\,grad\psi = 0 \qquad (3.10)$$

where p is the hydrostatic pressure. The left-hand side of this equation is the sum of the forces acting on a volume element of the liquid. The first term represents the friction between this volume element and surrounding portions of the liquid;

the second is the result of the volume element tending to move toward regions of low hydrostatic pressure and the third is the electrical force on the ions in the volume element. The latter force is transferred to the liquid. The third term corresponds to the electrophoretic retardation.

The primary assumptions in deriving these equations are that the solvent is continuous and characterized by a constant dielectric permittivity. The latter is assumed unaffected by the overall field strength or the local field in the neighbourhood of an ion. It is also assumed the ions act as point charges, the fluid is simple Newtonian with a viscosity independent of position and the flow is slow and steady.

These three equations are general and apply to a particle of any shape. Solution is only possible when boundary conditions appropriate to a particular shape of particle are known.

The solution cannot be expressed in analytical form. It requires sophisticated computer solution. Wiersema et al. (1966) developed such a solution using a model of a rigid, electrically-insulating sphere surrounded by a Gouy-Chapman double layer. O'Brien and White (1978) provided a more effective numerical solution of the electrophoresis problem for a sphere.

The zeta potential can be calculated via the theory developed by O'Brien (1988) from the dynamic mobility of a suspension of spheres (particle concentrations up to 10 volume percent), determined by electroacoustics.

For aqueous media, assuming thin double layers ($\kappa a > 50$),

$$U_d = \frac{\varepsilon\zeta}{\eta} G(\frac{\omega a^2}{\nu}) \qquad (3.11)$$

Here the G term corrects for the inertia of the particle in the alternating field which acts to reduce the velocity amplitude for a given zeta potential. G depends on the frequency, ω, of the measurement, on the radius, a, of the particles, and on their kinematic viscosity ν (= η/ρ_s where ρ_s is the density of the solvent).

For non-aqueous media, assuming thick double layers ($\kappa a < 0.02$),

$$U_d = \frac{2\varepsilon\zeta}{3\eta} G'(\frac{\omega a^2}{\nu}) \qquad (3.12)$$

Eqs.3.11 and 3.12 are identical to the well known Smoluchowshi and Huckel equations for the dc electrophoretic mobility except for the G and G' terms.

III-4 Electroviscous Effects

The presence of charged species in a suspension influences its viscosity. There can be a dramatic change in the viscosity of suspensions of charged particles with changes in the electrolyte concentration of the suspending medium. This is most marked in concentrated dispersions.

Three distinct electroviscous effects have been identified (Conway and Dobry-Duclaux, 1960). The primary electroviscous effect results from deformation of the diffuse part of the double layer formed around charged particles from spherical symmetry by a shear field. The Maxwell stresses due to the asymmetric

electric field tend to restore the equilibrium double layer, thus oppose the flow. The primary electroviscous effect is small compared to other electroviscous effects.

The second electroviscous effect is the augmentation of the viscosity of a suspension by the ionic interaction between particles due to overlap of their double layers. The mechanism is an increase of the collision diameter of the particles due to the ionic repulsive force. Thus, the excluded volume is greater than for uncharged particles and the ionic particle-particle interactions in a flowing dispersion constitute an additional source of energy dissipation.

A tertiary electroviscous effect exists due to the expansion and contraction of particles made up of polyelectrolytes on changing the electrolyte concentration of the medium. This effect is non-active in the presently studied systems.

CHAPTER IV

MATERIALS PREPARATION AND CHARACTERIZATION

IV-1 Introduction

The oxides of the world are either acidic, basic or amphoteric in suspension. One oxide of each type (acidic: silica, basic: magnesia, amphoteric: alumina) was selected for study. The characteristics thereof will potentially facilitate prediction of the behaviour of all oxides.

Magnesia, alumina and silica and combinations thereof are contained in > 90% of ceramics.

When a surface is created by cleavage of the solid, some chemical bonds are broken. In the case of ionic or strongly polar compounds like oxides, the surface becomes reactive and is able to chemisorb water vapour that can be removed from the surface only by drastic means. Water may be chemisorbed on oxides through a hydrogen bond or it may undergo dissociation. In the latter case, surface hydroxyl groups (MOH) are formed.

The surface of magnesia is almost fully hydrated. The rate of hydroxylation of MgO is high probably because of the high solubility of MgO in water.

Alumina has both basic and acidic sites on its surface (Tanabe, 1970). Alumina surfaces are partially hydrated and the surface is covered by AlOH that acts as basic sites. Upon calcination, dehydration begins and Lewis acid (Al^+) and base (O^-) sites may form. Even if the powder is carefully dried and stored, some degree of hydroxylation remains on the surface. Upon re-adsorption of water from the atmosphere, these sites may be converted to Bronsted acid and base sites. Therefore, the exact surface chemical nature of an alumina powder will depend on the thermal history of the particles.

Silica is an acidic oxide. Its surface structure is complex. It is now generally accepted that surface silicon atoms tend to complete tetrahedral configuration forming silanol groups.

Ethyl alcohol (EtOH) and dimethyl sulphoxide (DMSO) are used as polar organic media in this study.

IV-2 Powder Characterization

IV-2.1 Alumina

The powder used was high purity alumina (purity > 99.99%; Sumitomo Chemical Co., Tokyo, Japan) designated AKP-50.

The particle size of the alumina powder was determined by sedimentation (Model CAPA 700, Horiba, Ltd., Tokyo, Japan), giving, D_{vel}, the "diameter" of an

imaginary "equivalent sphere" with the density of alumina and whose settling velocity is the same as the particle. The powder was dispersed in ethanol and sonicated for 10 minutes to break up agglomerates. The suspension was then diluted for measurement.

The particle size frequency distribution is plotted in Figure 4.1 and the cumulative distribution in Figure 4.2, reporting the total cumulative mass of particles that are smaller than a given diameter, D_{vel}. The powders show a log-normal size-distribution. The geometric mass average, ${}_G\langle D_{vel}\rangle_{43}$, and the geometric standard deviation, σ_G, were determined from Figure 4.2 directly, i.e. 0.22 μm, 1.64, respectively.

However, to characterize the suspension stability due to surface charge and the interaction, the equivalent surface area diameter, D_s, is most appropriate for individual non-spherical particles, and the geometric equivalent surface average of the surface equivalent diameter, ${}_G\langle D_s\rangle_{32}$, is needed to represent the area of the group particles.

According to Kapteyn's rules (Woods, 1983) which are

$$\ln {}_G\langle D_{vel}\rangle_{32} = \ln {}_G\langle D_{vel}\rangle + 2 \ln^2\sigma_G \quad (4.1)$$

$$\ln {}_G\langle D_{vel}\rangle_{43} = \ln {}_G\langle D_{vel}\rangle + 3 \ln^2\sigma_G \quad (4.2)$$

$$\ln {}_G\langle D_{vel}\rangle_{32} = \ln {}_G\langle D_{vel}\rangle_{43} - \ln^2\sigma_G \quad (4.3)$$

where ${}_G\langle D_{vel}\rangle$ is the geometric number average of equivalent settling velocity diameter. The geometric surface average of equivalent settling velocity diameter, ${}_G\langle D_{vel}\rangle_{32}$, can be calculated, i.e. 0.17 μm.

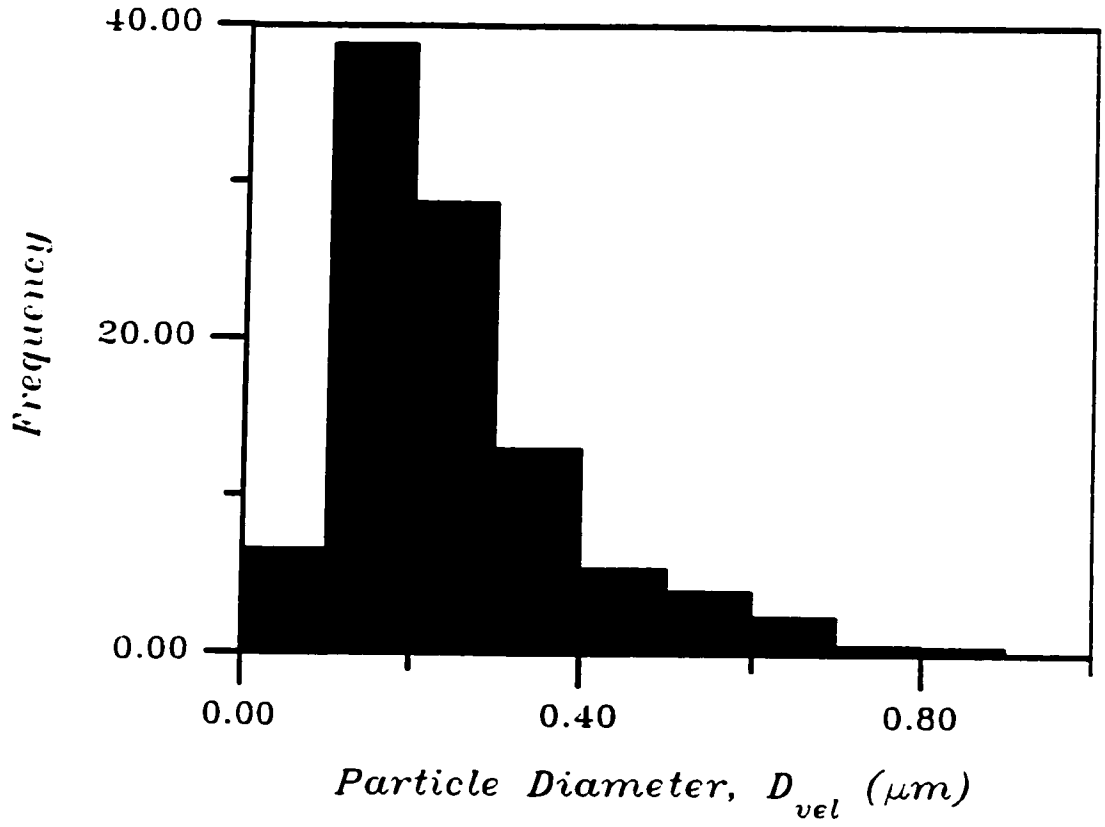

Figure 4.1 The particle size frequency distribution of alumina powders

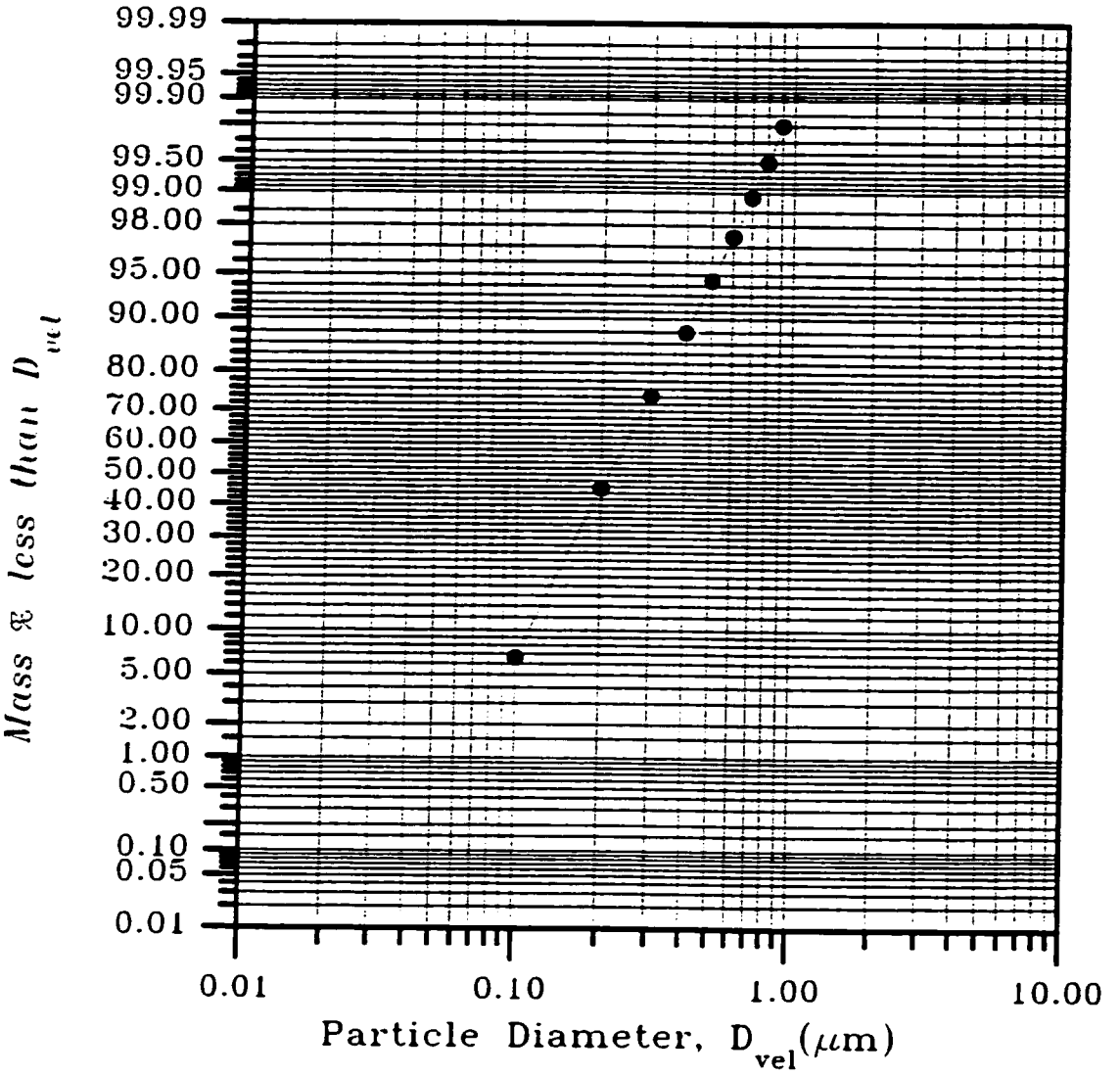

Figure 4.2 The cumulative particle size distribution of alumina powders

The geometric equivalent surface average of the surface equivalent diameter, ${}_G\langle D_S\rangle_{32}$, can be calculated via (Woods, 1983)

$$ {}_G\langle D_S \rangle_{32} = \frac{(0.37)6}{\pi} \frac{1}{(\alpha_V)^{\frac{1}{2}}} {}_G\langle D_{vel} \rangle_{32} \quad (4.4) $$

where α_v is volume shape factor.

A DS130 scanning electron microscope was employed to observe the alumina particles. The powder was dispersed in ethanol and sonicated for 10 minutes. Several drops of the suspension were placed on an SEM sample holder and gold was coated on via a SPI-MODULE Sputter Coater (SPI Supplies Division of Structure Probe, Inc.). The coating current was ~ 20 mA under a vacuum of ~ $2x10^{-2}$ atm. The coating time was 3 minutes. Micrographs of the powder are shown in Figure 4.3.

Values of shape factor were estimated, i.e., surface shape factor, α_s, 2.3, and volume shape factor, α_v, 0.25, respectively. Therefore, the geometric surface average of the equivalent surface area diameter, ${}_G\langle D_S\rangle_{32}$, can be calculated (Equation 4.4), i.e., 0.24 μm.

Specific surface area was measured by multiple-point BET (Autosorb 1, Quantachrome, USA) i.e. 11.5 m^2/g.

X-ray diffraction analysis (CN2005 Miniflex x-ray diffractometer, Rekagu) of the sample revealed it was α-alumina. Figure 4.4 is the x-ray diffraction pattern of the alumina powder.

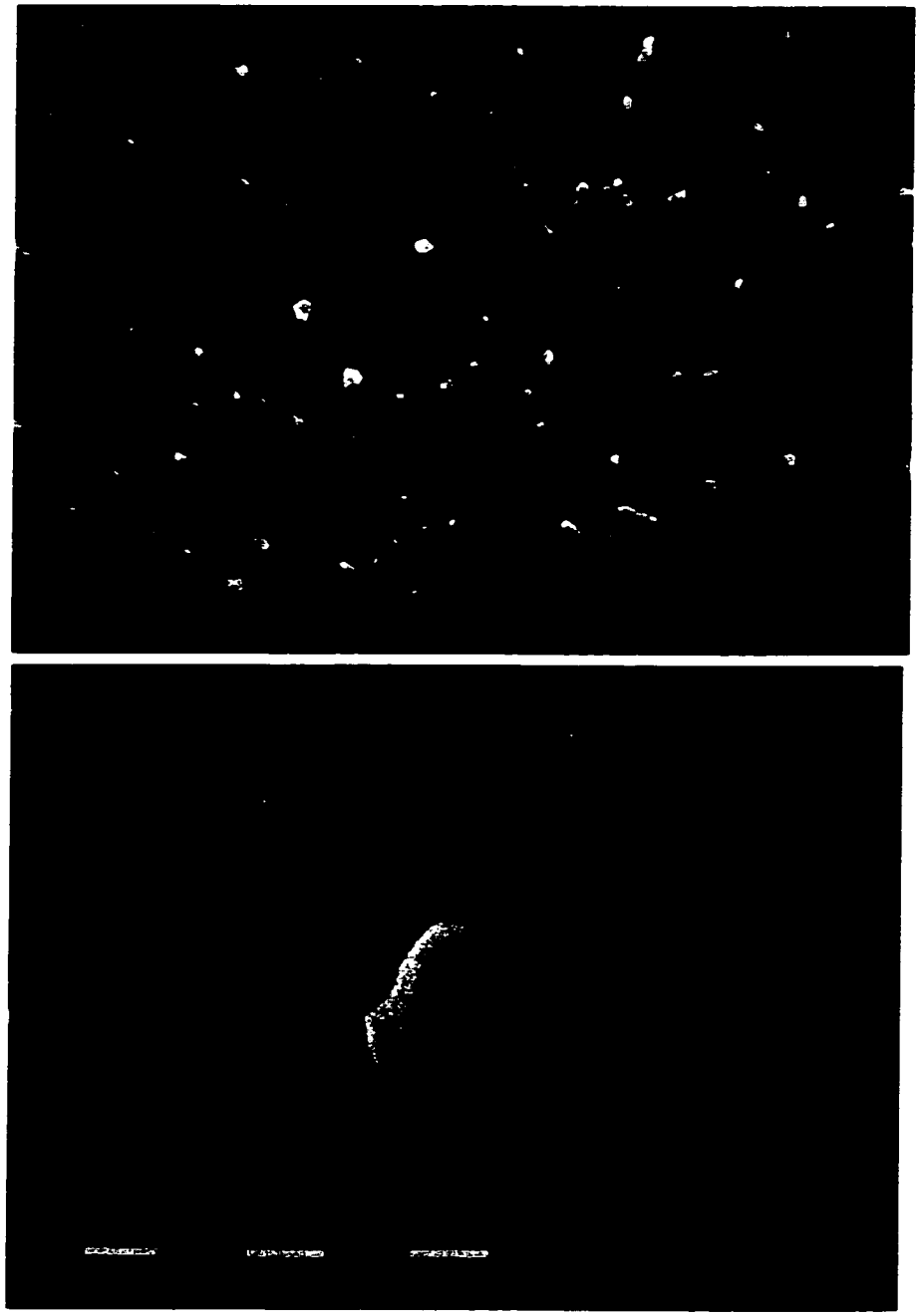

Figure 4.3 SEM micrographes of alumina powders

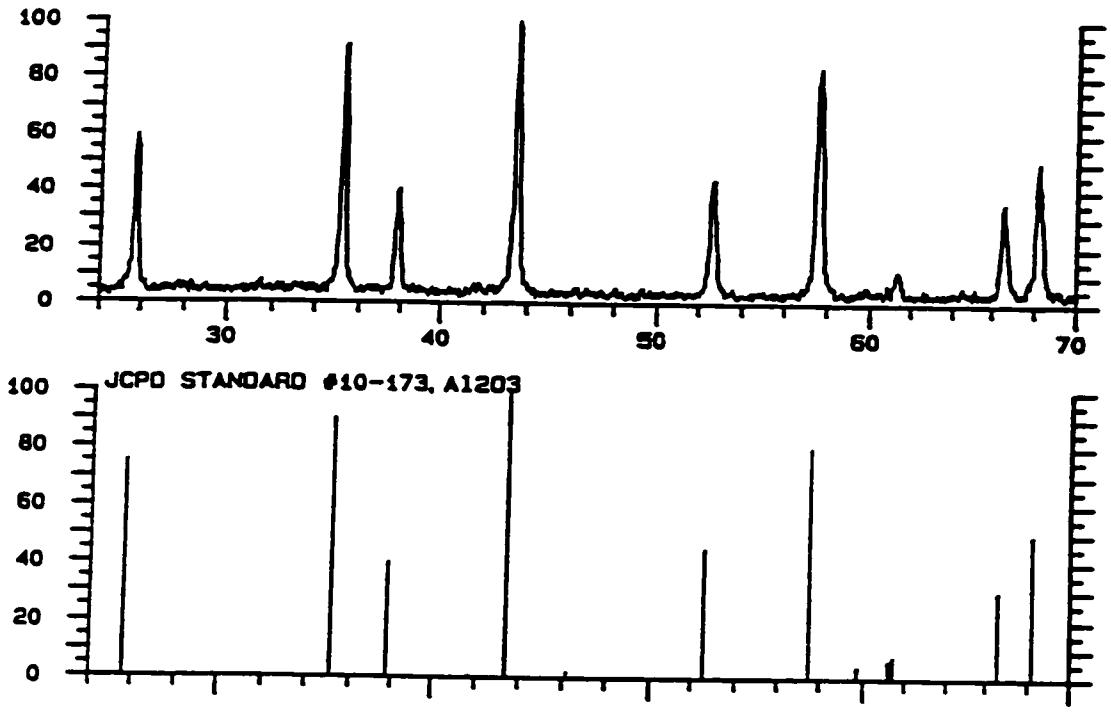

Figure 4.4 XRD pattern of alumina powders

All alumina powders were washed until the supernatant liquid electrical resistivity was equal to that of distilled, deionized water. These washed powders were then dried at a temperature of 100° C for 24 h. Fourier transform infrared spectroscopy (FTIR) (Bio-Rad Laboratories, Ltd.) spectra showed the surfaces of the alumina powders were partially hydrated (Figure 4.5). The additional weight loss of the powder on calcination at 400° C for 1 d was 0.38%.

IV-2.2 Silica

High purity (>99.9%) silica powder (PCR Inc., Florida, USA) was used in this study.

These silica particles are monodispersed and spherical, with diameter 0.5 μm via a CM12 (Philips) transmission electron microscope (TEM) (Figure 4.6).

The specific surface area is 6.19 m^2/g via multiple-point BET (Autosorb 1, Quantachrome, USA).

X-ray diffraction analysis (CN2005 Miniflex x-ray diffractometer, Rekagu) of the sample revealed that it was amorphous (Figure 4.7).

Dialysis was used to clean the silica of surfactants at the particle surfaces. Silica powders were placed in Spectra Por 4 cellulose dialysis membranes. The filled sacks were immersed in Milli-Q treated distilled water for 30 days. The dialysate was changed at regular intervals (once a day). After dialysis, powders were dried at 100° C for 24 h.

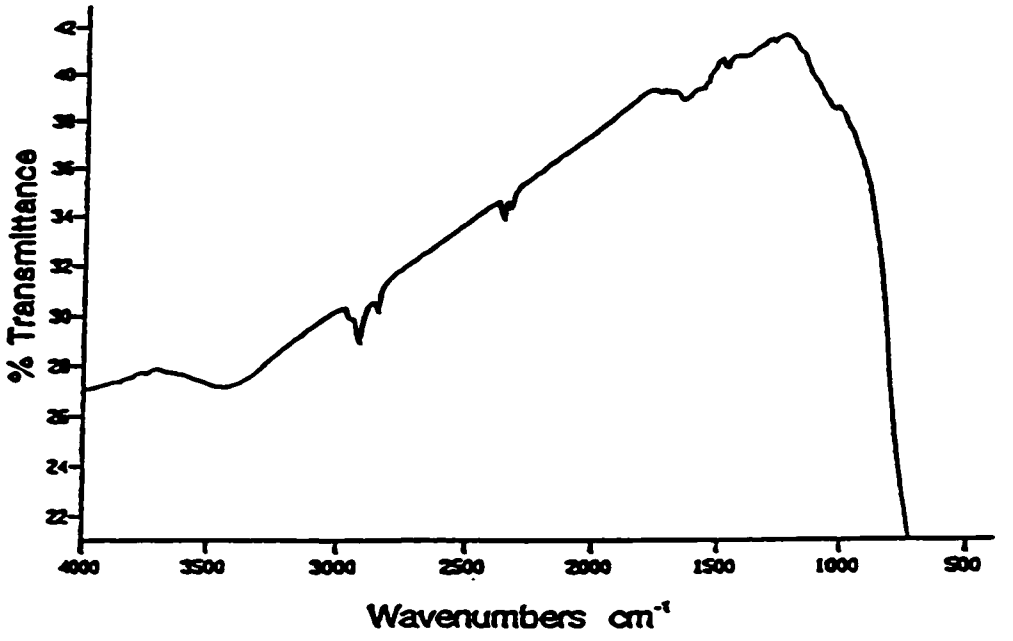

Figure 4.5 Transmittance FTIR spectra of alumina powders showing that the powders are partially hydrated by the broad peak in the 3000 – 3500 cm^{-1} region

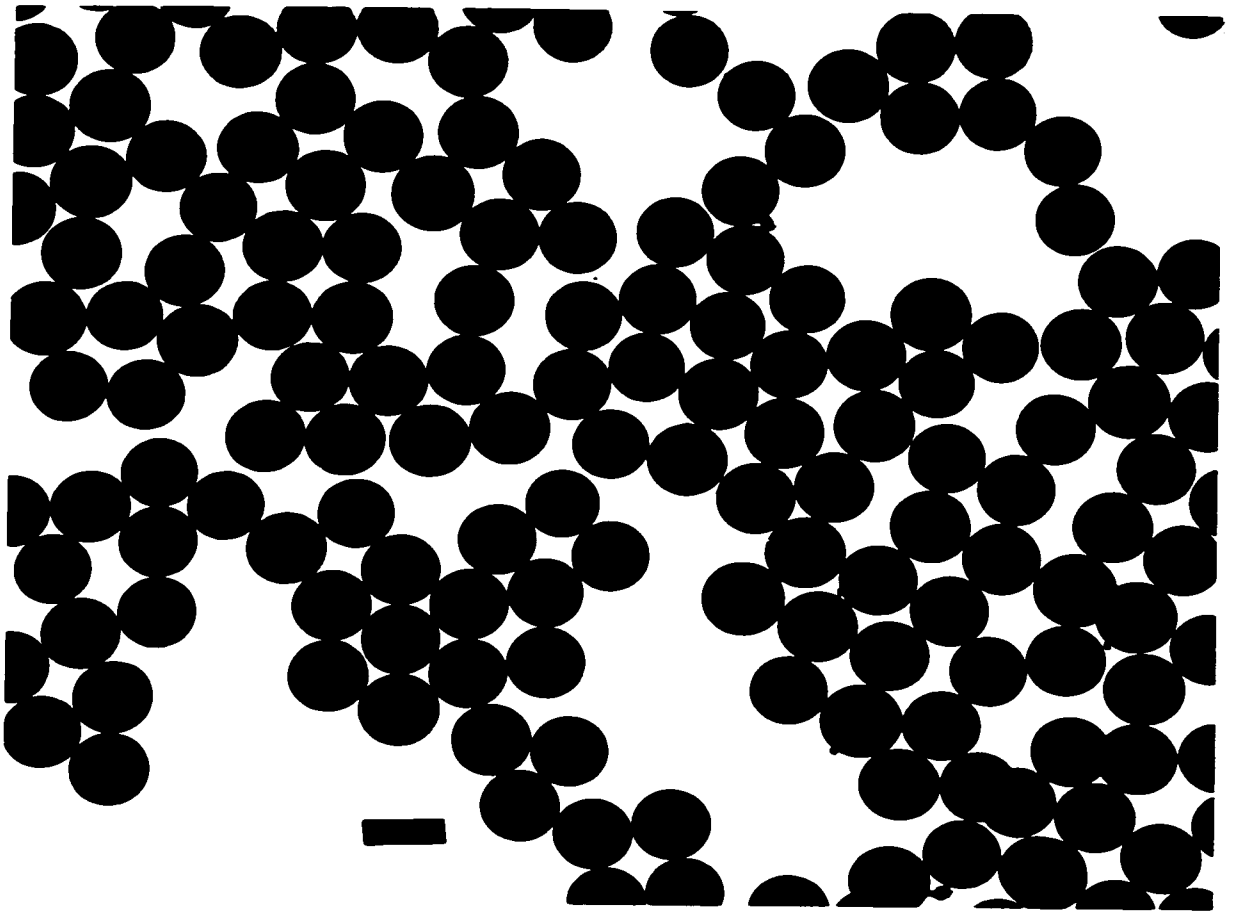

Figure 4.6 TEM micrograph of silica powders (Bar = 0.5 μm)

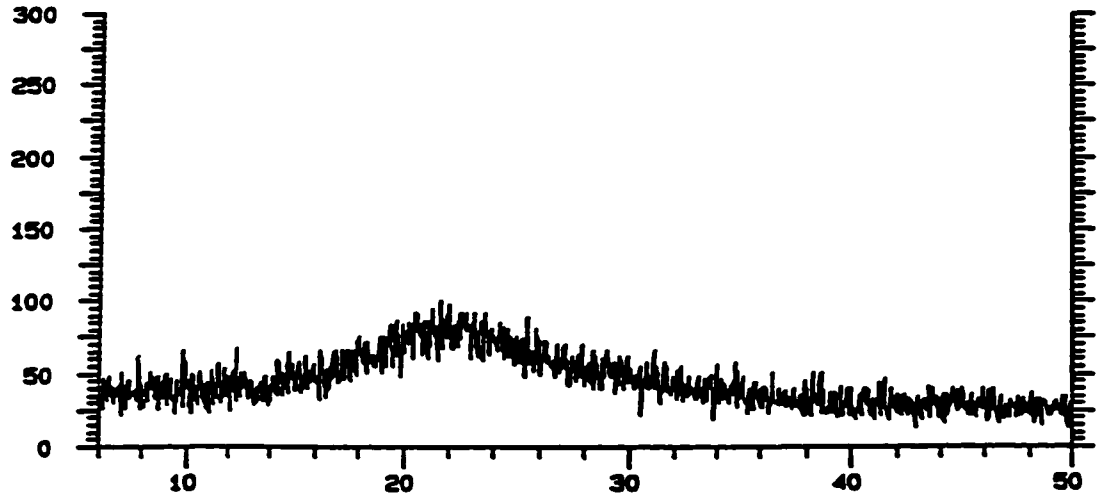

Figure 4.7 XRD pattern of silica powders

IV-2.3 Magnesia

The powder was magnesia from Cerac, Inc., USA (purity > 99.5%). This powder is porous with low density, i.e., 2.87 g/cm^3, measured by a multipicnometer (Quantachome, USA). The specific surface area is 85 m^2/g via multiple-point BET (Autosorb 1, Quantachrome, USA).

This powder was calcined at 1800°C for 1 hour then ground by vibromilling for 48 hours and dried at 100° C for 24 h.

The particle size frequency distribution of the calcined magnesia powder, (designated C-1), as determined by sedimentation, is plotted in Figure 4.8 (a) and the cumulative distribution in Figure 4.8 (b). The latter shows the powder has a log-normal size-distribution. The geometric mass average, ${}_G\langle D_{vel}\rangle_{43}$, and the geometric standard deviation, σ_G, were determined from Figure 4.8 (b) directly, i.e. 1.15 μm and 1.92. The geometric surface average of equivalent settling velocity diameter, ${}_G\langle D_{vel}\rangle_{32}$, was calculated (Equation 4.3), i.e., 0.78 μm.

SEM micrographs of the C-1 powder (Figure 4.9) give information on the particle shape. Values of shape factor were estimated, i.e., surface shape factor, α_s, 1.5, and volume shape factor, α_v, 0.1, respectively. Therefore, the geometric equivalent surface average of the surface equivalent diameter, ${}_G\langle D_s\rangle_{32}$, was calculated (Equation 4.4), i.e., 1.73 μm.

The specific surface area is 3.5 m^2/g via multiple-point BET.

The packing density of the powder after calcination is 3.47 g/cm^3.

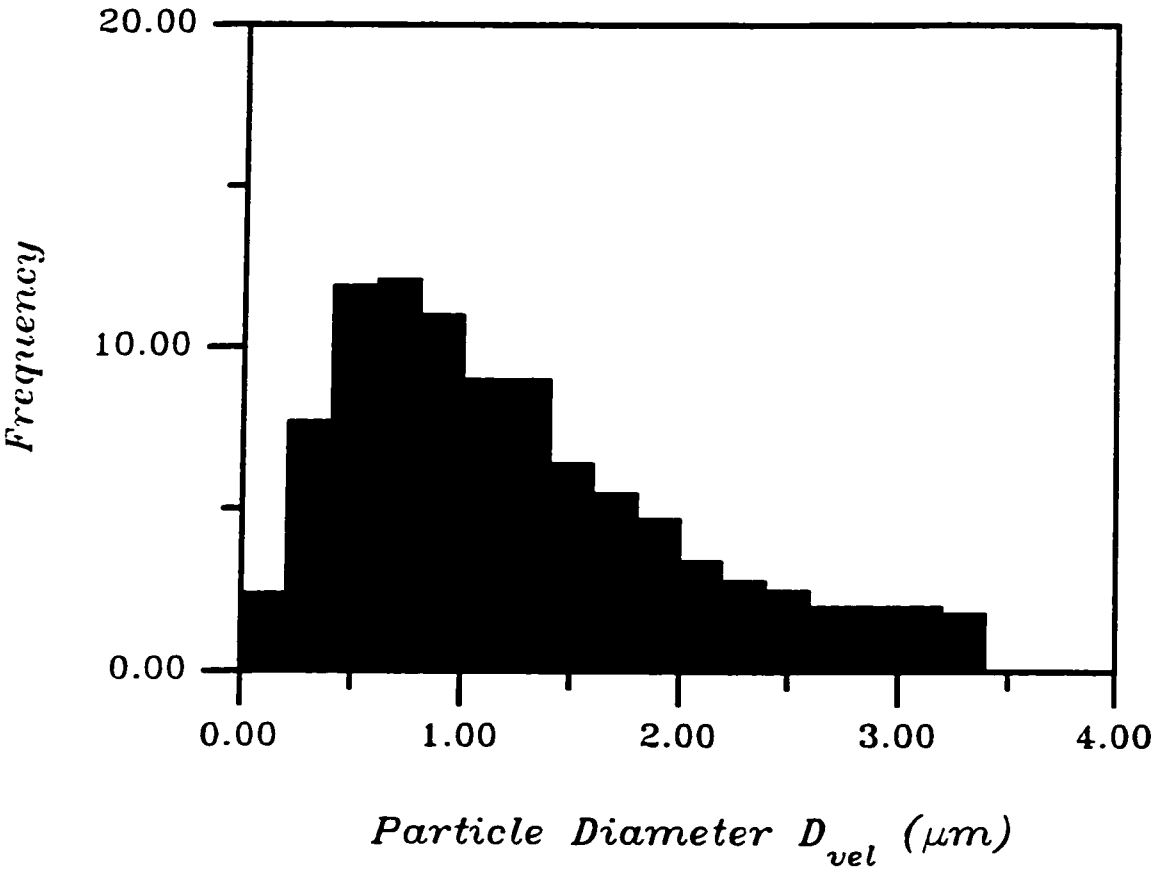

Figure 4.8 (a) Particle size frequency distribution of calcined magnesia powders (C-1)

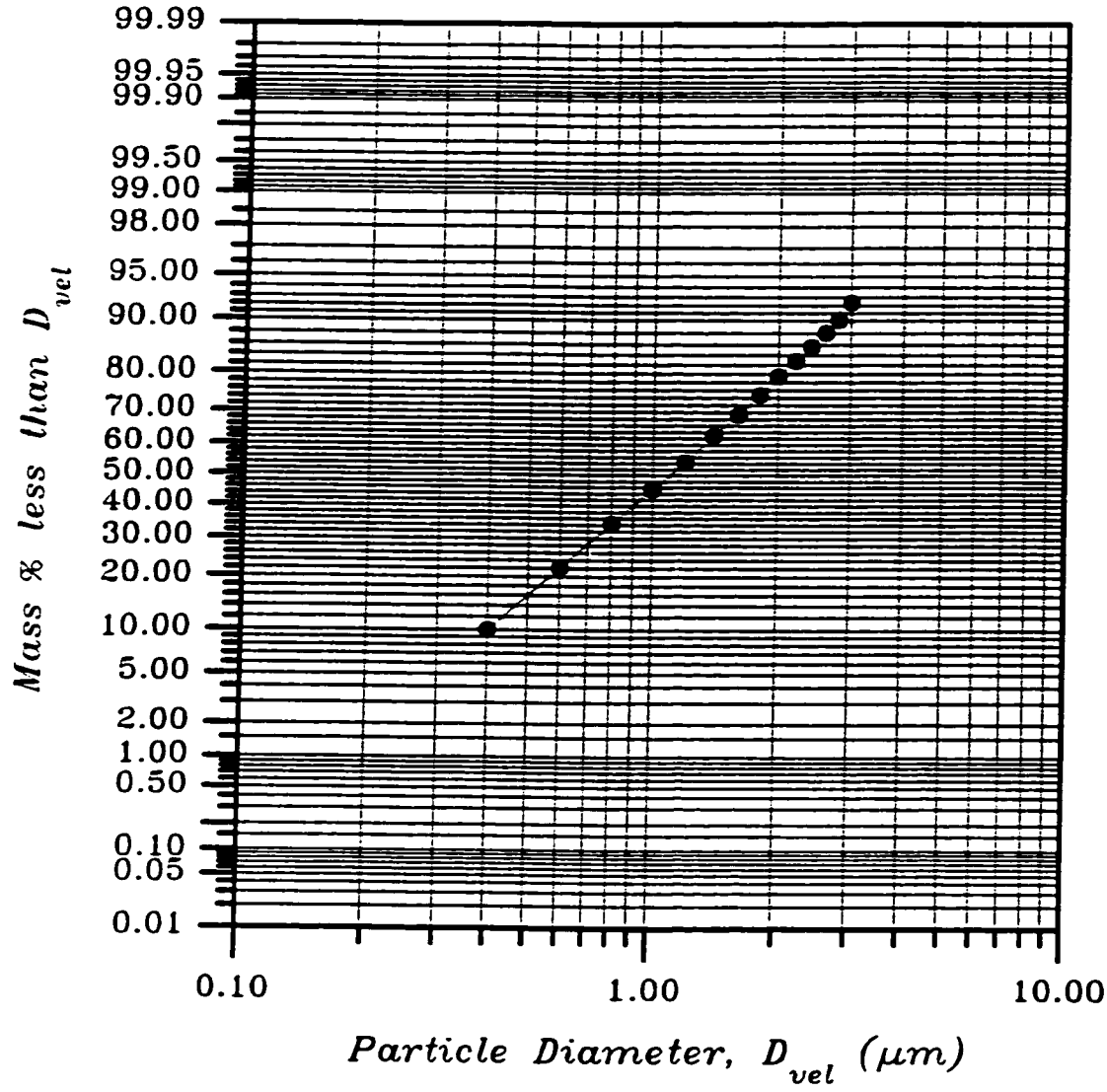

Figure 4.8 (b) Cumulative particle size distribution of calcined magnesia powders (C-1)

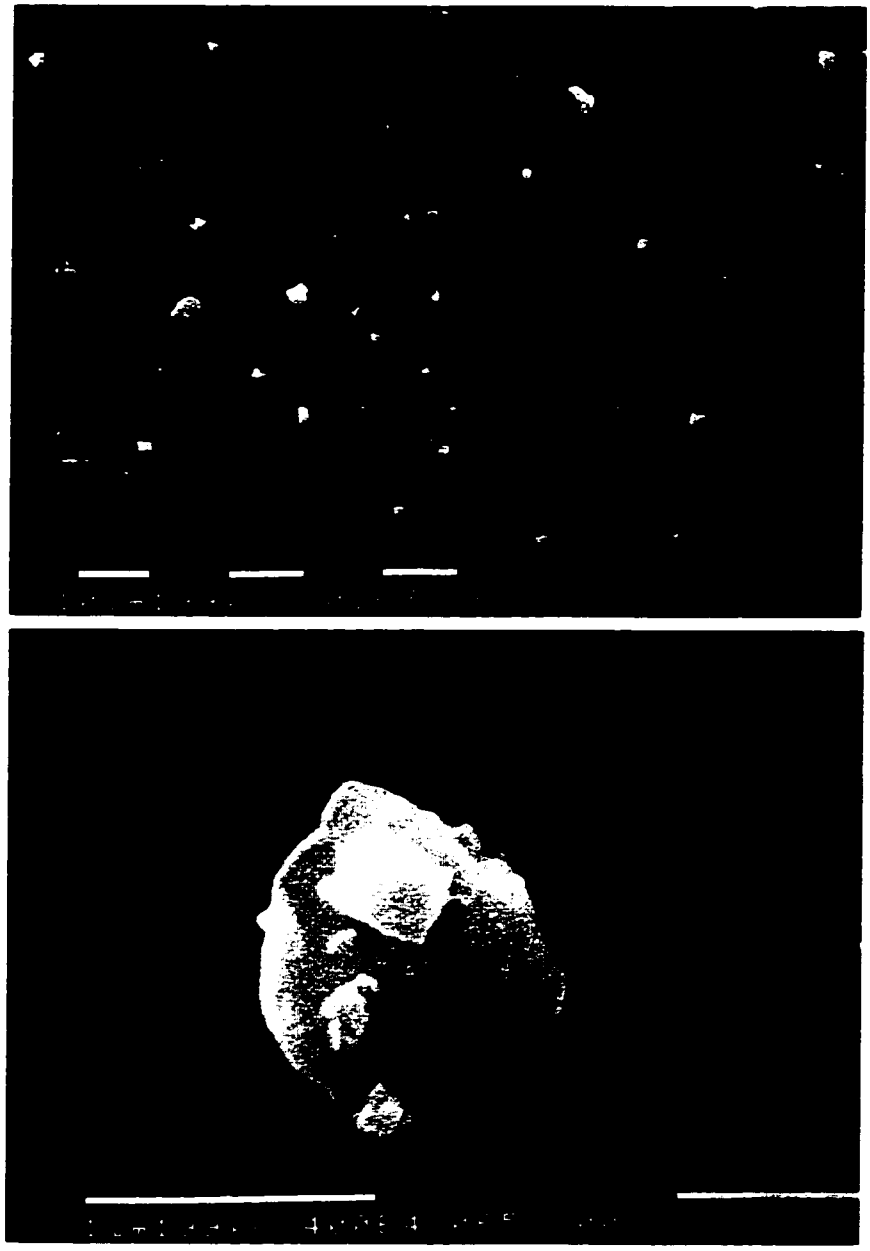

Figure 4.9 SEM micrograph of calcined magnesia powders (C-1)

Figure 4.10 is the x-ray diffraction pattern of the magnesia after calcination.

Some of the calcined magnesia powder (C-1) was separated into narrow size fractions by sedimentation. The particle size frequency distribution of the fine calcined magnesia powder, (designated C-2), determined by sedimentation is plotted in Figure 4.11 (a) and the cumulative distribution in Figure 4.11 (b). The size-distribution is log-normal. The geometric mass average, $_G\langle D_{vel}\rangle_{43}$, and the geometric standard deviation, σ_G, were determined directly from Figure 4.11 (b), i.e. 0.28 μm and 1.79. The geometric surface average of the equivalent settling velocity diameter, $_G\langle D_{vel}\rangle_{32}$, was calculated (Equation 4.3), i.e., 0.20 μm. The geometric equivalent surface average of the surface equivalent diameter, $_G\langle D_s\rangle_{32}$, was calculated (Equation 4.4), i.e., 0.45 μm. The specific surface area is 8.9 m^2/g via multiple-point BET.

The characteristics of three oxide powders are listed in Table 4.1.

Table 4.1 Characteristics of Oxide Powders

Oxide	Alumina	Silica	Magnesia	
			C-1	C-2
Crystal type	α-alumina	amorphous	magnesia	
$_G\langle D_s\rangle_{32}$ (μm)	0.24	0.5	1.73	0.45
Specific surface area (m^2/g)	11.5	6.19	3.5	8.9

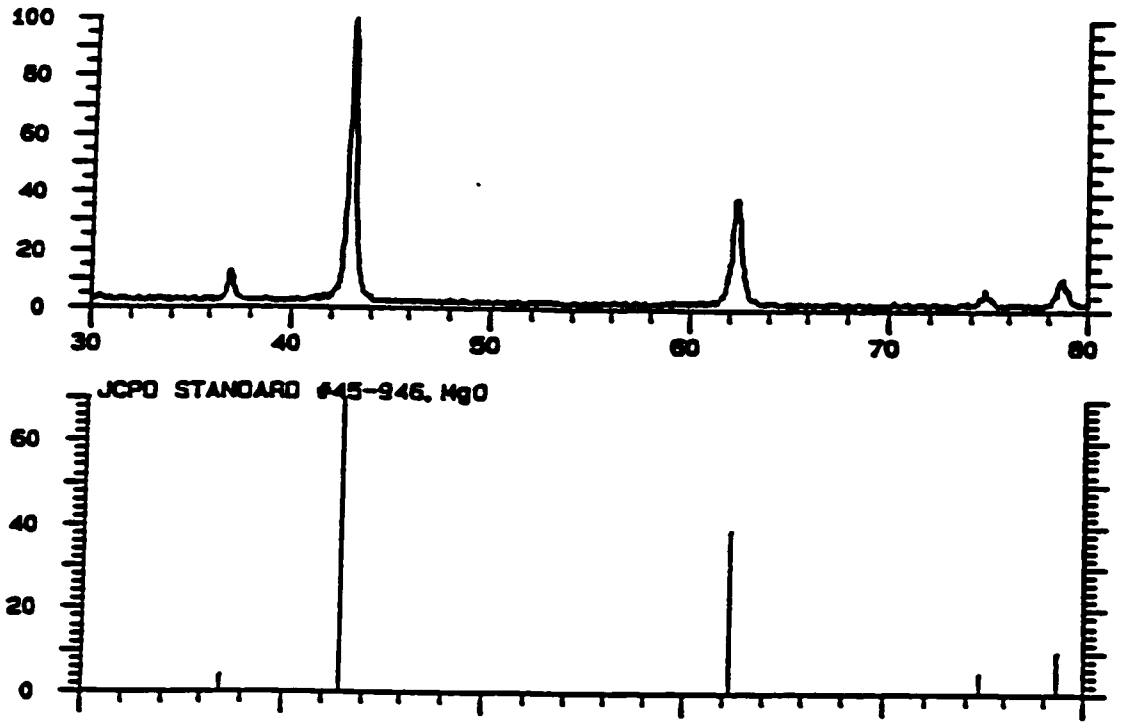

Figure 4.10 XRD pattern of calcined magnesia powders

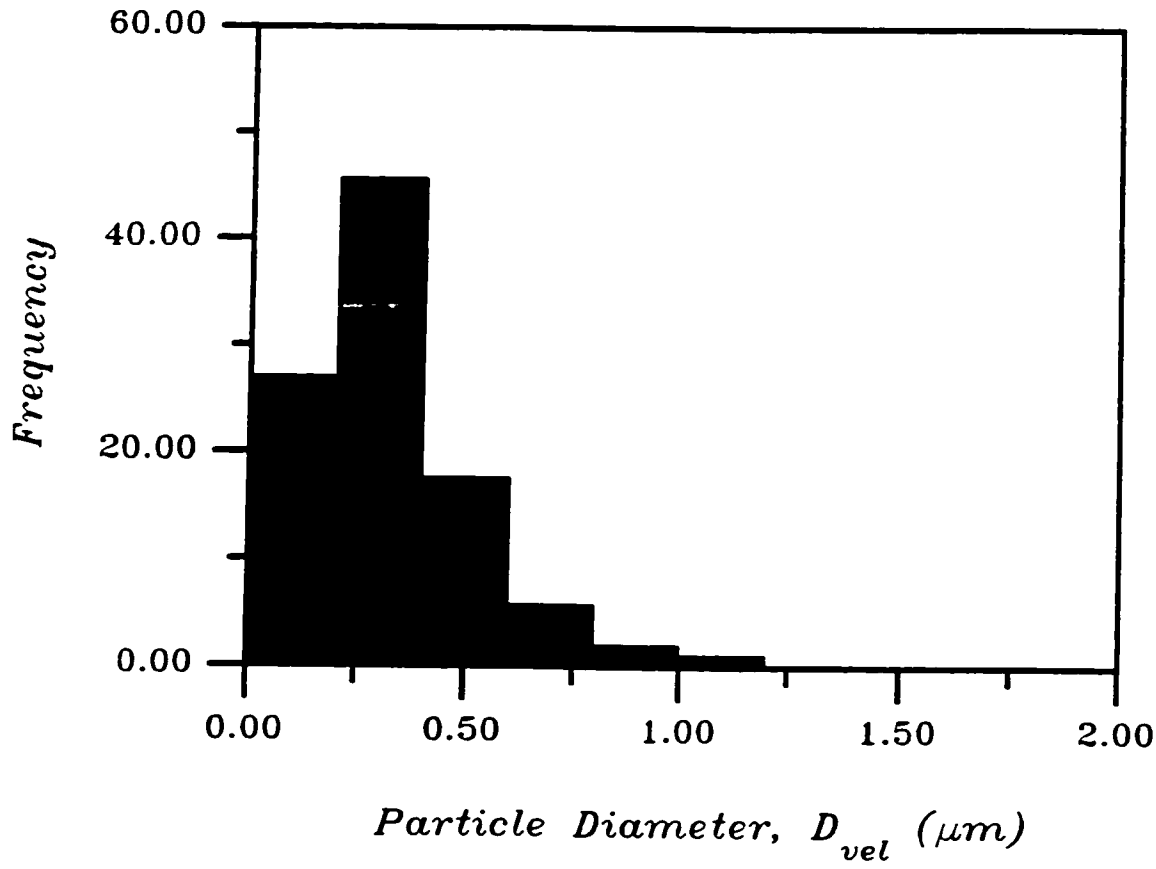

Figure 4.11 (a) Particle size frequency distribution of fine calcined magnesia powders (C-2)

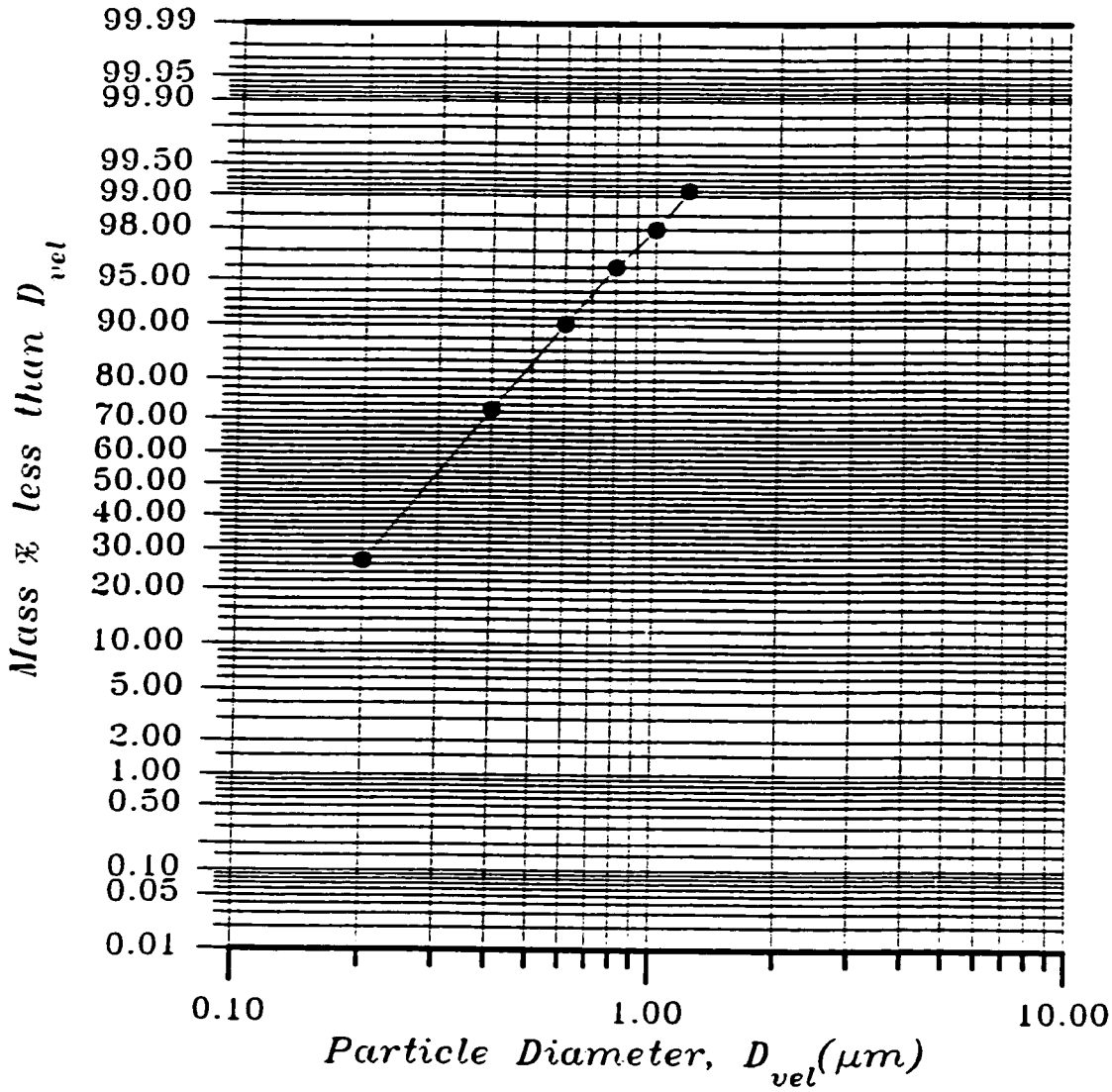

Figure 4.11 (b) cumulative particle size distribution of fine calcined magnesia powders (C-2)

IV-3 Solvent Characterization

Anhydrous, absolute ethyl alcohol (EtOH) (Commercial Alcohol Inc., Canada) and dimethyl sulphoxide (DMSO) (Caledon Laboratories Ltd., Canada) were used without further purification. Water-content measurement of the EtOH and DMSO by Karl Fisher titrations was performed by Galbraith Laboratories, Inc., Knoxville, TN. Analysis of the ethanol and dimethyl sulphoxide without further purification showed 0.20% and 0.72% water respectively.

The relevant physical and chemical properties of the solvents (Weast, 1990) are listed in Table 4.2.

Table 4.2 Relevant Properties of Solvents

Solvent	Viscosity at 25°C (mPa.s)	Dielectric Constant (ε_r)	Refractive Index (n)	Hamaker Constant (A_{33}) (10^{-20} J)
Ethanol (EtOH)	1.078	24.3	1.361	4.2*
Dimethyl Sulphoxide (DMSO)	2.24	45.0	1.476	

* Taken from Israelachvili (1985).

CHAPTER V

EXPERIMENTAL PROCEDURE

V-1 Electrokinetic Study

V-1.1 Electrophoretic Light Scattering

Dilute suspensions for electrophoresis (100 mg dm^{-3}) measurement were made by ultrasonically dispersing oxide particles in the media.

The acidity of solutions was adjusted by glacial acetic acid (HAc), hydrochloric acid (HCl) or tetramethyl ammonium hydroxide (TMAH) (25% in Methanol) and measured with a pH meter (Model Accumet 1002, Fisher Scientific Co., PA) employing glass and calomel electrode pairs connected by a concentrated aqueous KCl salt bridge. Due to the lack of standard buffer solutions in EtOH, two aqueous standards of pH values of 4 and 7 were used during standardization. Because of the slow response of pH electrodes in EtOH, it took 1/2 to 1 hour to obtain stable operational-pH readings. Typical examples of operational-pH readings vs. time are shown in Figure 5.1.

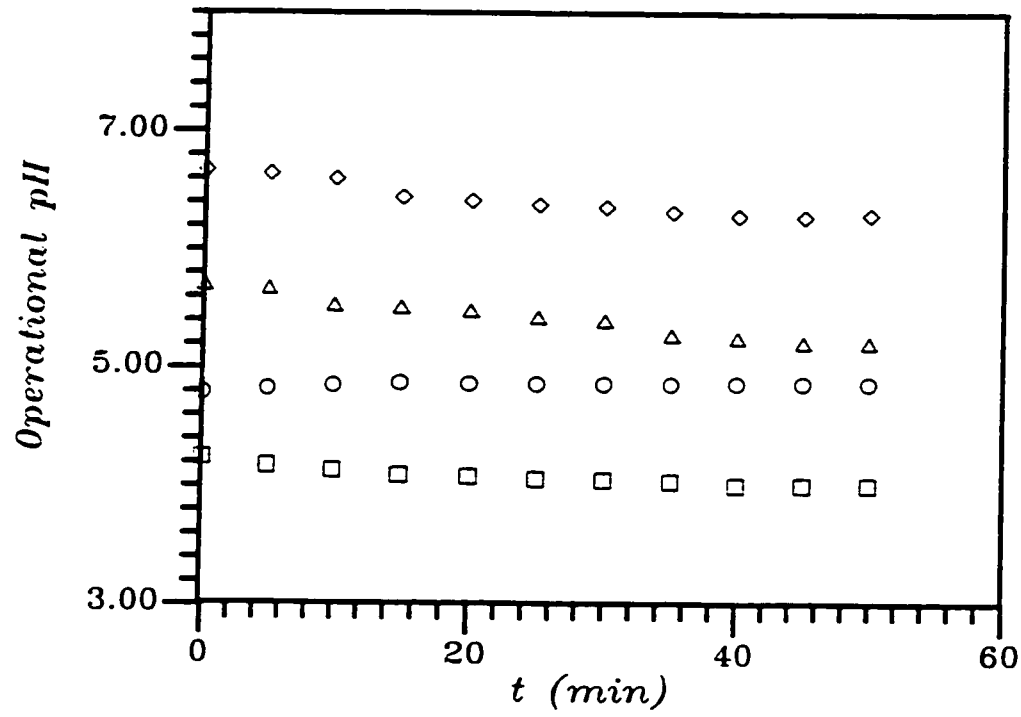

Figure 5.1 Measurement of operational pH as a function of time

Analytical-grade LiCl was used to adjust the ionic strength of the suspensions as desired.

Electrophoretic mobility measurements were made at 25.0 ± 0.3 °C (Model DELSA 440, Coulter Electronics, FL). The resolution of mobility spectra increases with increasing electric field, but increased resolution is "paid for" by increased noise on the spectra. Therefore field strengths of 4 to 6 kV m^{-1} were chosen as the standard electric field for all measurements. The mobility of an oxide particle in this range was independent of the field strength applied. The direction of the static electric field was alternated to prevent polarization. Field-off times were used to reduce heat generation. The run time was 30 s, with field-on and field-off times of 2.0 and 0.5 s, respectively.

The apparent mobility was measured as a function of position across the cell to reduce the measurement error of electrophoretic mobility due to electroosmosis. Particle mobilities were determined at seven positions across the cell and the stationary mobility values calculated by fitting the data to a linearized form of the Komagata equation. This procedure is based on that of Pelton (1993) for producing valid electrophoresis data from the same equipment. The true mobility of the particles was thus determined.

V-1.2 Electroacoustics

Experiments on moderately-concentrated suspensions were carried out at 25.0 ± 0.5°C using an electroacoustic analysis system (ESA 8000, Matec Applied Sciences, Hopkinton, MA). During the analysis, a high frequency (~1 MHz) electric field was applied to the suspension which generated a sound wave at the electrode surface. The pressure amplitude of this wave, termed the electrokinetic sonic amplitude (ESA), and the phase angle relative to a standard of known polarity, were measured.

Suspensions were prepared by ball-mixing the oxide powder in ethanol for 12 h to achieve homogeneous dispersion. Considering the long equilibration time for non-aqueous systems, the single point module was used for the ESA measurements. Five individual measurements were made at each operational pH, giving the average value and the standard deviation. A series of single point measurements were started at the 'natural' acidity (i.e., no preadjustment). The acidity was then adjusted by HAc or TMAH. Samples were aged for 12 hours before the operational pH and ESA measurements. Samples were stirred rapidly during ESA measurement, using an overhead propeller and a magnetic stirrer.

V-2 Stability Ratio Study

The stability ratio (W) of the oxide dispersions was determined by measuring the rate of constant of the initial stage of coagulation reaction between the oxide particles. Prepared samples with different operational pH were added to a quartz sample cell and the absorbance measurement commenced 10 s after cessation of the ultrasonic dispersion. The change of absorbance as a function of time was recorded with a UV/VIS spectrophotometer (Model 8452A UV/VIS diode array spectrophotometer, Hewlett Packard, CA).

Dilute suspensions for turbidity (250 mg dm^{-3}) measurement were made by ultrasonically dispersing the oxide particles in EtOH.

Timasheff (1966) has shown that turbidity or absorbance of a given coagulating dispersion may initially increase, remain constant, or decrease, depending on the wavelength of the incident light. In the present study (e.g., for alumina samples), the maximum rate of decrease of the turbidity of rapidly coagulating dispersions occurred at 450 nm. Therefore, the rate of decrease of turbidity at 450 nm was used as a measure of the rate of coagulation. Under these conditions according to Timasheff;

$$d\tau/dt = -k_s K N_o^2 \lambda^2 / (1 + k_s N_o t)^2 \quad (5.1)$$

where τ is the turbidity, t the time, K a proportionality constant, λ the wavelength of the incident light, N_0 the initial number of primary colloid particles, and k_s the initial

rate constant for actual slow coagulation. Equation 5.1 shows that, as $t \rightarrow 0$, $d\tau/dt$ becomes directly proportional to the rate constant k_s. Thus the relative rate of coagulation can be obtained from the initial slope of a plot of turbidity or absorbance as a function of time, as the plot should be linear in this region. The experimental stability ratio (W) of the suspension at a particular operational pH was calculated by dividing the maximum observed rate of change of absorbance for a given dispersion, by the observed rate at a particular operational pH (Wiese and Healy, 1975).

V-3 Rheology Study

All suspensions for rheological study were prepared by ball-mixing the oxide powder in the solvent for 12 h to achieve homogeneous dispersion. Rheological measurements were conducted at 25°C using a Bohlin controlled-shear-rate VOR rheometer (Bohlin Rheologie, Lund, Sweden). A concentric-cylinder measuring system (C25) was used with a moving cup of radius 27.5 mm and a fixed bob of radius 25.0 mm. A range of shear rate was applied to the sample. This was programmed to sweep from the lowest value in the range selected, upwards to the highest value, in steps (each step at a fixed shear rate); this order was then reversed. A 20 to 150 s shear was applied prior to the measurement at each shear rate; then, the viscosity and shear stress were measured over a twenty-second period.

V-4 Conductivity Measurements

Suspension conductivity was measured at 25°C using impedance spectroscopy (4192A LF Impedance Analyzer, Hewlett-Packard).

A sinusoidal voltage, $V(t) = V_o\exp(i.\omega.t)$, was applied to the sample-filled capacitor (consisting of two parallel platinum plates enclosed in a glass tube) and measurements were made from 10 Hz to 10 MHz.

The suspension can be modeled by the equivalent R-C circuit shown in Figure 5.2(a). The resistance, R_s, and capacitance, C_s, are those for the bulk suspension; R_e and C_e are the resistance and capacitance of the electrodes. Since the double layer thickness around the electrodes is small, their capacitance is orders of magnitude higher than the bulk suspension. Thus the characteristic time-constant (i.e. the product of the resistance and the capacitance, RC) of the electrode is high and therefore, the low frequency impedance response must correspond to the electrode and that at high frequency to the suspension.

Figure 5.2(b) is the complex impedance plot for a suspension. Z' is the real part of the impedance and Z" the imaginary part. Figure 5.2(b) shows the complete semi-circle of the high frequency region which corresponds to the response of the suspension. The intersection of the semicircle with the x-axis defines the resistance of the sample.

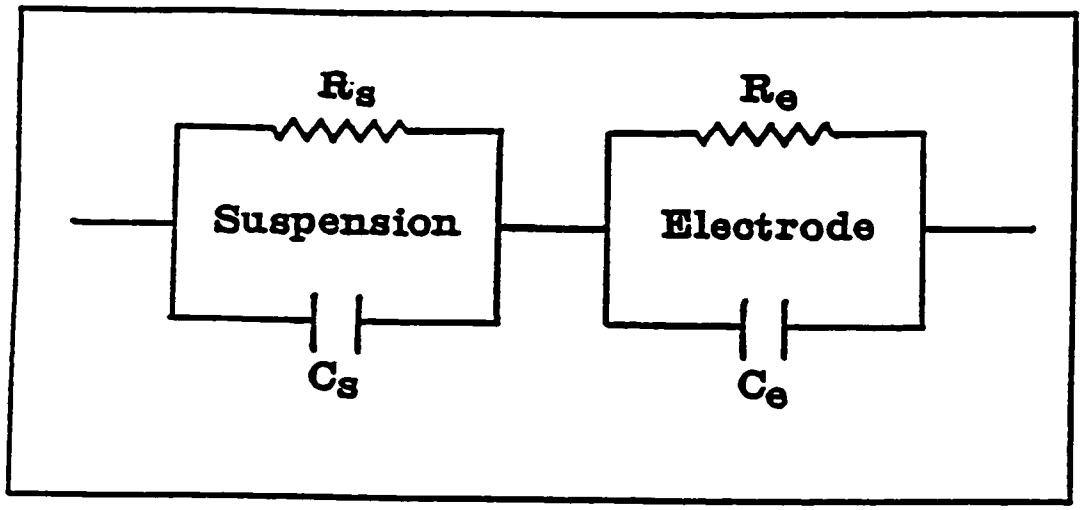

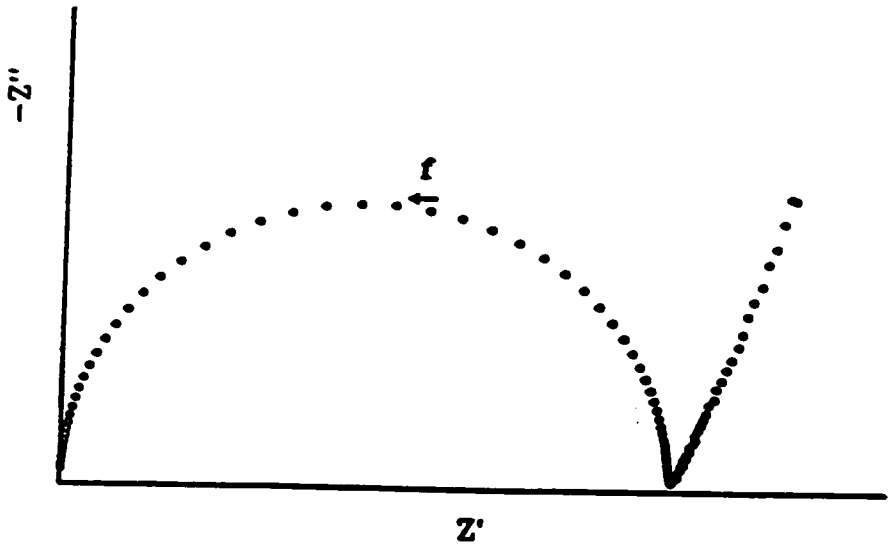

Figure 5.2 (a) Equivalent circuit and (b) corresponding complex plane impedance diagram for suspension conductivity measurement

A NIST traceable, conductivity-calibration standard with conductivity 101.4 μS/cm was used to determine the cell constant.

V-5 Heterocoagulation Processes

Heterocoagulates were prepared by mixing the constituent oxide dispersions. Unary oxide/EtOH suspensions of various operational pH were first made. The initial, volume-based concentration of particulates was 0.25 vol%. The unary suspensions of same operational pH values were then mixed to give 5, 10 vol% Al_2O_3 (or MgO) in SiO_2 (with respect to the total solids content). After rotating end-over-end (10 min^{-1}) for 30 min, samples of the mixture were subjected to electrophoretic mobility measurement and TEM observation.

CHAPTER VI

RESULTS AND DISCUSSION

VI-1 The Acidity-Stability Relationships for Oxide Powders in Ethanolic Suspensions

VI-1.1 The Influence of Acidity on the Surface Charge of Oxide Particles in Ethanol

Figure 6.1 plots electrophoretic mobility for SiO_2, Al_2O_3 and MgO, determined by electrophoretic light scattering, vs. operational pH and pa_H (referred to the aqueous standard state, according to Eq.2.61, with both δ and $\log {}_m\gamma_H$ taken from Popovych and Tomkins (1981)). The identified isoelectric points (IEP) of oxide particles in EtOH are listed in Table 6.1.

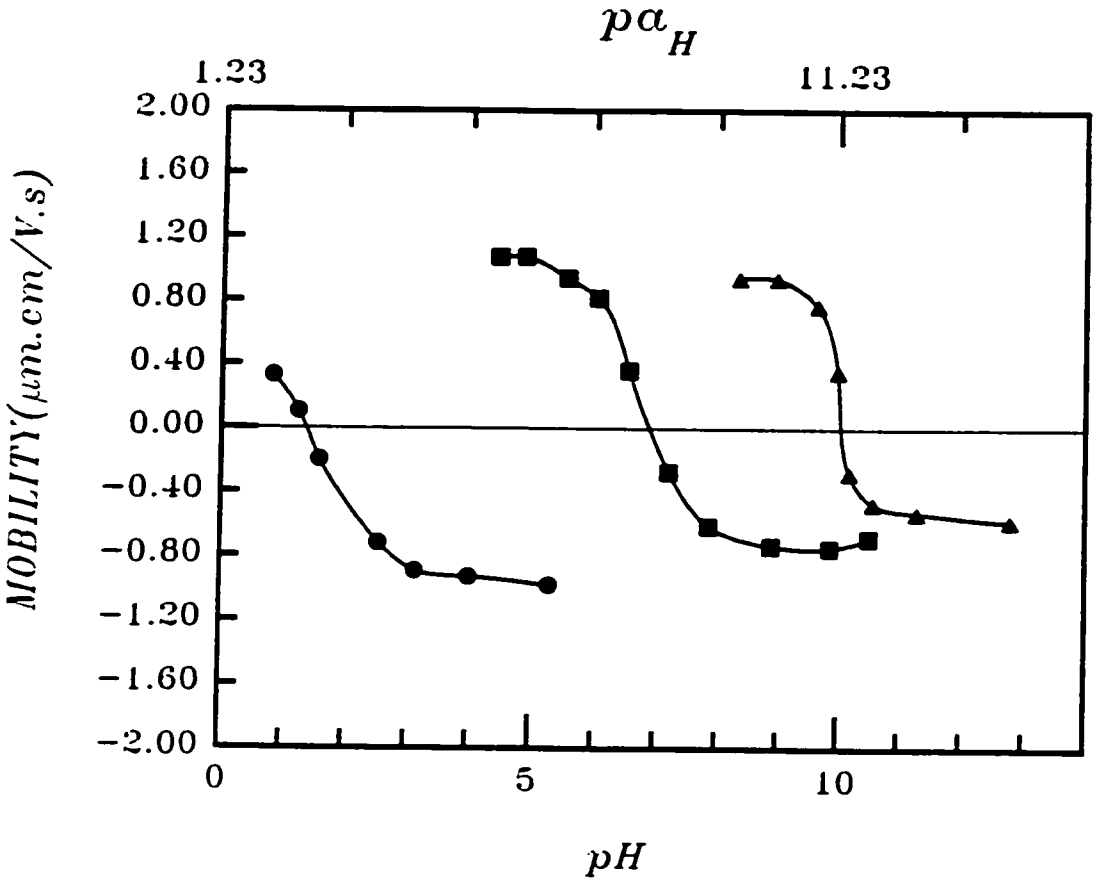

Figure 6.1 Electrophoretic mobility of oxide particles in EtOH as a function of operational pH and pa_H (●: silica; ■: alumina; ▲: magnesia (C-2))

Table 6.1 Isoelectric Point of Oxide Particles in Ethanol

Oxide	Operational pH	pa_H
Silica	1.43	2.66
Alumina	7.10	8.33
Magnesia	10.08	11.31

These results suggest there is an acidity-dependent surface charge on all three oxide particles suspended in EtOH. The charging mechanism of the surface could be:

$$MOH_2^+ \overset{H^+}{\longleftarrow} MOH \overset{OH^-}{\longrightarrow} MO^- + H_2O$$

These reactions describe the adsorption of protons or hydroxyls as potential-determining-ions onto the surface sites of the three oxide particles.

VI-1.2 Calculation of Zeta Potential

Acetic acid (hydrochloric acid or TMAH) was the only electrolyte species in the system without salt addition (assuming EtOH dissociation is negligibly small). Eq.2.65 and Eq.2.66 can thus be used to estimate the limiting equivalent conductivity (Λ_o). The Λ_o of acetic acid, hydrochloric acid and TMAH in EtOH solution was estimated as 325 $ohm^{-1}cm^2$ $equiv.^{-1}$, 354 $ohm^{-1}cm^2$ $equiv.^{-1}$ and 213

ohm^{-1} cm^2 $equiv.^{-1}$, respectively (Moelwyn-Hughes, 1957, Weast, 1990). The ionic concentration (n^o) is calculated from these via Eq.2.64. The calculated values of n^o, Debye parameter (κ), and Debye length ($1/\kappa$) at 25°C for EtOH solutions are listed in Table 6.2.

The values of Debye parameter (κ) shown in Table 6.2 prohibit use of the simple expressions of Smoluchowski and Huckel. Henry's theory is only valid for particles with low surface potential ($\zeta < 25$ mV) and it also fails to account for field distortion induced by movement of the particles, i.e.; the relaxation effect (Hunter, 1981). O'Brien and White (1978) developed a theoretical treatment for the electrophoresis of spherical particles. Their analysis is based on a numerical calculation procedure and is capable of providing reliable ζ values.

Zeta potentials were calculated via a computer program (WinMobil, Department of Mathematics, University of Melbourne, Australia), based on the expressions derived by O'Brien and White (1978). This procedure takes account of retardation and relaxation effects. These are significant in the presently studied systems; thus, the simple Henry expression is not applicable. Figure 6.2 is a plot of the calculated zeta potential for the three oxide particles dispersed in ethanol vs. operational pH and pa_H.

Table 6.2 Conductivity Data and Resulting Values of Ethanolic Solution

pH	Specific conductivity ($\times 10^6$ ohm^{-1}cm^{-1})	Ionic concentration number, n° ($\times 10^{-16}$ cm^{-3})	Concentration ($\times 10^5$ M)	κ $\times 10^{-7}$ (m^{-1})	Debye length (nm)
0.84	103	19	32	11	9.5
1.26	69.6	13	22	8.8	11
1.60	38.1	7.1	12	6.4	16
2.55	23.5	4.3	7.1	5.0	20
3.15	15.8	2.9	4.8	4.1	24
3.72	6.37	1.2	2.0	2.6	38
4.01	5.06	0.94	1.6	2.3	42
4.45	2.48	0.46	0.76	1.6	61
4.87	1.39	0.26	0.43	1.2	82
5.45	1.10	0.20	0.34	1.1	92
6.56	4.75	1.3	2.2	2.0	50
7.41	9.23	2.6	4.3	3.9	25
7.87	14.7	4.2	6.9	4.9	20
8.90	29.6	8.4	14	7.0	14
9.30	40.5	11.5	19	8.1	12
9.87	62.8	18	30	10	9.8
10.52	144	41	68	15	6.5

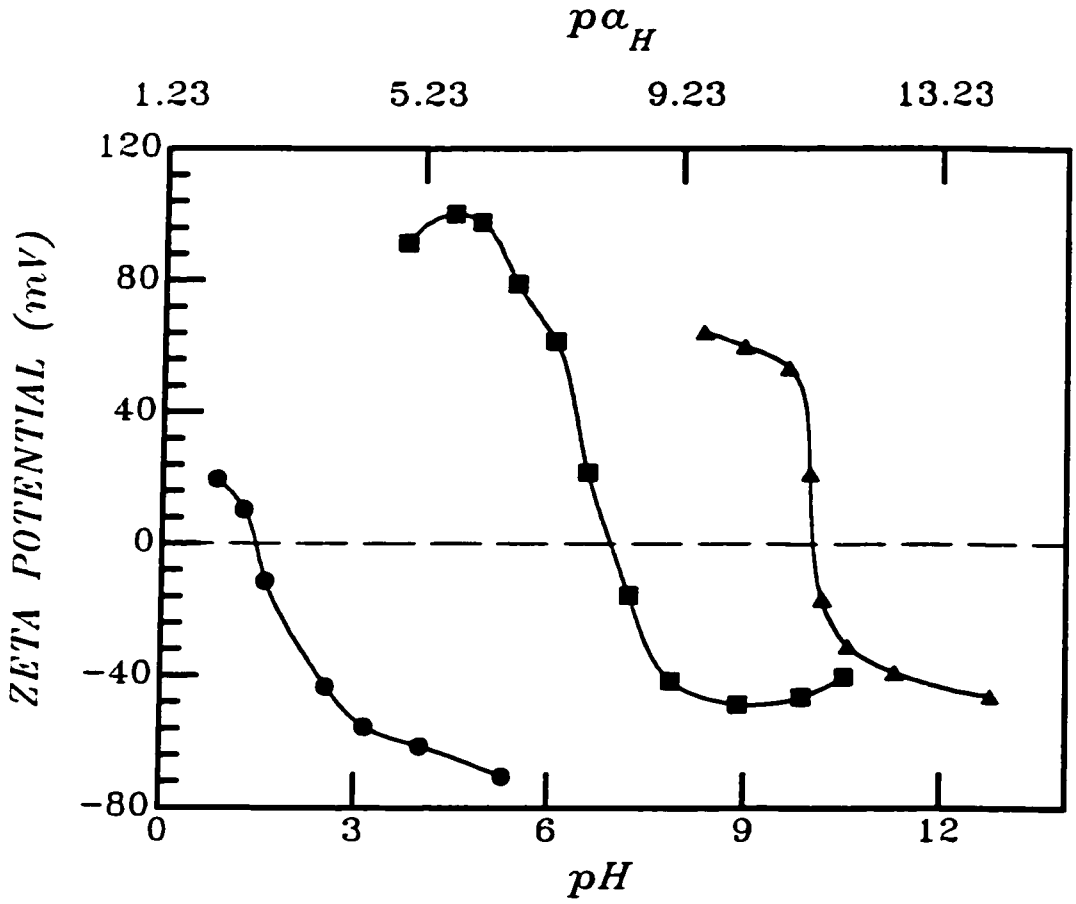

Figure 6.2 Zeta potential of oxide particles in EtOH as a function of operational pH and pa_H (●: silica; ■: alumina; ▲: magnesia (C-2))

VI-1.3 Calculation of Interparticle Interaction Energy and Force

DLVO theory was used to calculate the net interaction potential energies (Eqs. 2.40 and 2.44) and forces (Eqs. 2.42 and 2.45) for pairs of identical oxide particles. Previous estimates of κ (see Table 6.2) were used in Eqs.2.40 and 2.42. The interaction between charged particles is governed predominantly by the overlap of diffuse layers so the potential most relevant to the interaction is that at the boundary between the Stern and diffuse layers (the Stern potential, Ψ_δ, is generally assumed equal to the zeta potential), rather than the potential at the particle surface. So, zeta potential, ζ, versus acidity data (see Figure 6.2) were used to replace the surface potential, ψ_o, in Eqs.2.40 and 2.42. The Hamaker constants for the three oxide particles were taken from recently published data (Bergstrom, 1997) and listed in Table 6.3.

Plots of total interaction energies, V_T, and forces, F_T, vs particle separation, H, for (oxide-EtOH) + (HAc or TMAH) suspensions are shown in Figure 6.3 to 6.6. The maximum repulsive force, F_T(max), corresponds to the steepest part of the energy curve. The 'effective' surface area for repulsion, A(eff.) = $\pi a/\kappa$ as defined by Van der Hoeven and Lyklema (1992), allows calculation of the maximum repulsive pressure, P_T(max), between two identical oxide particles. The repulsive energy barrier, maximum repulsive force and pressure for the three oxide particles at various operational pH values are

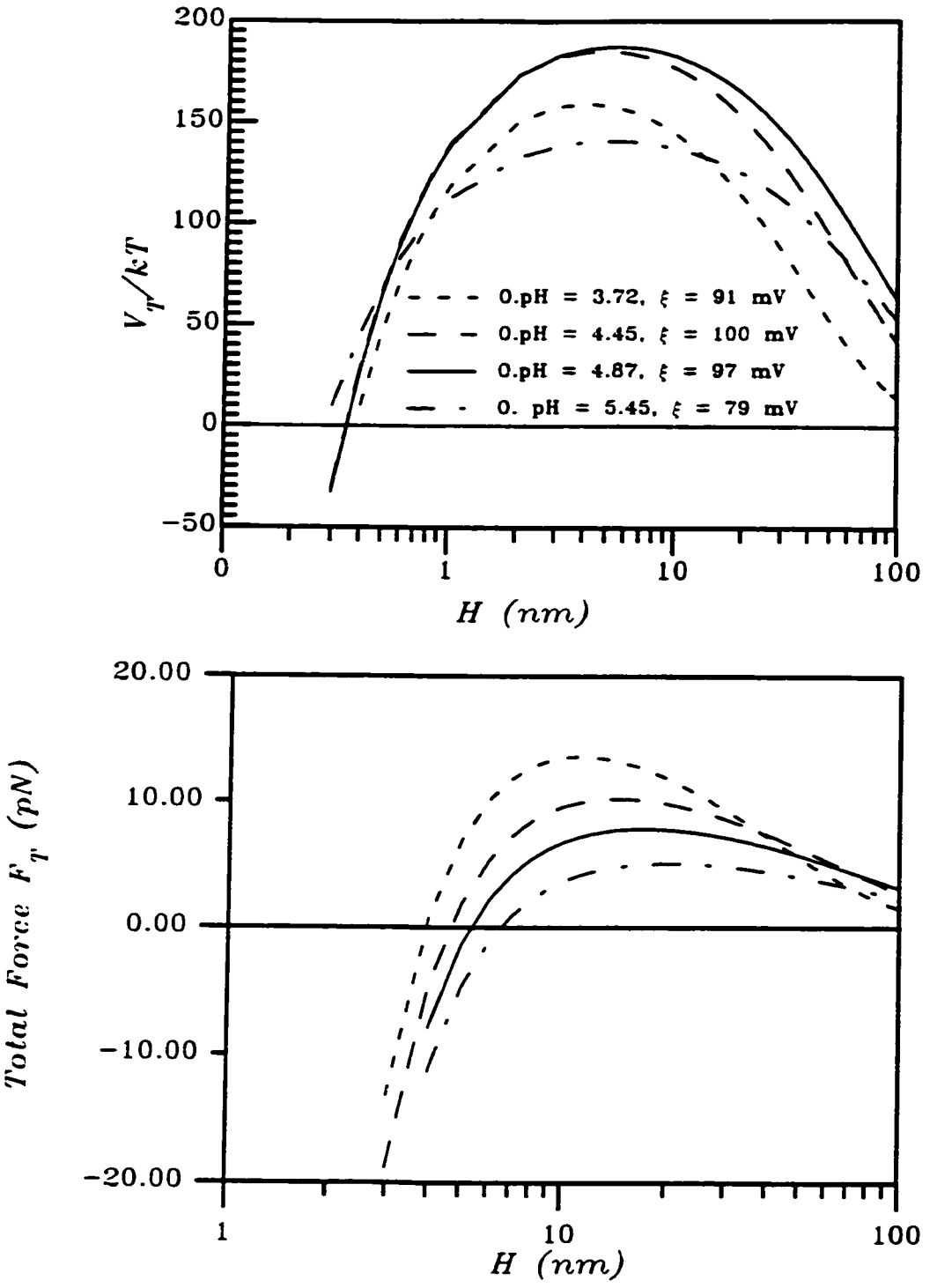

Figure 6.3 Total interaction energies (a) and forces (b) as a function of particle separation between two positively charged alumina particles for various O. pH (operational pH) and ζ values

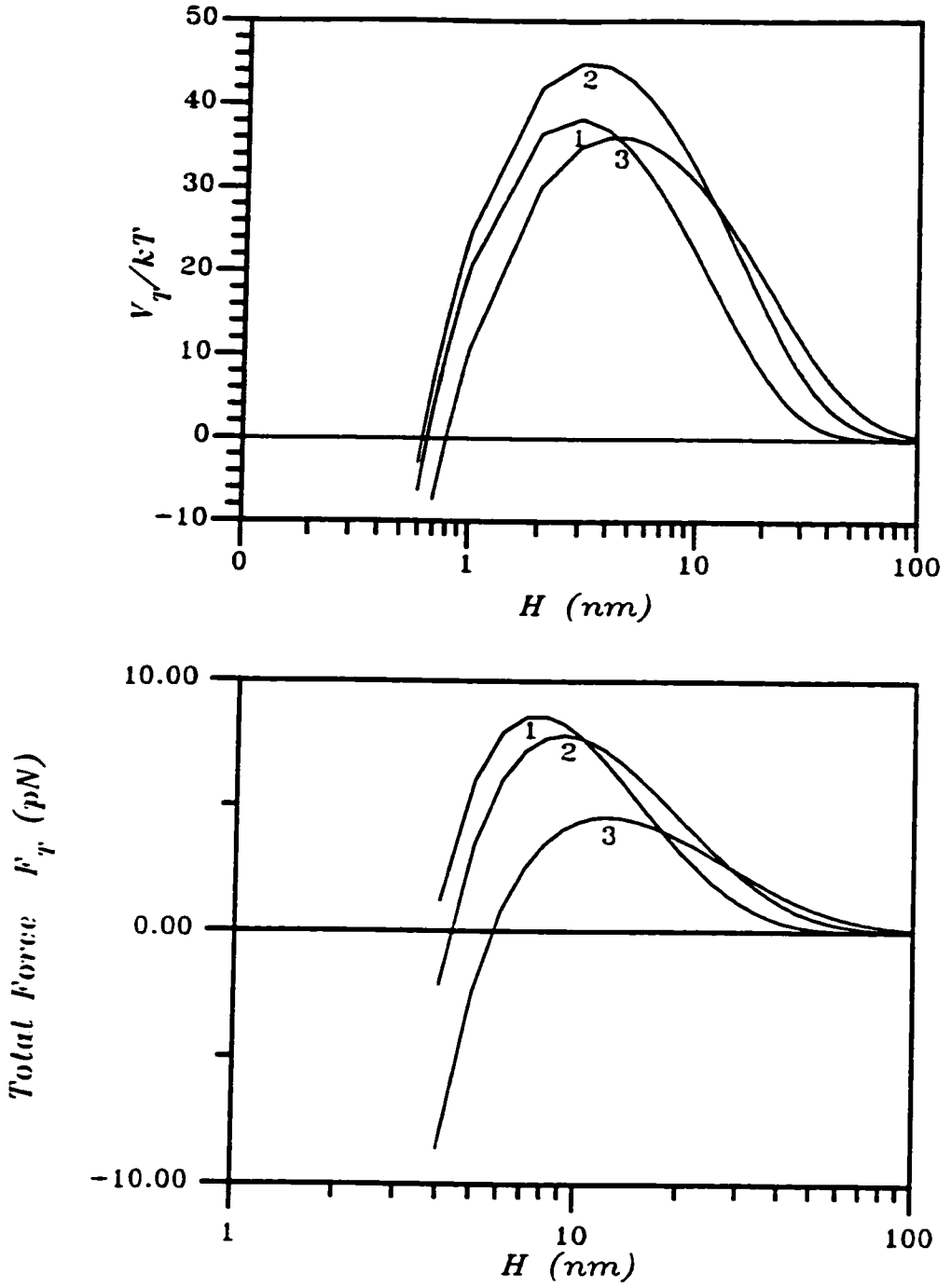

Figure 6.4 Total interaction energies (a) and forces (b) as a function of particle separation between two negatively charged alumina particles for various O. pH (operational pH) and ζ values (line 1: O. pH = 9.87, ζ = - 47 mV; line 2: O. pH = 8.90, ζ = - 49 mV; line 3: O. pH = 7.87, ζ = - 42 mV)

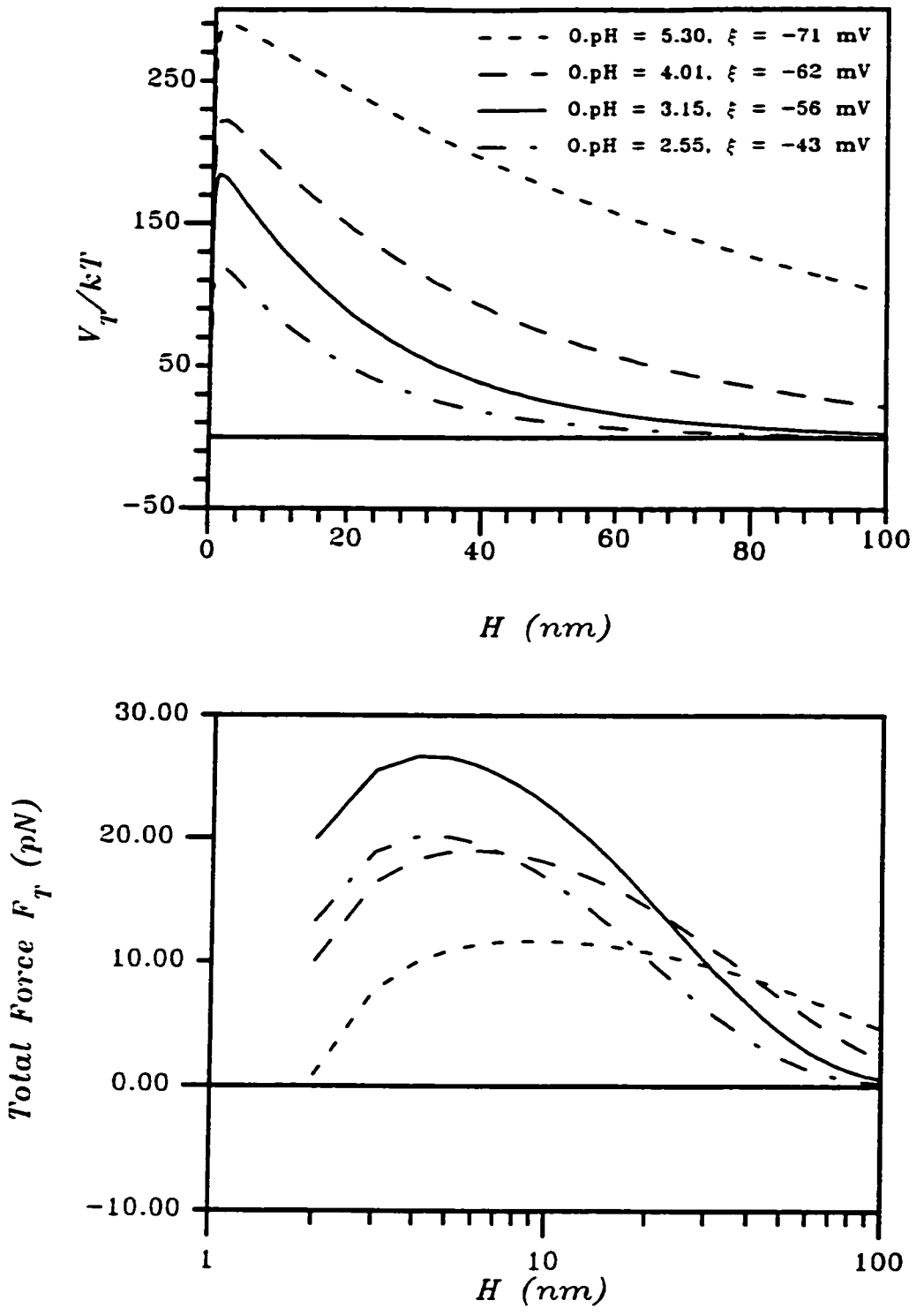

Figure 6.5 Total interaction energies (a) and forces (b) as a function of particle separation between two spherical silica particles for various O. pH (operational pH) and ζ values

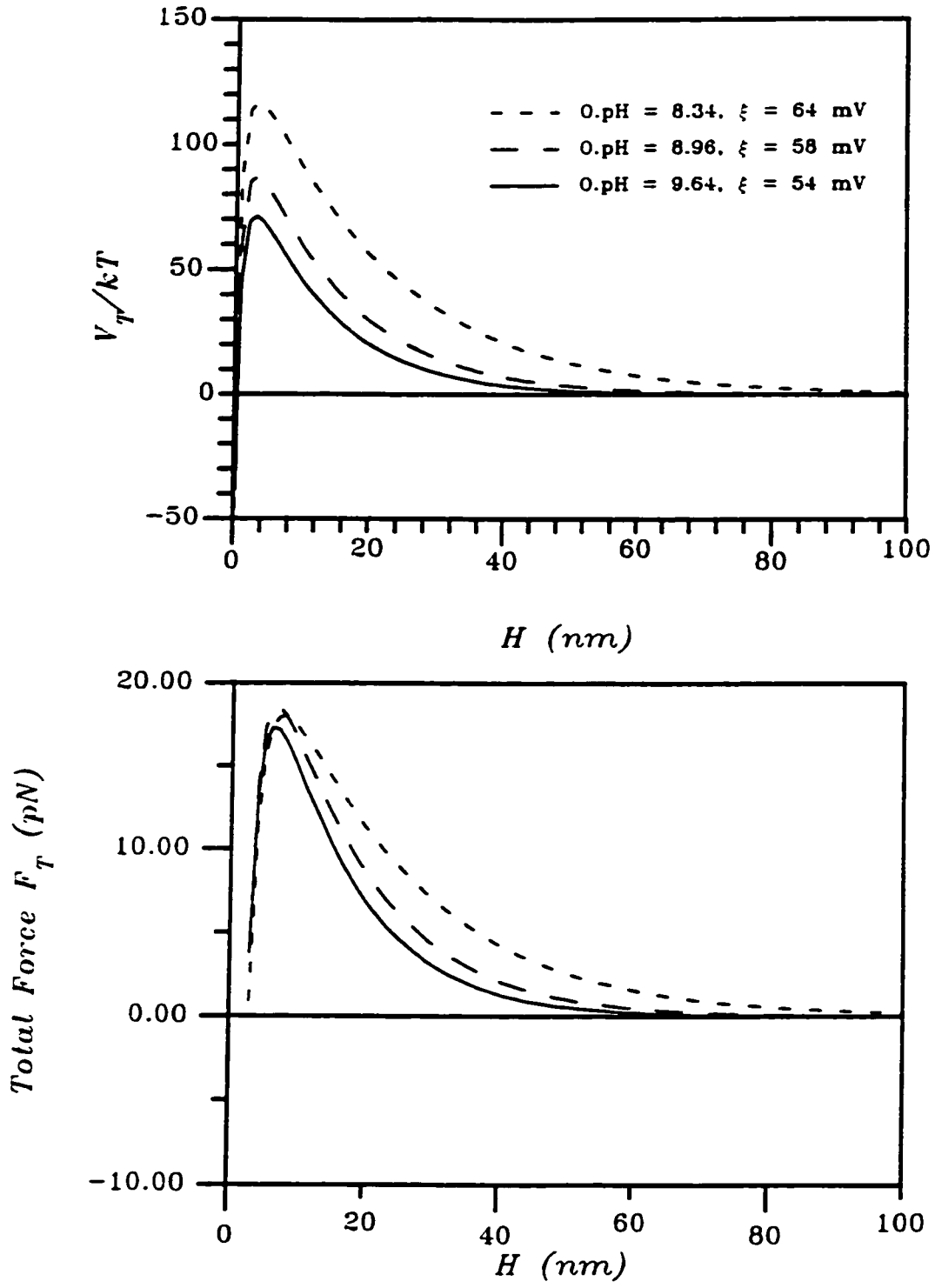

Figure 6.6 Total interaction energies (a) and forces (b) as a function of particle separation between two magnesia (C-2) particles for various O. pH (operational pH) and ζ values

summarized in Table 6.4. These are determined by combination of the data from Figure 6.3 to 6.6 and Table 6.2.

Table 6.3 Nonretarded, Effective Hamaker Constants for the Oxide Particles Interacting across Air and Ethanol at Room Temperature (298 K)

Oxide	Hamaker constant (10^{-20} J)	
	Medium	
	Vacuum[1] (A_{11})	Ethanol[2] (A_{131})
α-Al_2O_3	15.2	3.37
MgO	12.1	2.00
SiO_2 (amorphous)	6.50	0.24

1. From Bergstrom (1997).
2. The values calculated using Eq.2.48. The Hamaker constant of ethanol A_{33}=4.2 x 10^{-20} J taken from Israelachvili (1985).

The value of the minimum repulsive energy necessary to stabilize a suspension is 15 kT (Verwey and Overbeek, 1948). The plots indicate considerable repulsive barriers develop in the suspensions studied. However, a high repulsive potential is not sufficient for ionic stabilization in media of low dielectric constant. In addition, a sufficiently high repulsive force (pressure) must exist (Albers and Overbeek, 1959). Table 6.4 demonstrates that, for oxide particles dispersed in EtOH, this condition can be met by controlling the acidity

Table 6.4 Total DLVO Interaction Energy, Force and Pressure for Two Oxide Particles at Different Operational pH Values in EtOH

Oxide	Operational pH	V_T (max) (kT)	F_T(max) (pN)	A(eff.) ($x10^{15}$ m^2)	P_T(max) (kN/m^2)
SiO_2	5.30	289.9	11.7	72.2	0.16
	4.01	222.5	19.0	33.0	0.58
	3.15	184.5	26.7	18.8	1.4
	2.55	119.0	20.1	15.7	1.3
Al_2O_3	3.72	159.3	13.6	13.1	1.0
	4.45	185.1	10.2	21.1	0.48
	4.87	187.4	7.8	28.3	0.28
	5.45	140.9	5.1	31.8	0.16
	7.87	36.1	4.6	6.9	0.66
	8.90	45.0	7.8	4.8	1.6
	9.87	38.3	8.6	3.4	2.5
MgO (C-2)	8.34	116.8	18.0	9.4	1.9
	8.96	87.2	18.5	6.6	2.8
	9.64	71.4	17.3	5.7	3.1

of the suspensions. Addition of acid or base induces (i) a surface charge, (ii) to increase the ionic strength of the continuous phase. Regarding the three conditions for ionic stabilization, i.e., (i) a high surface potential (ii) particular levels of ionic strength and (iii) low van der Waals attraction, two are fulfilled by addition of a simple acid or base.

The total interaction-potential-energy remains repulsive up to 100 nm and no secondary minimum is observed due to slow decay of the interaction energy with distance. The repulsive energy barrier developed in the SiO_2-EtOH suspensions is higher than for the other oxide-EtOH systems, owing to the weaker van der Waals attraction.

Table 6.4 shows that, at certain operational pH values, low ionic strength results in low repulsive force (pressure), eventhough the zeta potential is high. At a given zeta potential, the repulsive force, i.e., the slope of the potential curves, increases with increasing ionic strength. The latter increase can also be achieved by salt addition thus salt (LiCl) was introduced into the (Al_2O_3-EtOH) + (HAc or TMAH) suspensions to increase the ionic strength and the repulsive force, whilst maintaining ζ high enough to stabilize the colloids.

VI-1.4 The Acidity-Stability Relationships for Alumina in Ethanolic Suspensions with Salt (LiCl) Addition

Figures 6.7 show the effect of salt (LiCl) addition on the electrophoretic mobility, (determined by electrophoretic light scattering), of alumina particles in EtOH as a function of operational pH and pa_H. The isoelectric point (IEP) is independent of LiCl concentration, suggesting that LiCl is an indifferent-electrolyte in this system.

The conductivities of the suspensions were measured, and the ionic concentration calculated thereafter. Tables 6.5 and 6.6 give the calculated values of ionic concentration (n^o), Debye parameter (κ) and Debye length ($1/\kappa$) for the suspensions.

Zeta potentials were then calculated and the results are shown in Figure 6.8. The values of electrophoretic mobility and zeta potential decrease in the presence of LiCl because of compression of the double layer (previously suggested by de Rooy et al. (1980)).

Figures 6.9 to 6.12 are plots of total interaction energies, V_T, and forces, F_T, vs H (particle separation), using DLVO theory for suspensions with $5x10^{-5}$ M and 10^{-3} M LiCl addition at various operational pH values. Note the shallow secondary minimum in Figure 6.12 as a consequence of the high ionic strength. The depth of the energy of this secondary minimum is –0.2 kT and is at distance of ca 35 nm.

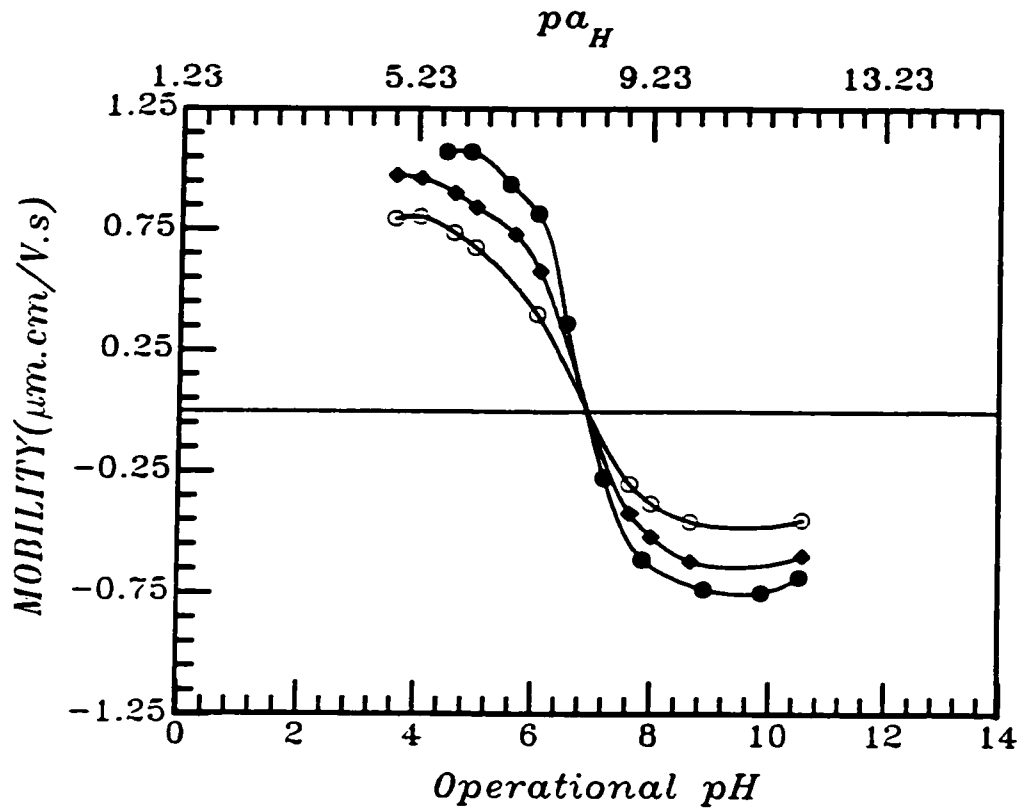

Figure 6.7 The effect of LiCl addition on electrophoretic mobility of alumina particles in EtOH as a function of operational pH and pa_H ((●) EtOH, (◆) EtOH (5×10^{-5} M LiCl) and (○) EtOH (10^{-3} M LiCl))

Table 6.5 Conductivity Data and Resulting Values with the Addition of 5×10^{-5} M LiCl

Operational pH	Specific conductivity ($x10^6\ \Omega^{-1}.cm^{-1}$)	Debye parameter κ, ($x10^{-7}\ m^{-1}$)	Debye length $1/\kappa$, (nm)	κa
3.60	8.21	6.52	15.3	7.2
4.02	7.16	6.03	16.6	6.6
4.60	6.35	5.64	17.7	6.2
4.97	5.58	5.46	18.3	6.0
5.65	5.26	5.28	18.9	5.8
6.05	4.03	4.17	23.9	4.6
7.65	15.1	8.26	12.1	9.1
8.00	28.9	9.87	10.1	10.8
8.66	59.6	10.4	9.7	11.4
10.56	148.2	16.3	6.1	17.9

Table 6.6 Conductivity Data and Resulting Values with the Addition of 10^{-3} M LiCl

Operational pH	Specific conductivity ($x10^6\ \Omega^{-1}.cm^{-1}$)	Debye parameter κ, ($x10^{-7}\ m^{-1}$)	Debye length $1/\kappa$, (nm)	κa
3.60	35.4	11.1	9.0	12.2
4.02	36.3	11.2	8.9	12.3
4.60	34.6	11.1	9.0	12.2
4.97	33.3	11.0	9.1	12.1
6.05	33.2	11.0	9.1	12.1
7.65	43.6	12.0	8.3	13.3
8.00	57.9	12.3	8.1	13.6
8.66	89.8	13.9	7.2	15.2
10.56	151.8	18.2	5.5	20.2

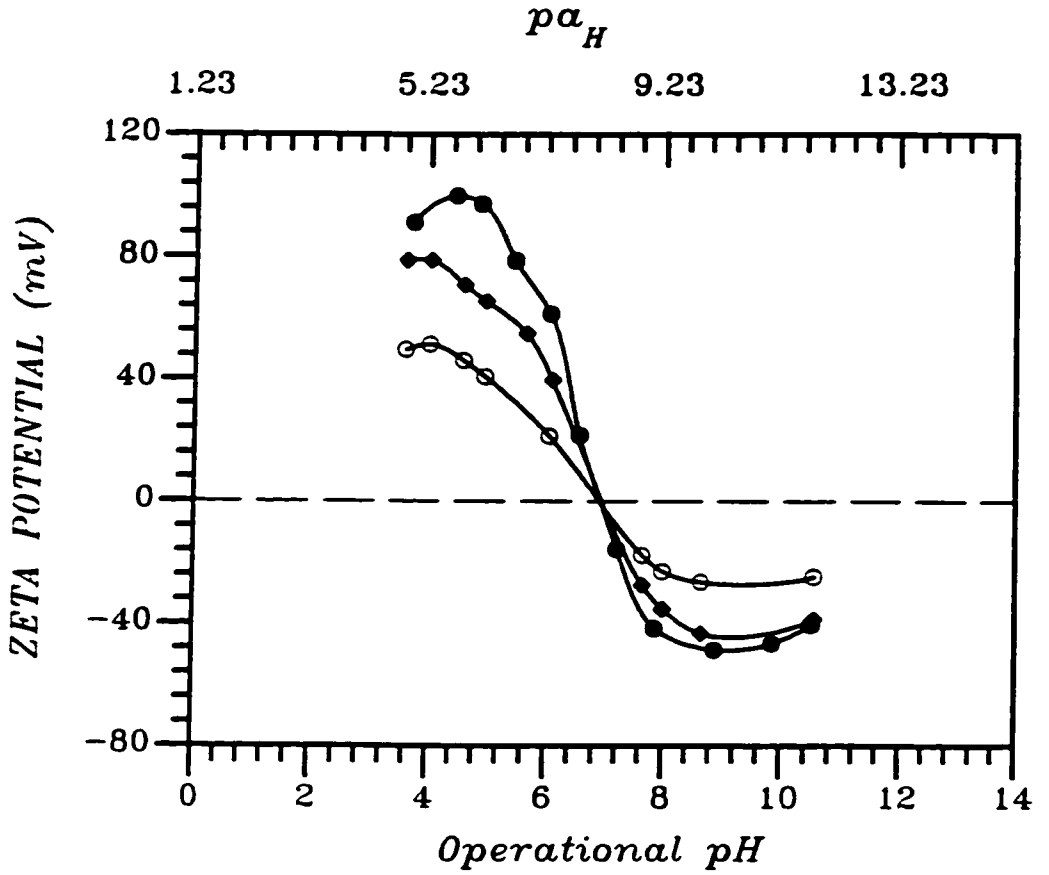

Figure 6.8 The effect of LiCl addition on zeta potential of alumina particles in EtOH as a function of operational pH and pa_H ((●) EtOH, (◆) EtOH (5×10^{-5} M LiCl) and (○) EtOH (10^{-3} M LiCl))

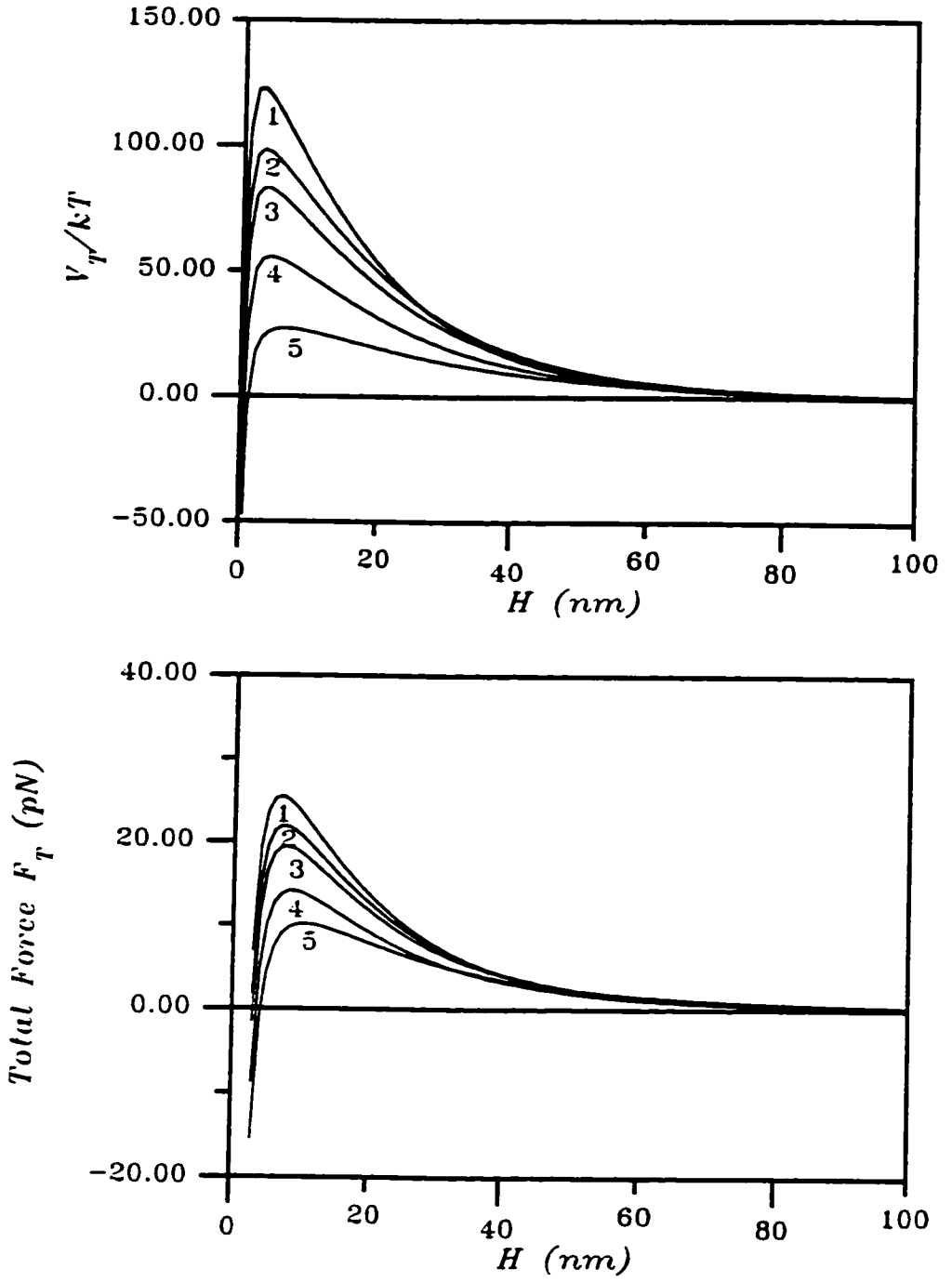

Figure 6.9 Total interaction energies (a) and forces (b) as a function of particle separation between two positively charged alumina particles with the addition of 5 x 10^{-5} M LiCl to an Al_2O_3-EtOH suspension for various O. pH (operational pH) and ζ values (line 1: O. pH = 4.02, ζ = 79 mV; line 2: O. pH = 4.60, ζ = 71 mV; line 3: O. pH = 4.97, ζ = 66 mV; line 4: O. pH = 5.65, ζ = 55 mV; line 5: O. pH = 6.05, ζ = 40 mV)

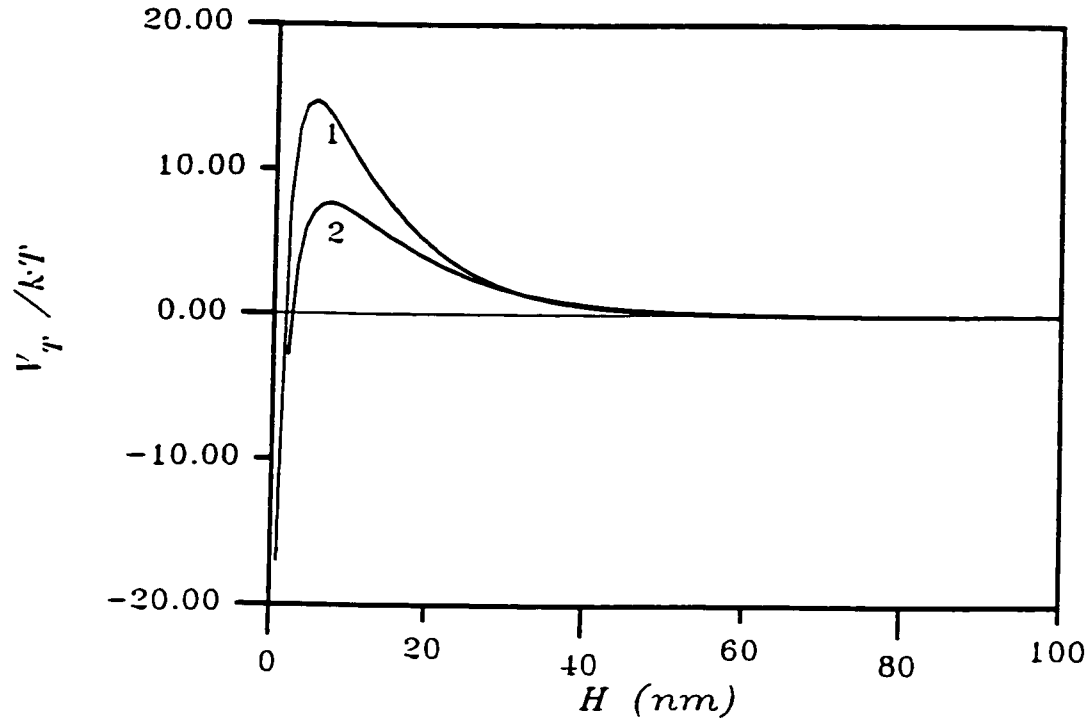

Figure 6.10 Total interaction energies as a function of particle separation between two negatively charged alumina particles with the addition of 5 x 10^{-5} M LiCl to an Al_2O_3-EtOH suspension for various O. pH (operational pH) and ζ values (line 1: O. pH = 8.00, ζ = - 35 mV; line 2: O. pH = 7.65, ζ = - 27 mV)

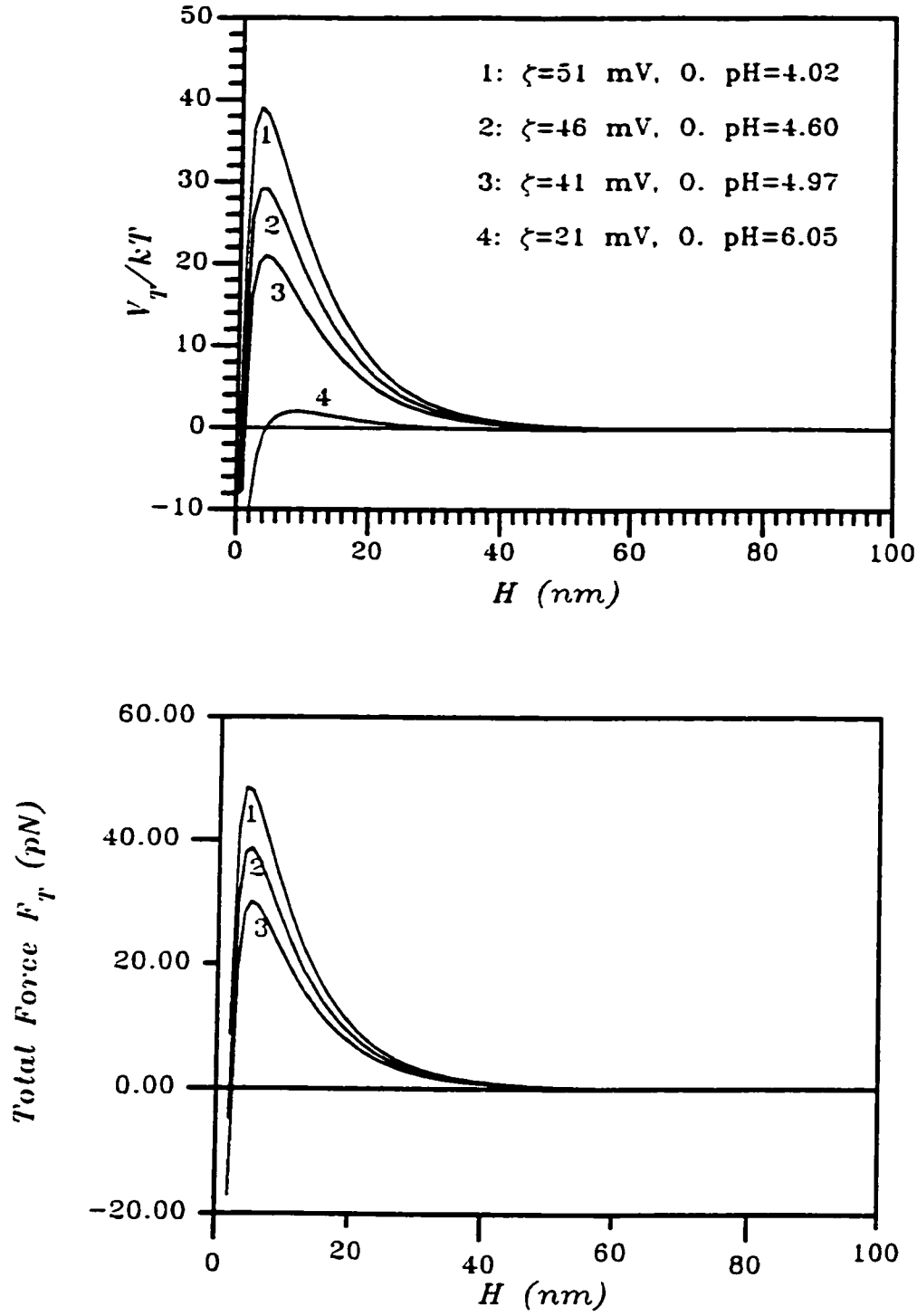

Figure 6.11 Total interaction energies (a) and forces (b) as a function of particle separation between two positively charged alumina particles with the addition of 10^{-3} M LiCl to an Al_2O_3-EtOH suspension for various O. pH (operational pH) and ζ values

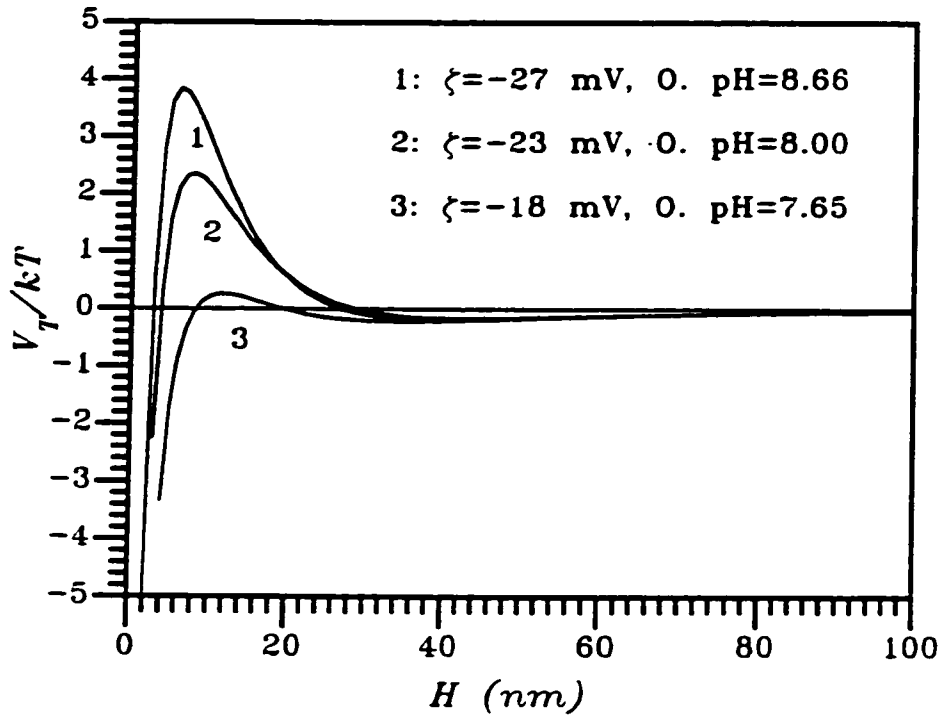

Figure 6.12 Total interaction energies as a function of particle separation between two negatively charged alumina particles with the addition of 10^{-3} M LiCl to an Al_2O_3-EtOH suspension for various O. pH (operational pH) and ζ values

The values of repulsive-energy-barrier, maximum-repulsive-force and pressure at various operational pH values are summarized in Table 6.7, and the results suggest the colloidal stability of alumina in ethanol is sensitive to salt addition. Alumina-EtOH suspensions with 5×10^{-5} M LiCl are stable as a result of the high repulsive potential barrier and repulsive force (pressure). However, suspension stability decreases with 10^{-3} M LiCl addition owing to the low repulsive potential. Therefore, it can be predicted that the ionic stability of oxide particles in EtOH can be better controlled by the combination of potential-determining-ions and indifferent-electrolyte. Combination optimizes both repulsive potential and repulsive force (pressure).

The rate of coagulation of Al_2O_3 (estimated via the stability ratio) was determined by turbidity measurement. The results of stability ratio, with and without, LiCl addition versus operational pH and pa_H are shown in Figure 6.13. This figure demonstrates close correlation with the stability predictions of Tables 6.7 and 6.4.

Table 6.7 Total DLVO Interaction Energy, Force and Pressure for Two Alumina Particles with LiCl Addition at Different Operational pH Values in EtOH

[LiCl] (M)	Operational pH	V_T (max) (kT)	F_T(max)* (pN)	A(eff.) ($x10^{15}$ m^2)	P_T(max)* (kN/m^2)
5×10^{-5}	4.02	122.9	25.5	5.73	4.5
	4.60	98.5	21.9	6.11	3.6
	4.97	83.2	19.4	6.32	3.1
	5.65	55.7	14.1	6.52	2.2
	6.05	27.2	10.2	8.26	1.2
	7.65	7.7			
	8.00	14.7			
10^{-3}	4.02	39.1	48.5	3.07	15.8
	4.60	29.2	38.7	3.10	12.5
	4.97	21.0	30.1	3.14	9.6
	6.05	1.99			
	7.65	0.26			
	8.00	2.36			
	8.66	3.84			

* F_T(max) and P_T(max) were calculated when V_T(max) > 15 kT.

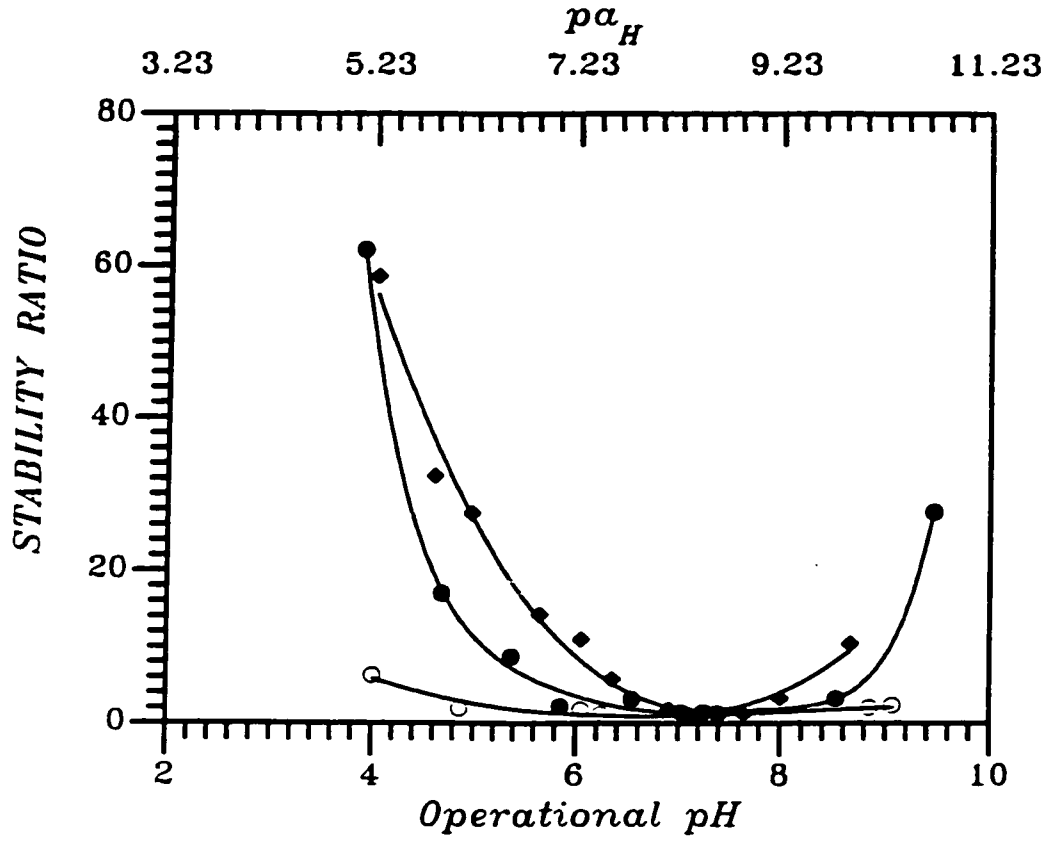

Figure 6.13 Stability ratio (W) as a function of operational pH and pa_H for alumina-EtOH suspension with and without LiCl addition ((●) EtOH, (◆) EtOH (5×10^{-5} M LiCl) and (○) EtOH (10^{-3} M LiCl))

VI-2 The Influence of Acidity on the Rheological Properties of Oxide Suspensions in Ethanol

In this section, interparticle forces are manipulated by controlling the acidity of ethanolic suspensions without dispersants. The influence of acidity on the surface chemistry of oxide particles suspended in ethanol is established and the relationship between surface chemistry and the rheological properties of suspensions of the three oxides in ethanol is presented. This facilitates macroscopic understanding of the dispersion phenomena.

VI-2.1 Rheological Studies of Alumina-EtOH and Magnesia-EtOH Suspensions

Figure 6.14 (a) shows the viscosity vs. shear-rate for suspensions containing 0.09 volume-fraction of alumina powder at different operational-pH values. The results show that the viscosity of suspensions at an operational pH of 5.08 were low and almost independent of the shear rate. This indicates a nearly Newtonian behaviour. The dispersed particles in this case are mutually repelled and they flow as individual units. On the other hand at other operational pH values, the suspensions exhibited shear-thinning behaviour and had a higher viscosity.

Figure 6.14 (b) shows the shear-stress vs. shear-rate for suspensions containing 0.09 volume fraction of alumina powder at different operational pH values. The measured flow curves were fitted with the Bingham model, the Herschel-Buckley model, the Ostwald-de Waele model and the Casson model. The Casson equation (Casson, 1959)

$$\tau^{1/2} = \tau_c^{1/2} + (\eta_c D)^{1/2} \qquad (6.1)$$

(where τ_c and η_c are the Casson yield value and the Casson viscosity, respectively) gave the best fit (the solid lines in the figure). The τ_c and η_c values obtained via fitting are listed in Table 6.8.

Table 6.8 Results of Fitting Flow Curves with the Casson Model for Al_2O_3-ethanol Suspensions with ϕ=0.09 at Different Operational pH

Operational pH	τ_c (mPa)	η_c (mPa.s)	R^2
5.08	10.28	4.09	0.997
4.63	1217	3.51	0.993
8.05	1926	2.32	0.999
10.71	2238	2.22	0.996
10.15	5899	2.84	0.975

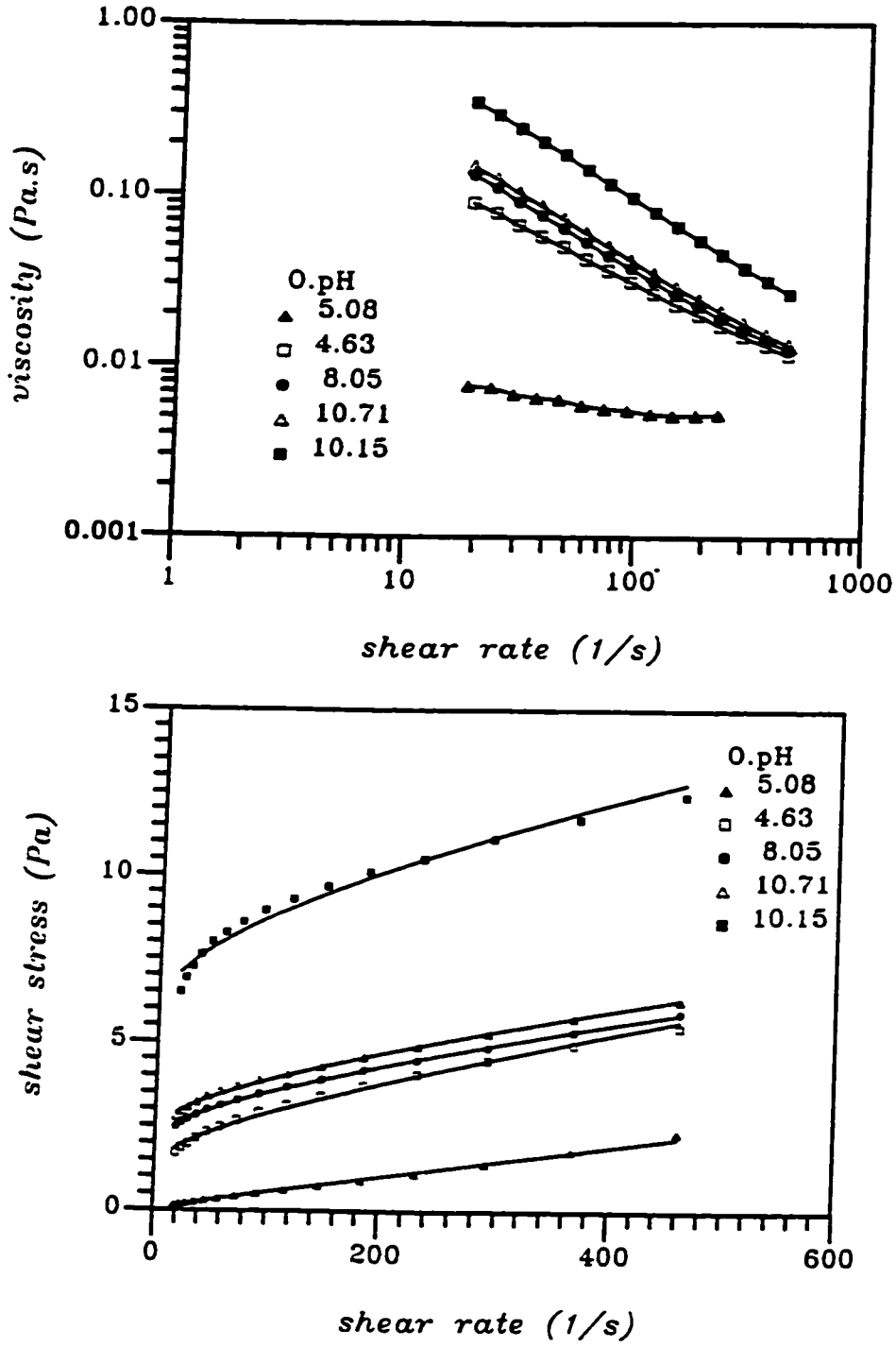

Figure 6.14 (a) Viscosity as a function of shear rate for Al_2O_3-ethanol suspensions with ϕ=0.09 at different operational pH (b) Fitting flow curves with the Casson model

According to the Casson model, the particles in a flocculated suspension form floc groups or a network because of mutual attraction between particles. The Casson yield value, τ_c, can be used as a parameter to indicate the degree of flocculation. The value of τ_c listed in Table 6.8 is acidity dependent. This is due to the different degree of flocculation at different operational pH values.

The Casson yield value (τ_c)-operational pH (pa_H) behaviour is shown in Figure 6.15. It is clearly attributable to the effect of acidity on the particle surface charge (zeta-potential). Maximum τ_c was observed at an operational pH value of 10.15. This should correspond to the iso-electric point (IEP) (zeta potential = zero). Ionic double-layer interactions are absent at this condition, i.e., the repulsive component is nonexistent and the net potential between particles is attractive. Particles are expected to flocculate and form a strongly attractive network throughout a still sample. This network is broken down into smaller units of flocculated particles under shear. The smaller units can withstand the shear field. The size of the units which survive is determined by a balance between the shear forces which tend to break the structure down and the forces of attraction which hold the particles together (Firth and Hunter, 1976). Such flocculated suspensions will exhibit high viscosity beyond the yield stress because both the network and its entrapped liquid must be moved to induce flow. Viscosity decreases when the network is sheared because it breaks into smaller and smaller flow units. More liquid will thus be liberated thereby reducing the effective

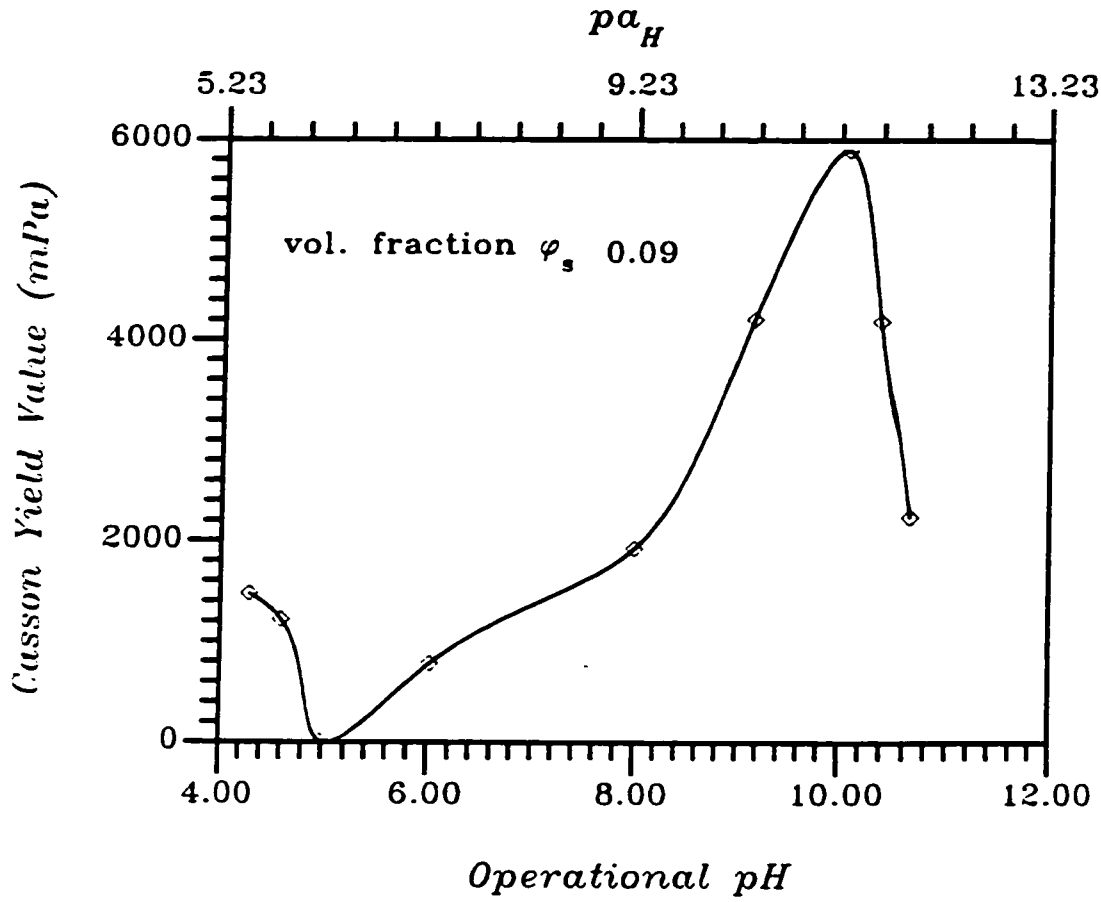

Figure 6.15 Casson yield value-operational pH behaviour of Al_2O_3-ethanol suspensions.

volume of solids. The shear rate required to achieve a given viscosity is indicative of the work required to break apart the network and produce a certain average flow unit size. It can be expected that the strength of this network, viz., how difficult it is to break it apart into smaller flow units, will depend on the magnitude of the attractive force between particles, the volume fraction of particles and the network connectivity or structure.

Away from the iso-electric point, as the zeta potential increases, the repulsion increases accordingly and, eventually, attains a level that is strong enough to overcome the van der Waals forces. Above this zeta potential level, the particles in suspension are dominated by repulsive forces; thus, the suspension is stabilized. This phenomenon can be seen on the flow curve at an operational pH value of 5.08 where the Casson yield stress is reduced to very low values.

Figure 6.15 shows that, at operational pH values below the iso-electric point, the value of τ_c decreases with operational pH, attains a minimum and then increases again. The latter indicates flocculation occurs again and becomes stronger as the operational pH decreases. This is due to the increase of ionic strength with increasing acid addition resulting in compression of the electrical double layer.

Similar rheological behaviour was observed for MgO (C-1)-EtOH suspensions. Figure 6.16 shows the viscosity and shear-stress vs. shear-rate for suspensions containing 0.15 volume fraction magnesia powder (C-1) at different

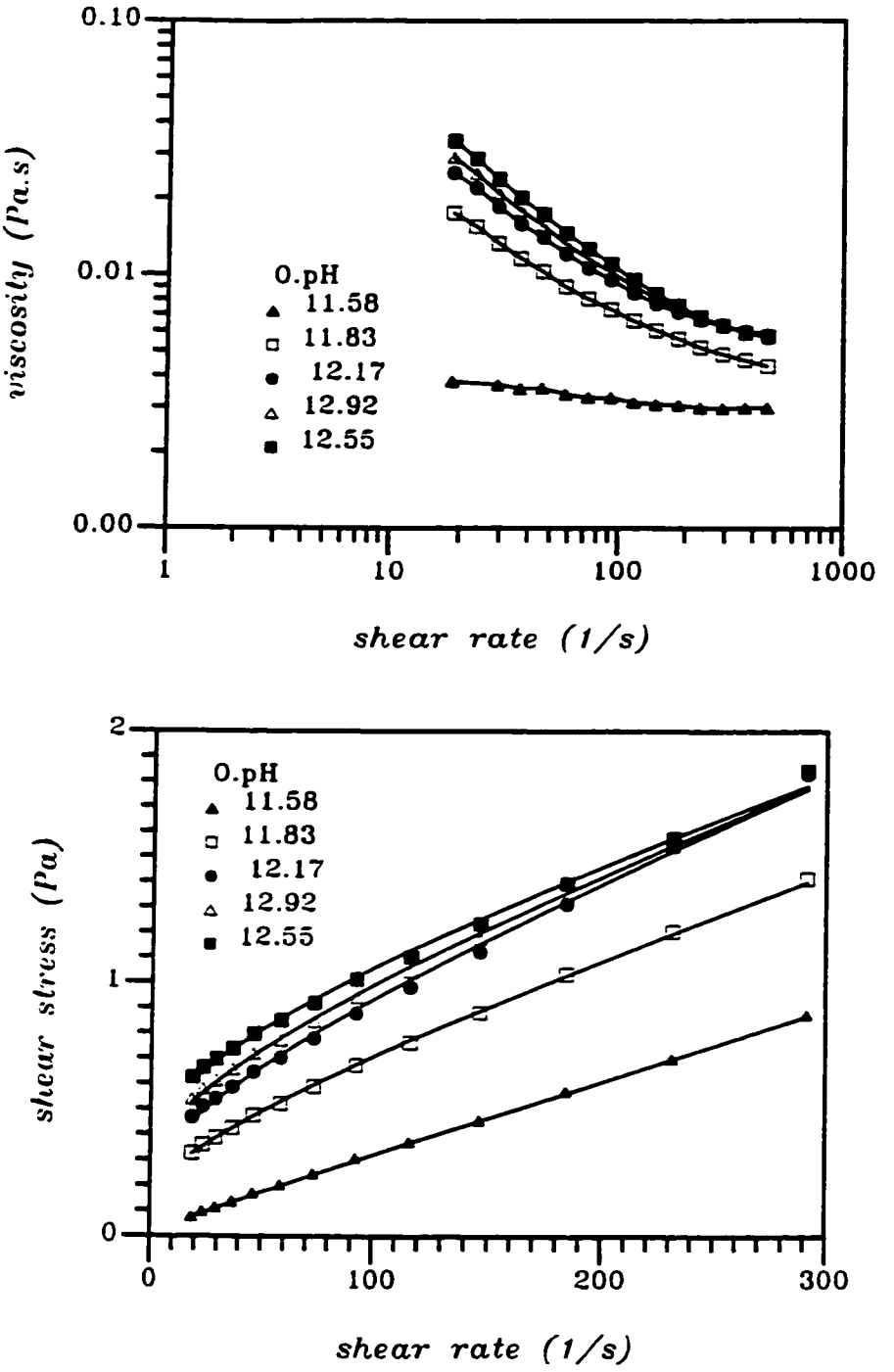

Figure 6.16 Rheology of MgO (C-1)-ethanol suspensions for 0.15 volume fraction at different operational pH (a) viscosity as a function of shear rate (b) shear stress as a function of shear rate. The experimental points were fitted to Casson model (solid line).

operational pH values. The figure shows the flow behaviour of the system follows the Casson model very well. The τ_c and η_c values are listed in Table 6.9.

Table 6.9 Results of Fitting Flow Curves with the Casson Model for MgO-ethanol Suspensions with ϕ=0.15 at Different Operational pH

Operational pH	τ_c (mPa)	η_c (mPa.s)	R^2
11.58	2.475	2.66	0.999
11.83	129.4	2.32	0.999
12.17	204.0	2.65	0.997
12.92	207.7	2.26	0.997
12.55	354.2	1.88	0.997

The Casson yield value (τ_c) of the magnesia (C-1) suspensions as a function of operational pH (pa_H) is shown in Figure 6.17. The Maximum value was observed at an operational pH value of 12.55.

The influence of acidity on the rheological properties of ethanolic alumina and magnesia suspensions should be correlated with the change of the surface chemistry of the alumina and magnesia with acidity. The isoelectric points (IEPs) of alumina and magnesia, as determined by electrophoretic light scattering and shown in Table 6.1, do not agree with the operational pH values for the maximum

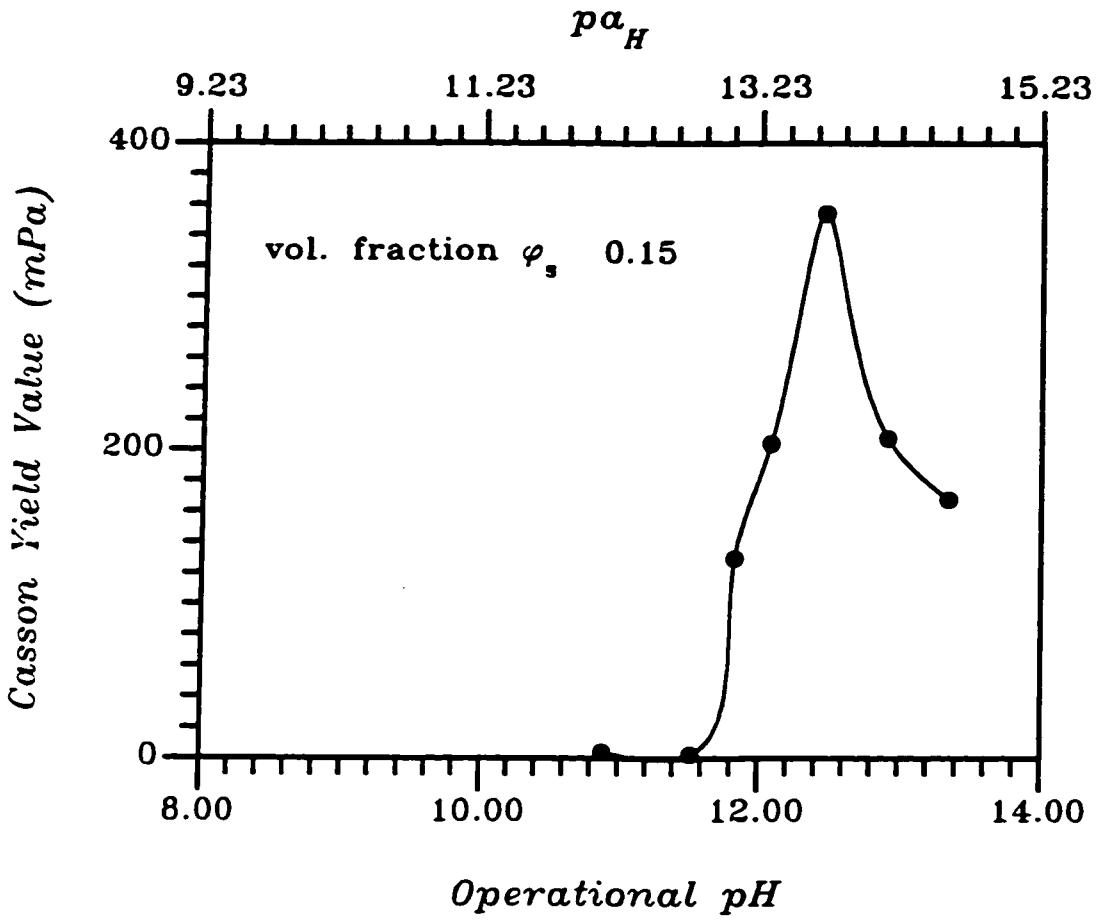

Figure 6.17 Casson yield value of MgO (C-1)-ethanol suspensions as a function of operational pH and pa_H.

Casson yield value (τ_c). To resolve this discrepancy, the dynamic electrophoretic mobility of moderately-concentrated suspensions was electroacoustically measured. Figures 6.18 and 6.19 show the dynamic mobility results for alumina and magnesia in EtOH determined by electrokinetic sonic analysis (Matec ESA 8000 system) as a function of operational pH and pa_H. The isoelectric points are at operational pH 10.11 and 12.58, respectively, for alumina-EtOH and magnesia-EtOH suspensions with φ_s above 0.01. These results agree with the operational-pH values for the maximum Casson yield value (τ_c) observed in the rheological measurements.

It is interesting to note that, in this case, the isoelectric points shift ~ 3 operational pH units in the basic direction compared to those determined by microelectrophoresis in dilute suspensions containing only 100 mg dm^{-3} solids. In comparison, electrophoretic mobility measurements in aqueous alumina suspensions give the same isoelectric point for both dilute and moderately-concentrated suspensions (Figure 6.20). Cannon and Mann (1988) have also reported the electrokinetic behavior and titratable surface charge for α-alumina in aqueous NaCl solution, using the Matec ESA 8000 system. They compared the dynamic mobilities for the 1.8 vol% sample with the static mobilities measured via microelectrophoresis. Both methods gave same value of pH=8.8 for the isoelectric point. Therefore, the experimentally-observed, positive isoelectric point shift with increasing solid content needs explanation, for alumina and magnesia in ethanolic suspensions.

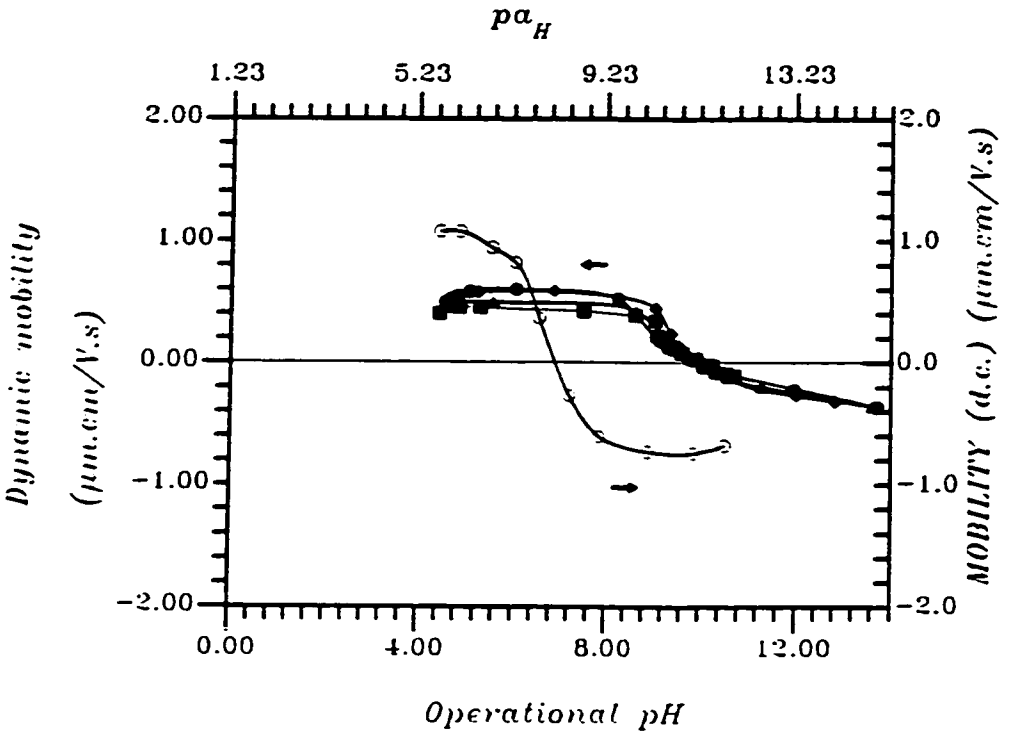

Figure 6.18 Dynamic and d.c. electrophoretic mobility of Al_2O_3 particles in EtOH as a function of operational pH and pa_H. (○-dilute suspension for microelectrophoresis (100 mg dm^{-3}), ●-1 vol%, ◆-2 vol%, ▲-4 vol% and ■-5 vol%.)

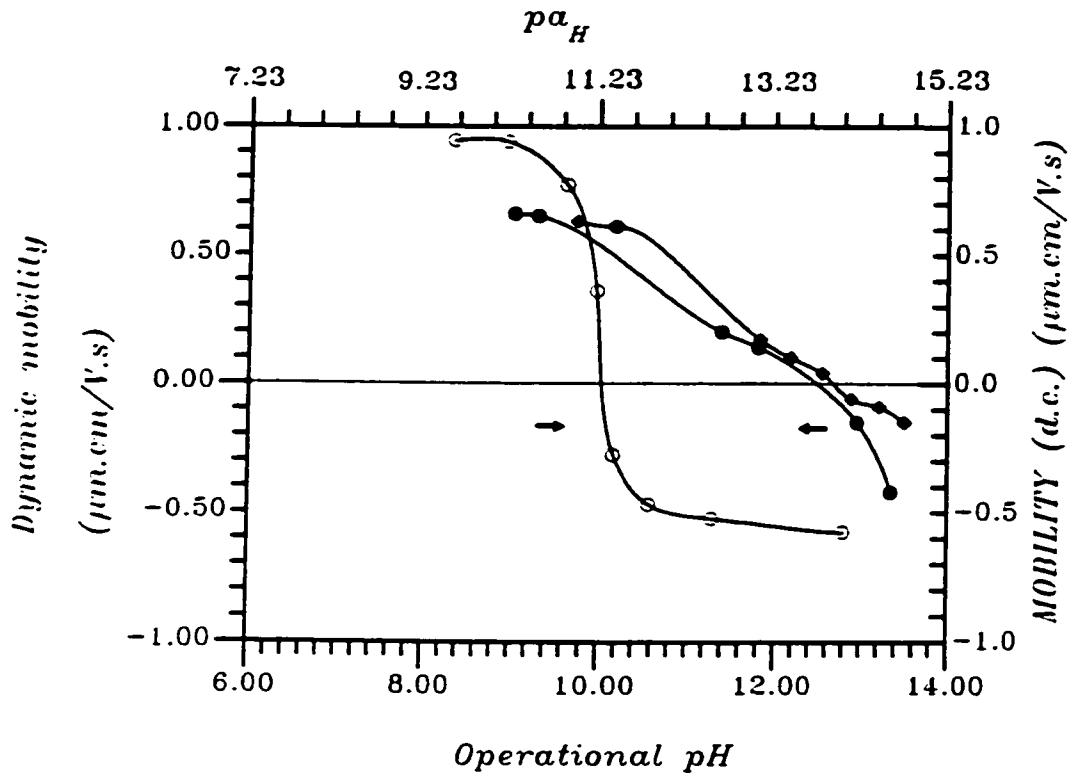

Figure 6.19 Dynamic and d.c. electrophoretic mobility of MgO particles in EtOH as a function of operational pH and pa_H. (o-dilute suspension for microelectrophoresis (100 mg dm^{-3}), ●-5 vol%, ◆-1 vol%)

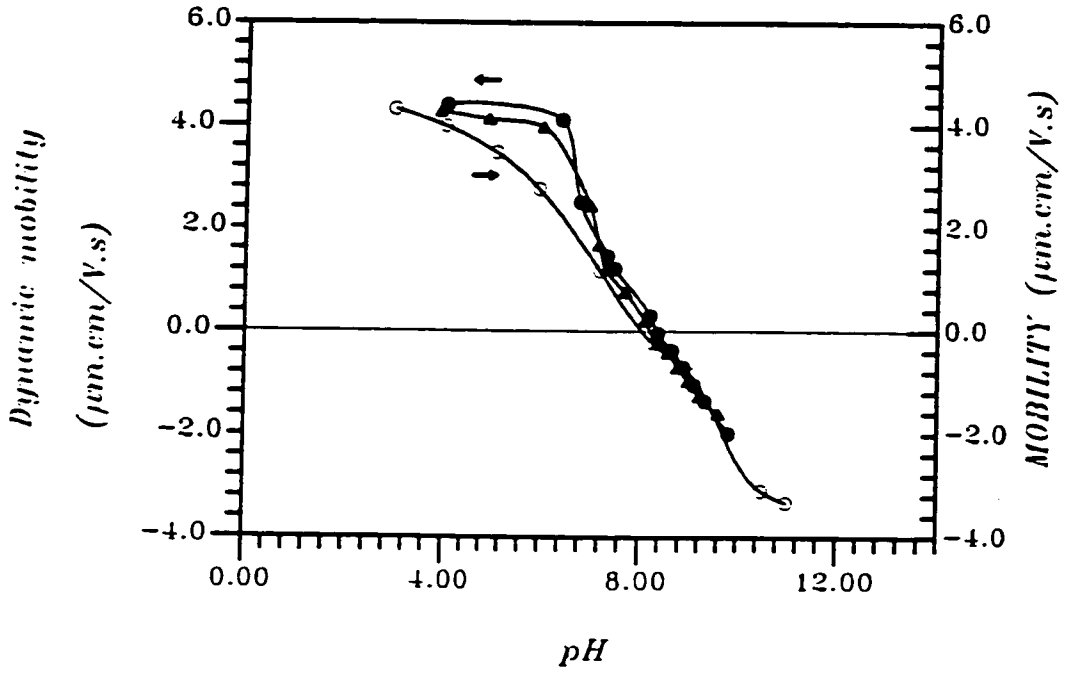

Figure 6.20 Dynamic and d.c. electrophoretic mobility of Al_2O_3 particles in water as a function of pH (o-dilute suspension for microelectrophoresis (100 mg dm^{-3}), ●-1 vol%, ▲-5 vol%)

Any metal oxide in solution is in "equilibrium" with a variety of species, e.g., hydrolyzed species in aqueous solution originating from dissolution of metal ions. It is known that such hydrolyzed species adsorb preferentially. It is believed that the adsorption of complex, hydrolyzed metal ions is responsible for the surface properties of metal hydrous oxides. The adsorptivities of these ions can be correlated to isoelectric points.

Any ion with a non-electrostatic adsorption energy contribution, can be regarded as preferentially or specifically adsorbed. Within this broad grouping, a further division can be made between those ions that adsorb chemically (sharing of electrons) and those that do not. For chemical interaction to occur, the ion must penetrate the compact layer (Stern layer). A chemical interaction with the surface is experimentally evidenced by superequivalent adsorption, reversal of the zeta potential sign or by a shift in the point of zero charge (PZC) or the isoelectric point (IEP) (Lyklema, 1983). In the absence of specific adsorption the PZC and IEP are identical. The direction of shift is indicative of the sign of the charge on the ion that is specifically adsorbing: if it is the cation, Δ(PZC) is negative and Δ(IEP) is positive; if it is the anion, the trends are reversed. This effect is due to the accumulation of excess positive or negative charge in the compact layer, which, to obtain charge neutrality, must be compensated for by the additional uptake of OH^- or H^+ potential determining ions, respectively. This opposite shift of PZC and IEP is a characteristic criterion for specific adsorption. Cannon and Mann (1988) found the point of zero charge is pH=7.4 for alumina in

aqueous suspension. This is 1.4 pH units lower than the isoelectric point indicating specific absorption of cations in the Stern layer.

Hirata et al (1995) investigated the dissolution behaviour of α-alumina particles in aqueous suspension. From the point of view of dissolving species from α-alumina, Al^{3+} cations exist in an acidic suspension and AlO_2^- anions in an basic suspension. It was found, the Al^{3+} concentration in a low-solid-content suspension (0.5 vol%) increased gradually with time, in the case of an acidic solution, and reached the solubility limit of α-alumina. On the other hand, a rapid increase of Al^{3+} concentration in a high solid content suspension (1 or 5 vol%) resulted in a supersaturated solution of Al^{3+} ions. The Al^{3+} concentration exhibited a maximum then decreased with time until the solubility limit of α-alumina was reached. The equilibrium value of Al^{3+} concentration at pH 4.4 was 0.42 mM. This value should be responsible for the experimentally-observed difference between the PZC and IEP of α-alumina in aqueous suspension via specific absorption of Al^{3+} in the Stern layer.

The dissolution behaviour of α-alumina (or magnesia) in ethanol is unclear. Some dissolving cationic species from α-alumina (or magnesia) may exist in ethanolic solutions and the concentration change with time may follow the same trend as water but the solubility limit of α-alumina (or magnesia) in ethanol should be lower than in water. Therefore, the equilibrium concentration of the dissolving cationic species obtained in dilute suspensions (containing only 100 mg dm^{-3} solids) for microelectrophoresis measurement, may be too low to cause

the IEP shift. However, for moderately concentrated suspensions with φ_s above 0.01, a rapid increase in the dissolving cationic species concentration can result in a supersaturated solution of cations. This will cause the positive shift of IEP via specific absorption in the Stern layer.

VI-2.2 Rheological Study of Silica-EtOH Suspensions and the Colloidal Stability of Silica in Ethanol

Figure 6.21 shows the flow curves and their fitting lines (indicated by the solid lines in the figure) with the Casson model, at different operational pH values for suspensions containing 0.15 volume fraction of silica. The τ_c and η_c values are listed in Table 6.10.

The Casson yield value (τ_c) of silica suspensions as a function of operational pH (pa_H) is shown in Figure 6.22. There is no maximum value of τ_c at the isoelectric point (IEP), in contrast with the Casson yield value-acidity behaviour of Al_2O_3-EtOH and MgO-EtOH suspensions. This observation means that SiO_2-EtOH suspensions are stable near the IEP in spite of the low zeta potential and consequent low repulsive energy barrier thereat. Clearly, the results do not follow the stability predictions based on DLVO theory, i.e., the colloidal stability of silica in ethanol cannot be exclusively explained by ionic stability as per DLVO theory. Similar conclusions were reached for silica in water (Iler, 1979). The rheological behaviour also parallels Ketelson's (1996) coagulation

results for Stober silica in acetone. The specifically different behaviour of silica was believed to be due to the presence of a steric barrier of a silicic acid gel network (proposed by Vigil et al. (1994)), which gives rise to a short-range steric repulsive force. Therefore, the rheological properties of silica-EtOH suspensions and the colloidal stability of silica in ethanol can be explained in terms of the accepted models of aqueous silica sols.

Table 6.10 Results of Fitting Flow Curves with the Casson Model for SiO_2-ethanol Suspensions with ϕ=0.15 at Different Operational pH

Operational pH	τ_c (mPa)	η_c (mPa.s)	R^2
5.08	2.196	2.57	0.998
4.23	75.67	2.28	0.998
3.85	80.70	2.38	0.998
2.31	112.2	2.32	0.998
1.89	113.2	2.37	0.998
1.21	110.9	2.39	0.998

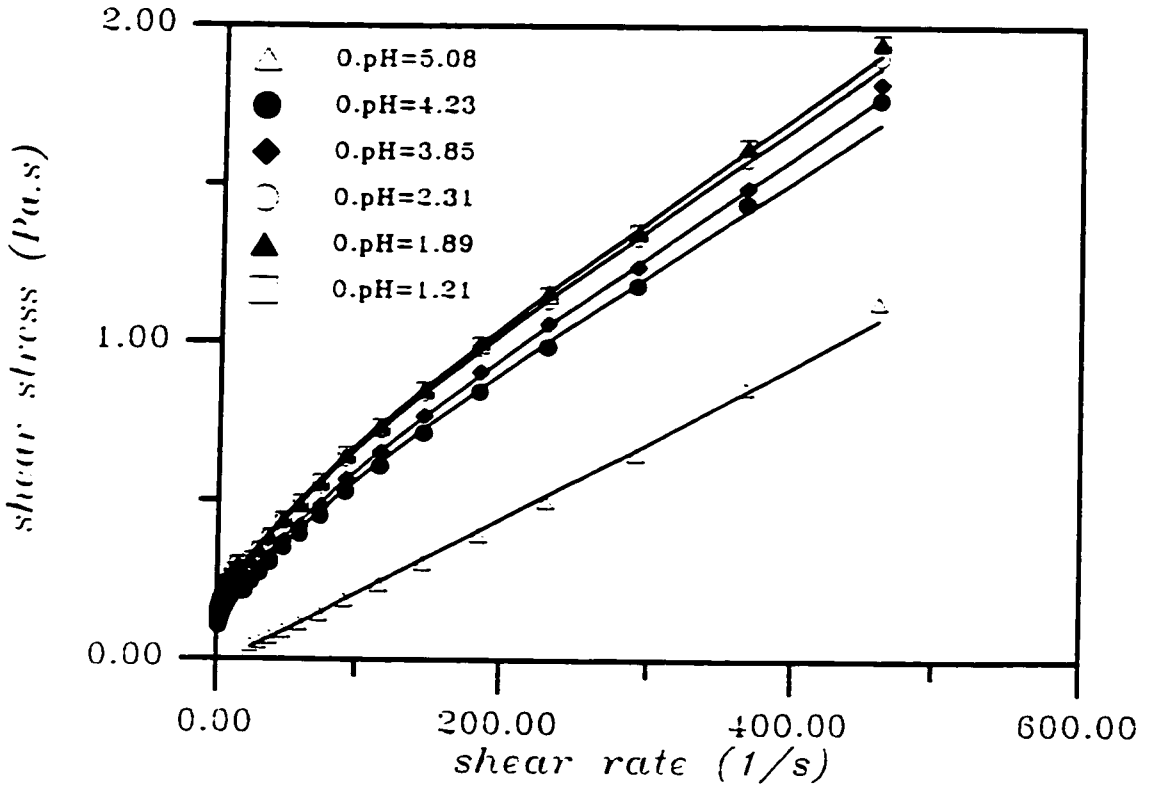

Figure 6.21 Fitting flow curves with the Casson model for silica-ethanol suspensions with ϕ=0.15 at different operational pH.

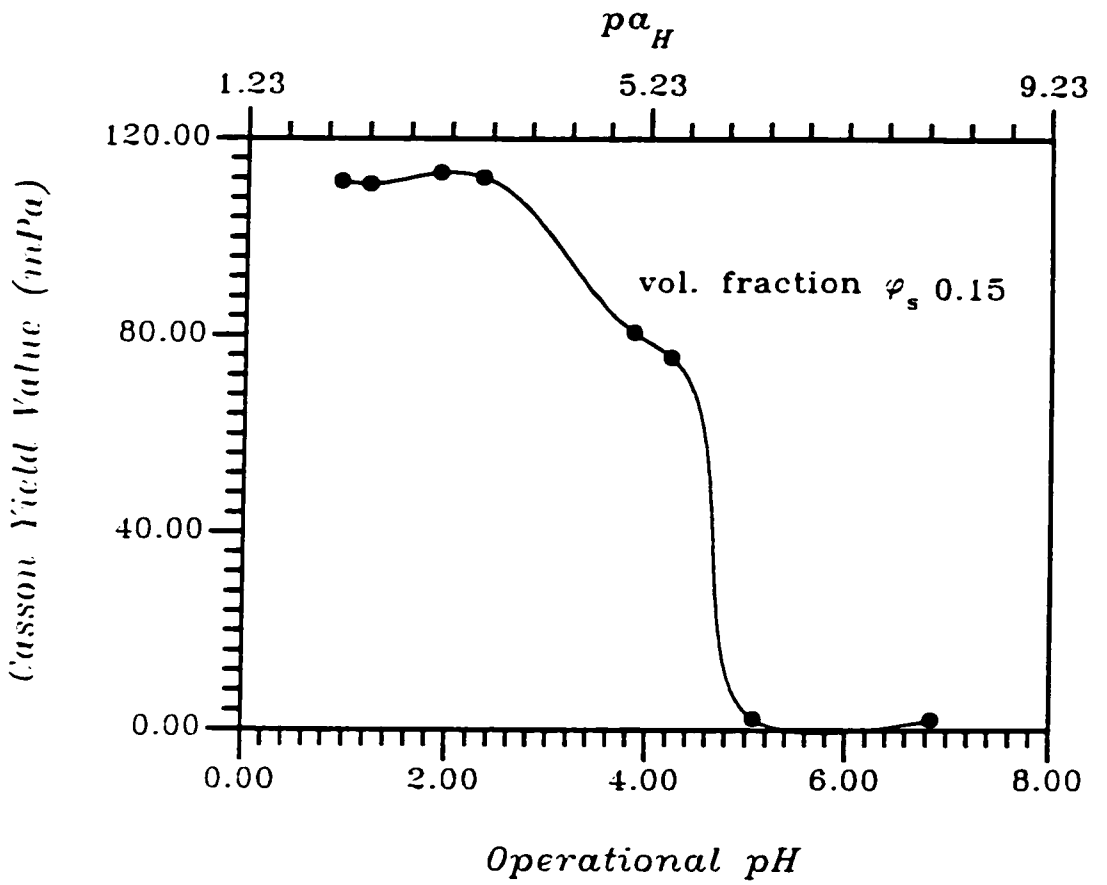

Figure 6.22 Casson yield value of silica-ethanol suspensions as a function of operational pH and pa_H.

VI-3 Heterocoagulation Behaviour of Oxide-mixture/Ethanol Suspension Systems

VI-3.1 Introduction

The majority of dispersions that occur in nature, or are used in various applications, contain particles which differ in composition, surface charge, shape, size and other properties. The structure and behaviour in mixed colloidal dispersions are critical in many areas of ceramic processing.

During the colloidal processing of ceramic composites (such as by EPD) of two or more oxide powders, the state of dispersion is strongly influenced by the differences of isoelectric point. This type of colloidal incompatibility leads to heterocoagulation of the powders. This phenomenon determines the degree of homogeneity of the final ceramic microstructure and the resulting properties of the composites.

The properties of the mixed system also depend strongly on the relative size of the particles. If the system consists of particles greatly different in size, electrostatic adsorption (colloidal coating) of small particles on the large ones may take place to form a coating layer.

In this section, the systems studied were chosen as model, ceramic-composite processing materials, i.e., the two components represent a pair of chemically reactive precursors for the final ceramic material. All the dispersions consisted of large, monodispersed, spherical silica and small alumina (or

magnesia) particles. These model systems confer the added advantage of making it easier to distinguish the two types of primary particle in photo-micrographs of the resulting, mixed aggregates. Heterocoagulation behaviour of small particle-size alumina (or magnesia) onto large particle-size silica was studied as a function of acidity and composition of the mixed suspension via the electrophoretic mobility. A series of experiments were designed to illustrate the application of colloid science principles to the design of heterocoagulates of controlled architecture containing more than one type of particle. The control of heterocoagulate structure in binary systems was achieved by exploiting the different susceptibilities of the components to changes in key colloidal parameters, i.e., the acidity of the suspension. Structure formation in binary dispersions was examined directly by transmission electron microscopy (TEM).

VI-3.2 Electrokinetic Behaviour of Mixed Oxide Suspension Systems

Figure 6.23 shows the electrophoretic mobility of alumina, silica and alumina-silica mixtures in ethanol as a function of acidity. The results show that the mixtures examined, exhibit electrokinetic behaviour intermediate between those of the pure oxides. The identified iso-electric points (IEP) for the alumina-silica mixtures together with those for the pure oxides are listed in Table 6.11. The IEP value of the mixture increases with alumina content and the iso-electric point (IEP) shifts from IEP_{silica} to $IEP_{alumina}$.

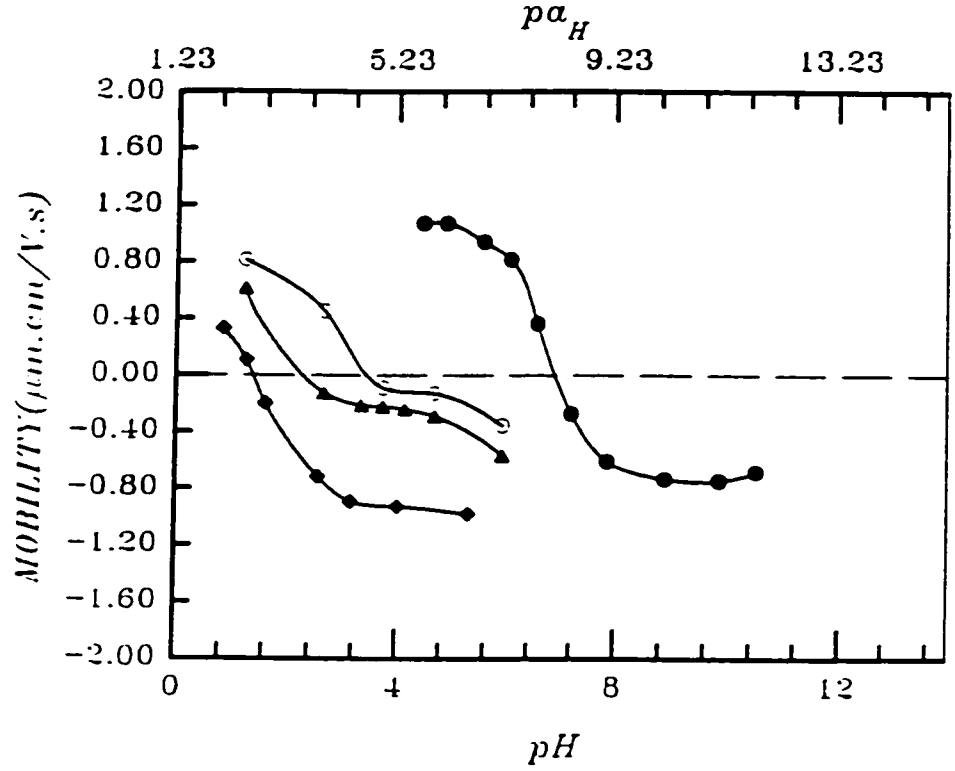

Figure 6.23 Electrophoretic mobility vs. operational pH and pa_H for alumina-silica heterocoagulate particles prepared at different compositions (◆-silica, ▲-5 vol% alumina, ○-10 vol% alumina, ●-alumina).

Table 6.11 The Iso-electric Point of Alumina–Silica Mixtures in Ethanol

Suspension Composition	IEP (Operational pH)
SiO_2	1.43
5 vol% Al_2O_3	2.45
10 vol% Al_2O_3	3.34
Al_2O_3	7.10

The electrostatic interactions between the particles of mixed oxides lead to heterocoagulation, the extent of which depends on the mixture composition. An average electrophoretic mobility of the heterocoagulates of the mixed powders is measured rather than the different mobilities of the individual powders.

Heterocoagulation between alumina and silica can be controlled by the acidity of the suspension. This effect is demonstrated by the change of electrophoretic mobility of the heterocoagulates with acidity. Thus, the differences in the observed values of electrophoretic mobility can be related simply to variations in the extent of electrostatic adsorption (surface coverage by alumina to give a colloidal coating).

Similar electrokinetic behaviour was observed for spherical-silica-/-fine-magnesia/ethanol suspension systems. Figure 6.24 shows the electrophoretic mobility of magnesia, silica and magnesia-silica mixtures in ethanol as a function

of acidity. The most pronounced change in the value of electrophoretic mobility was for small levels of magnesia (i.e., 5 vol%). This is expected because of the strong basic nature of magnesia. The IEP values determined for each magnesia-silica composition together with those for the pure oxides are listed in Table 6.12.

Table 6.12 The Iso-electric Point of Magnesia–Silica Mixtures in Ethanol

Suspension Composition	IEP (Operational pH)
SiO_2	1.43
5 vol% MgO	8.04
10 vol% MgO	8.74
MgO	10.08

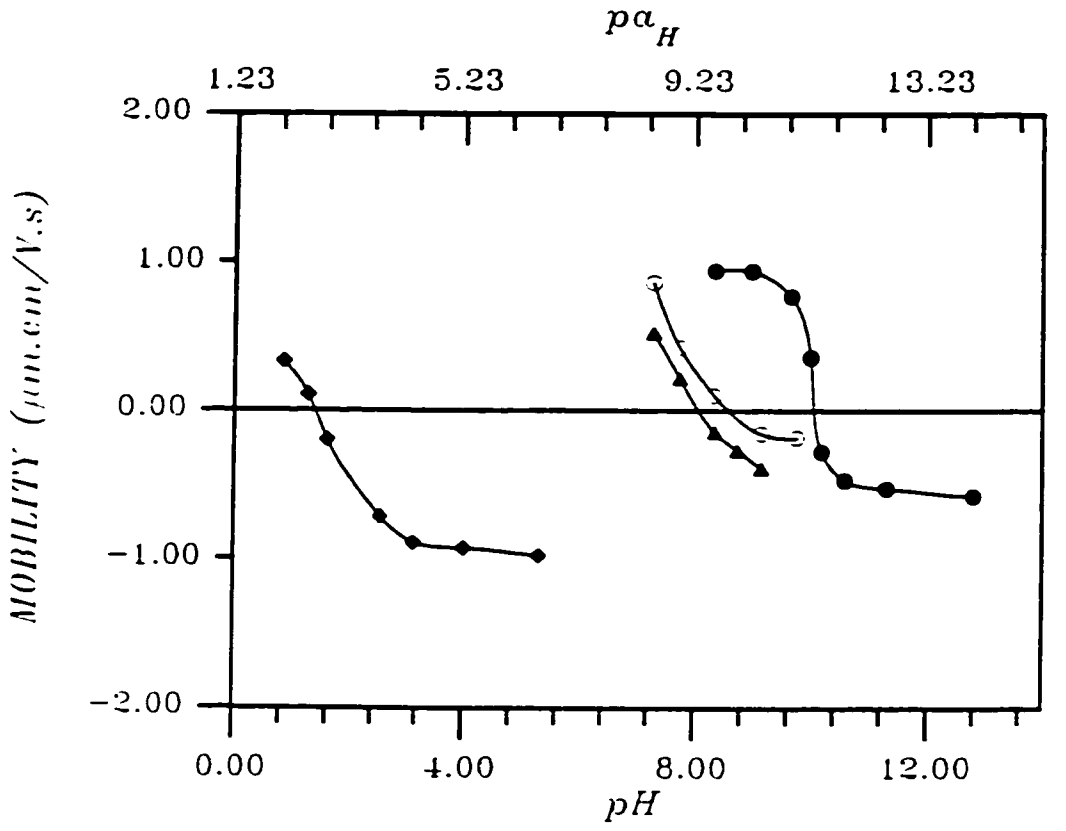

Figure 6.24 Electrophoretic mobility vs. operational pH and pa_H for magnesia (C-2)-silica heterocoagulate particles prepared at different compositions (◆-silica, ▲-5 vol% magnesia, ○-10 vol% magnesia, ●-magnesia).

VI-3.3 Structure Formation in Mixed Oxide Suspension Systems

There are three possible combinations of interparticle interaction in a mixed suspension system, i.e.;

1. Homocoagulation
2. Heterocoagulation plus homocoagulation
3. Heterocoagulation

These categories represent the clear-cut of behaviour. In practice, the composites obtained are intermediate in structure, exhibiting a predominance for one system of contacts rather than a total exclusion of all other possibilities. There are two possibilities in the first category, i.e., homocoagulation of one species and homocoagulation of both constituents. The latter is difficult to obtain in the systems studied, via acidity adjustment and unlikely to be of practical benefit, so no further discussion is merited.

VI-3.3.1 Homocoagulation of a Single-Oxide Particle Species

It is necessary to maintain colloidal stability of one type of particle with respect to homo- and heterocoagulation. The other type of particle must be destabilized. The obvious means of conferring such stability is via acidity adjustment to obtain stability, whilst the other particle suffers its iso-electric point.

For alumina-silica, acidity adjustment to an operational pH=1.31 is appropriate as both alumina and silica are positively charged. Preferential coagulation of the latter occurred due to its low zeta potential at this operational pH value.

Eqs 2.40 and 2.44 were used to calculate the net interaction potential energies for pairs of identical oxide particles, Eqs 2.51 and 2.52 were used for pairs of dissimilar oxide particles. The Hamaker constant (A_{132}) of Eq. 2.52 was calculated via Eq. 2.47 (using data of A_{11}, A_{22} and A_{33} from Tables 6.3 and 4.2), i.e., 0.925 X 10^{-20} J for alumina-ethanol-silica and 0.714 X 10^{-20} J for magnesia-ethanol-silica.

The total interaction potential curves are plotted in Figure 6.25 for silica-silica, alumina-alumina and silica-alumina particles at an operational pH=1.31. Homocoagulation of alumina-alumina particles hardly exists because of the high potential barrier that exists. The interaction-potential between silica and alumina particles has a high enough barrier to prevent heterocoagulation, however, the height of the potential barrier between silica-silica particles is < 15 kT, the lower limit for colloidal stability.

A transmission electron micrograph of the mixed aggregate structure at operational pH=1.31 is shown in Figure 6.26. The alumina particles are dispersed. There is no electrostatic adsorption of the fine alumina particles on the spherical silica particle surfaces. It is interesting to note that no big silica-silica aggregate (network structure) is observed, in spite of the low zeta potential near

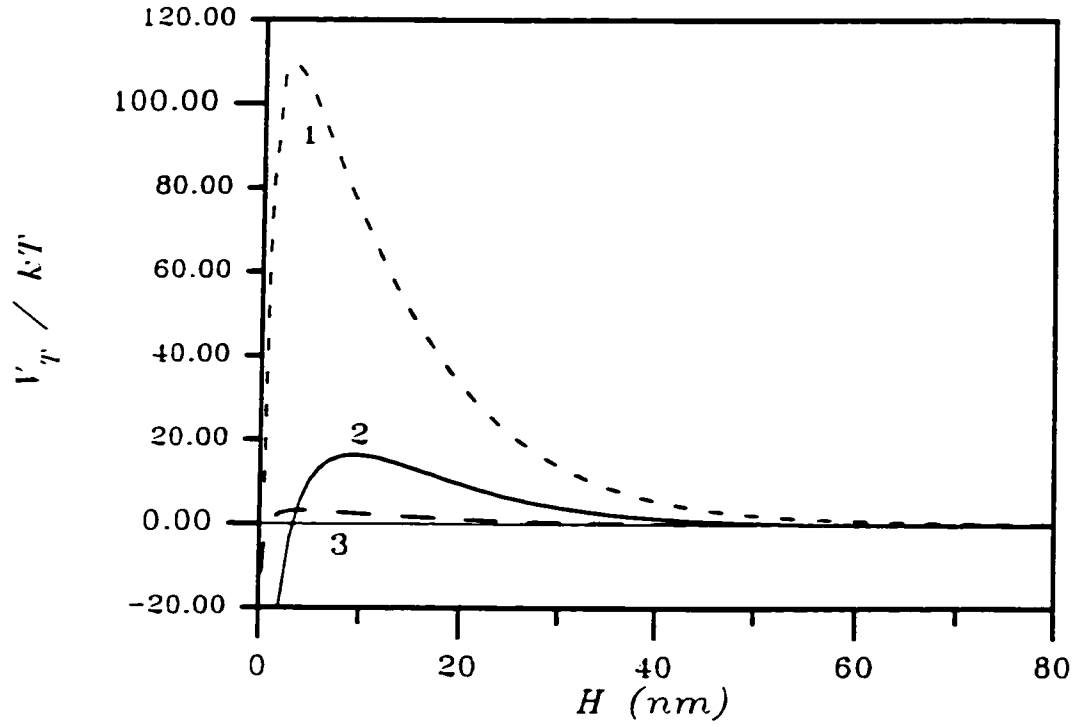

Figure 6.25 The total interaction potential between silica-silica (curve 3), alumina-alumina (curve 1) and silica-alumina (curve 2) particles in EtOH at operational pH 1.31.

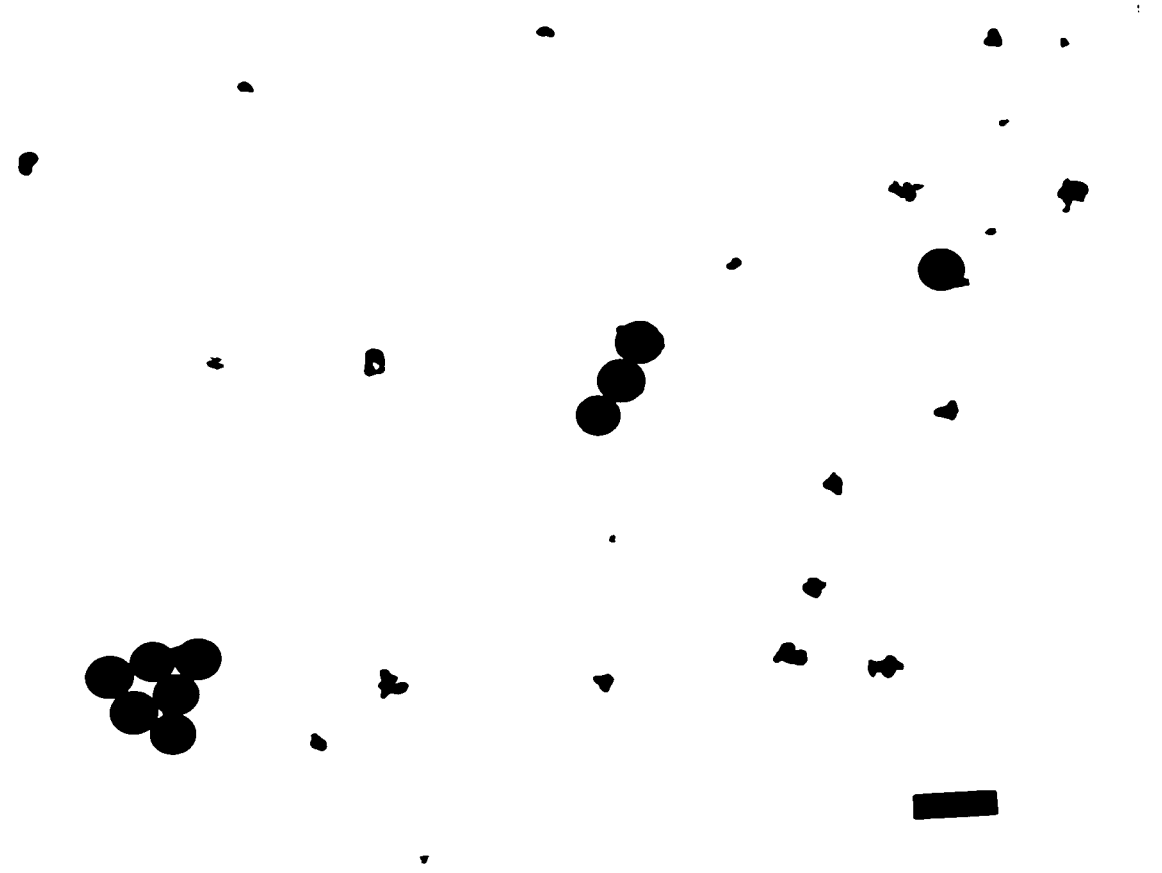

Figure 6.26 TEM micrograph of mixed suspension of alumina-silica at operational pH 1.31 with composition of 10 vol% alumina (Bar = 1 μm).

the iso-electric point. This is probably due to an additional, non-DLVO, short-range repulsive force due to a surface gel layer (Vigil et al., 1994).

VI-3.3.2 Heterocoagulation and Homocoagulation of a Single Component

The source of colloidal stability for one of the species with respect to homocoagulation is to be removed, whilst retaining the homostability of the other component. Heterocoagulation can be achieved by the electrostatic attraction between opposite-sign surface charges.

This strategy was demonstrated for a mixture of alumina and silica adjusted to an operational pH value of 6.68. The total interaction potential curves between silica-silica, alumina-alumina and silica-alumina particles are plotted in Figure 6.27. Silica has a strongly charged surface under this condition, thus preventing homocoagulation. The alumina particles on the other hand are destabilized as they approach their iso-electric point. The two types of particle adopt opposite charges as this operational pH value lies between the IEP of alumina and silica. This results in hetero-coagulation of the silica and alumina particles.

A TEM micrograph of the composite structure is shown in Figure 6.28. Homocoagulated alumina aggregates attach to isolated spherical silica surfaces to form heterocoagulates. This micrograph also illustrates the bridging role of the alumina particles in the aggregation of the stable silica spheres. This is evidence

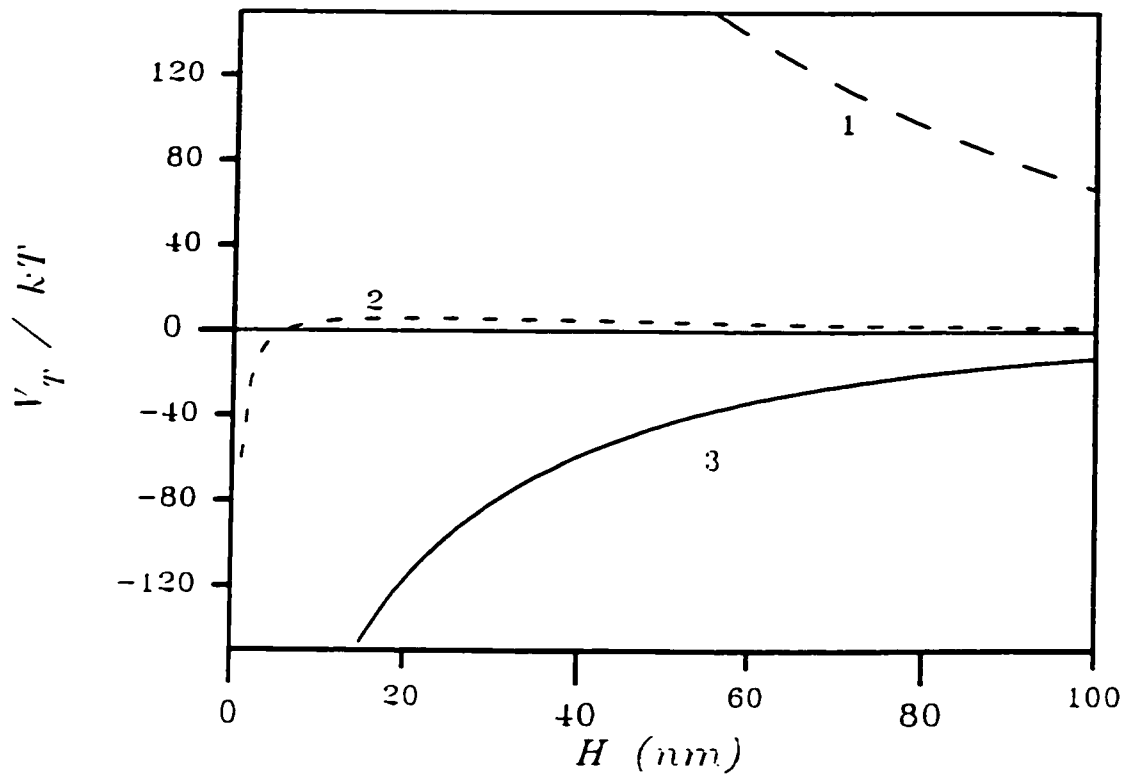

Figure 6.27 The total interaction potential between silica-silica (curve 1), alumina-alumina (curve 2) and silica-alumina (curve 3) particles in EtOH at operational pH 6.68.

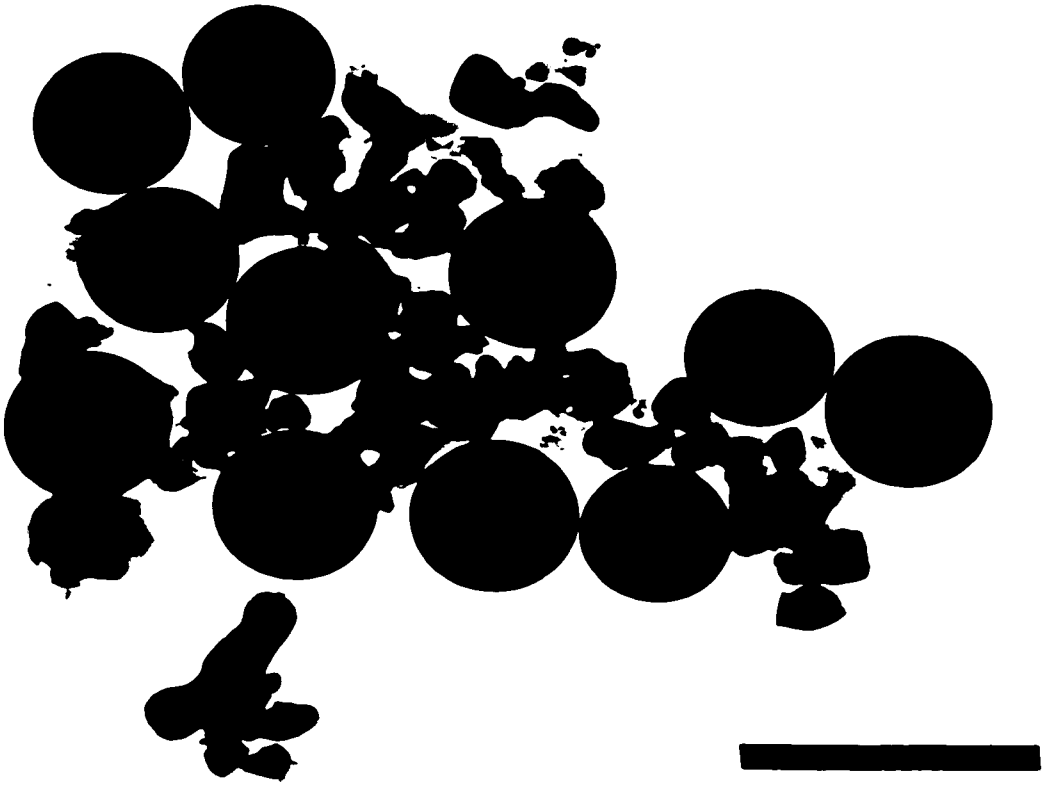

Figure 6.28 TEM micrograph of alumina heterocoagulated with silica at operational pH 6.68 with composition of 10 vol% alumina. Note the "bridging" action of the alumina particles (Bar = 1 μm).

that the positively-charged, alumina particles could promote silica-silica contacts via partial neutralization of the surface charge of the latter.

Similar behaviour was observed in the magnesia-silica system at an operational pH value of 9.89 (near the iso-electric point of the magnesia). The total interaction potential curves for the magnesia-silica system are plotted in Figure 6.29. The mixed-aggregate structure is shown in Figure 6.30. Although the silica spheres are, in some instances, constrained to be next to one another due to the "bridging" action of the magnesia particles, the colloidal stability has been preserved on aggregate formation so they are not strictly contiguous.

VI-3.3.3 The Achievement of Heterocoagulation

Predominant heterocoagulation is the most attractive architecture for a coated powder as a reactive ceramic precursor. This is a means of obtaining a very fine dispersion of one species in the other and providing a homogeneous mixture or distribution of two materials, with the scale of mixing, in principle, constrained only by the size of the primary particles. The most obvious way to promote heterocoagulation between unlike particles is to have the two components have opposite charge, whilst retaining their homostability. This can be achieved by acidity adjustment between the IEP values but away therefrom. Thus the two types of particle adopt opposite charges and heterocoagulation becomes the preferred mode of interaction. Under this condition, each component still has a strongly

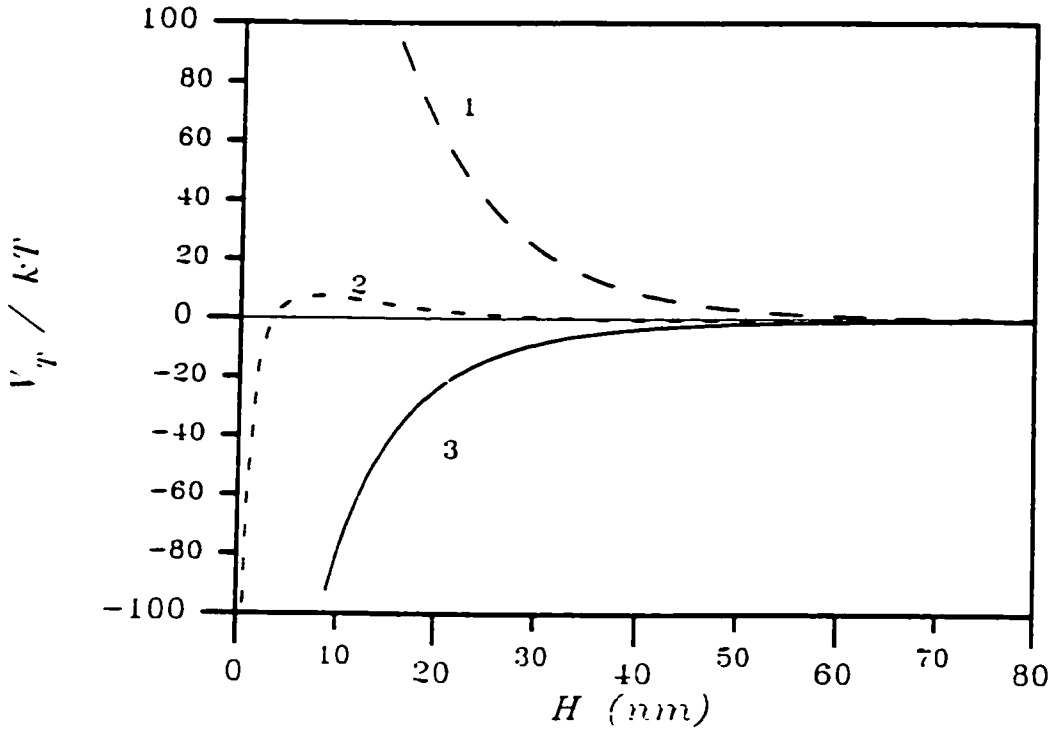

Figure 6.29 The total interaction potential between silica-silica (curve 1), magnesia-magnesia (curve 2) and silica-magnesia (curve 3) particles in EtOH at operational pH 9.89.

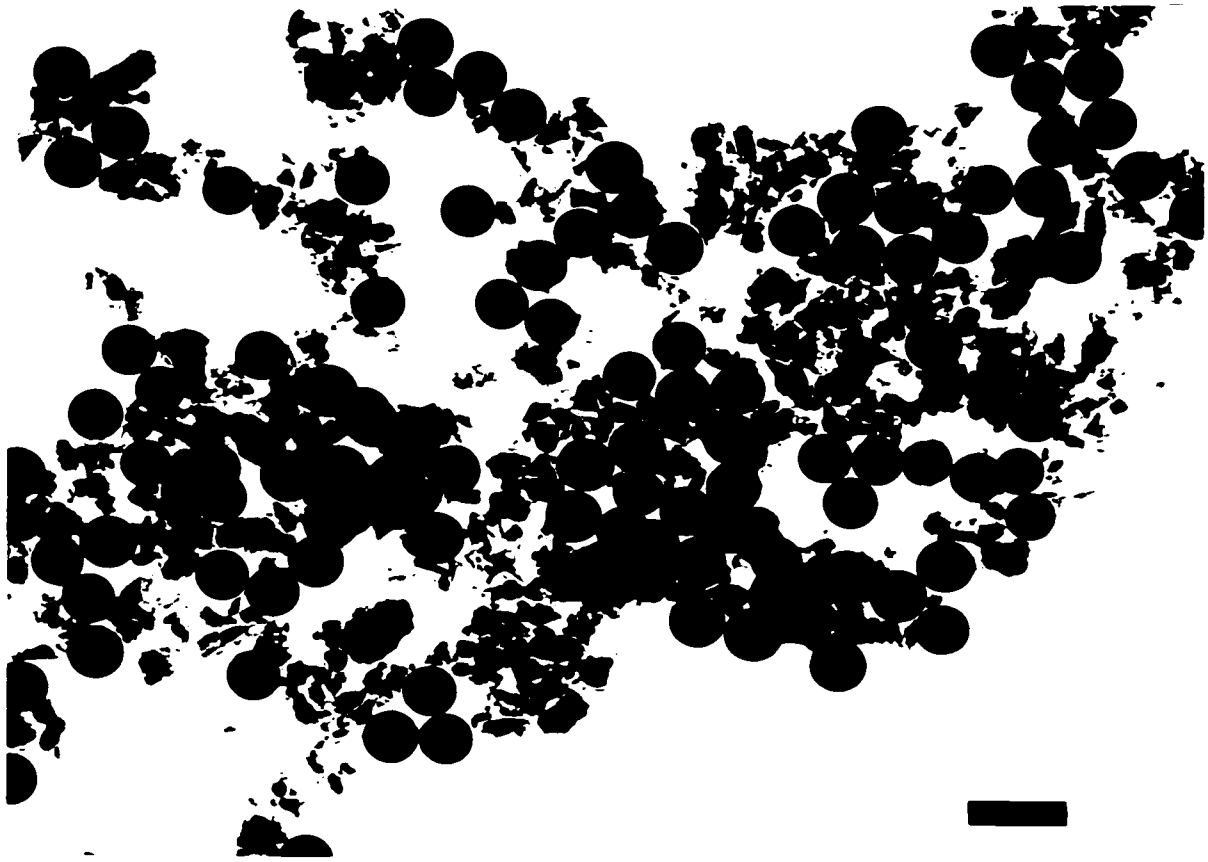

Figure 6.30 TEM micrograph showing the magnesia-silica heterocoagulate particles prepared at operational pH 9.89 with composition of 10 vol% magnesia (Bar = 1 μm).

charged surface (high zeta potential), thus homocoagulation is prevented.

Figure 6. 31 shows the total interaction potential curves for silica-silica, alumina-alumina and silica-alumina particles at an operational pH value of 2.77. The strong attraction energy between the silica and alumina particles results in heterocoagulation. A high potential barrier exists between same particles (alumina-alumina and silica-silica), thus preventing homocoagulation.

The morphology of heterocoagulate formed is shown in Figure 6.32. Heterocoagulation occurs predominantly in comparison with the other two homocoagulations.

Comparison of Figure 6.32 with Figure 6.28 Illustrates the level of structure control that may be imposed via selective destabilization. The fractional coverage of small alumina particles on the large silica spheres, decreases with selective destabilization of the alumina particles.

Similar behaviour was observed for the magnesia-silica system at an operational pH value of 8.73. The total interaction potential curves for this system are plotted in Figure 6.33. The morphology of the heterocoagulate formed is shown in Figure 6.34.

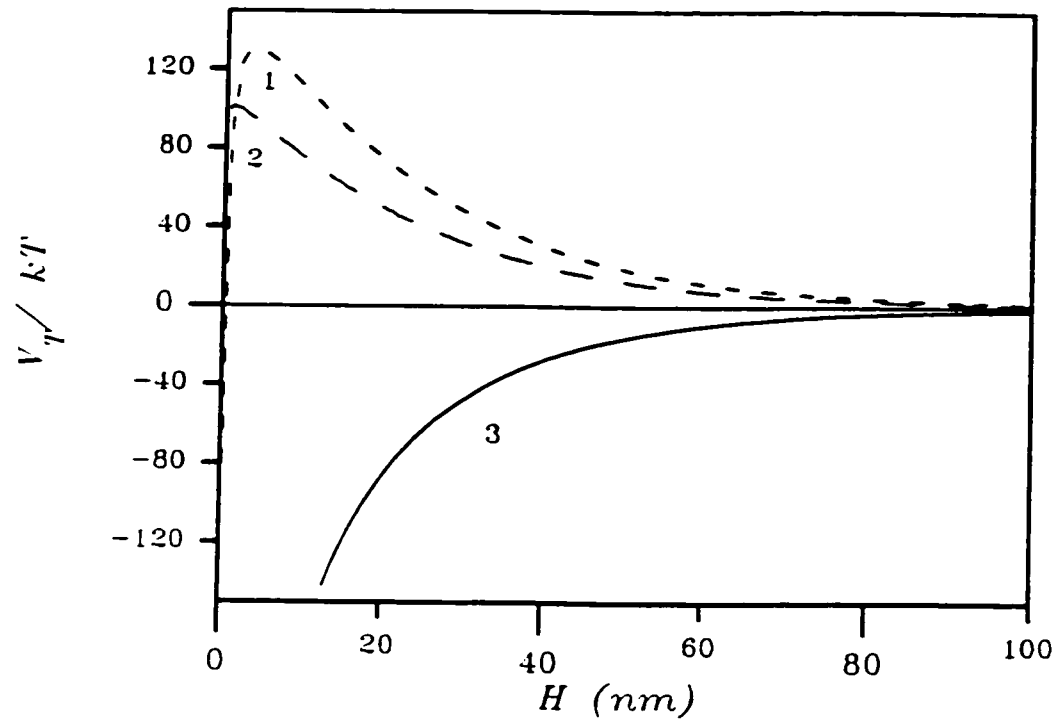

Figure 6.31 The total interaction potential between silica-silica (curve 2), alumina-alumina (curve 1) and silica-alumina (curve 3) particles in EtOH at operational pH 2.77.

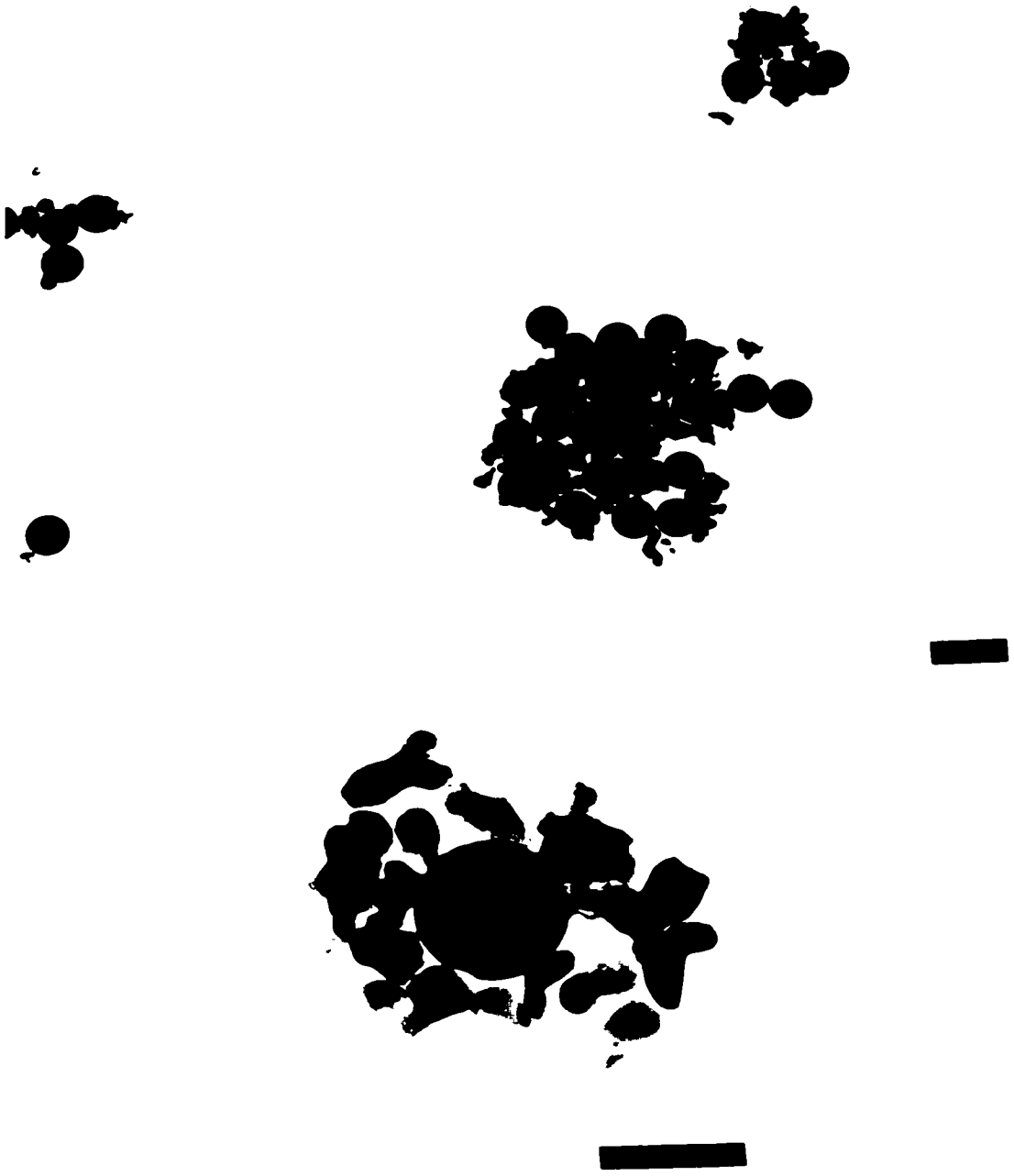

Figure 6.32 TEM micrograph showing achievement of predominantly heterocoagulation between alumina and silica at operational pH 2.77 with composition of 10 vol% alumina (Bar = 1 μm in (A) and 0.5 μm in (B)).

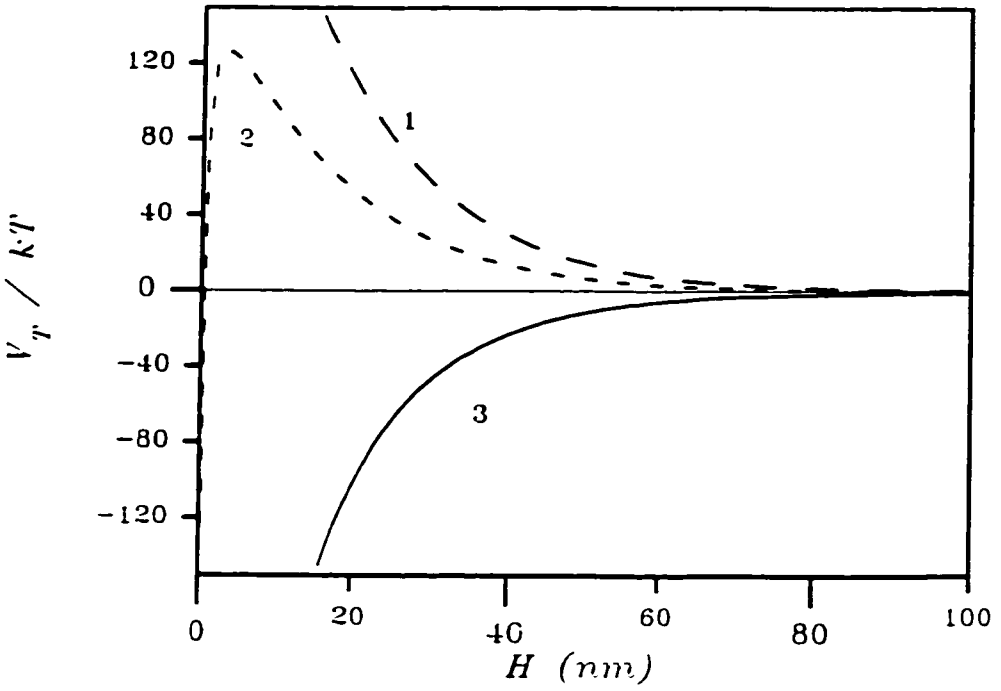

Figure 6.33 The total interaction potential between silica-silica (curve 1), magnesia-magnesia (curve 2) and silica-magnesia (curve 3) particles in EtOH at operational pH 8.73.

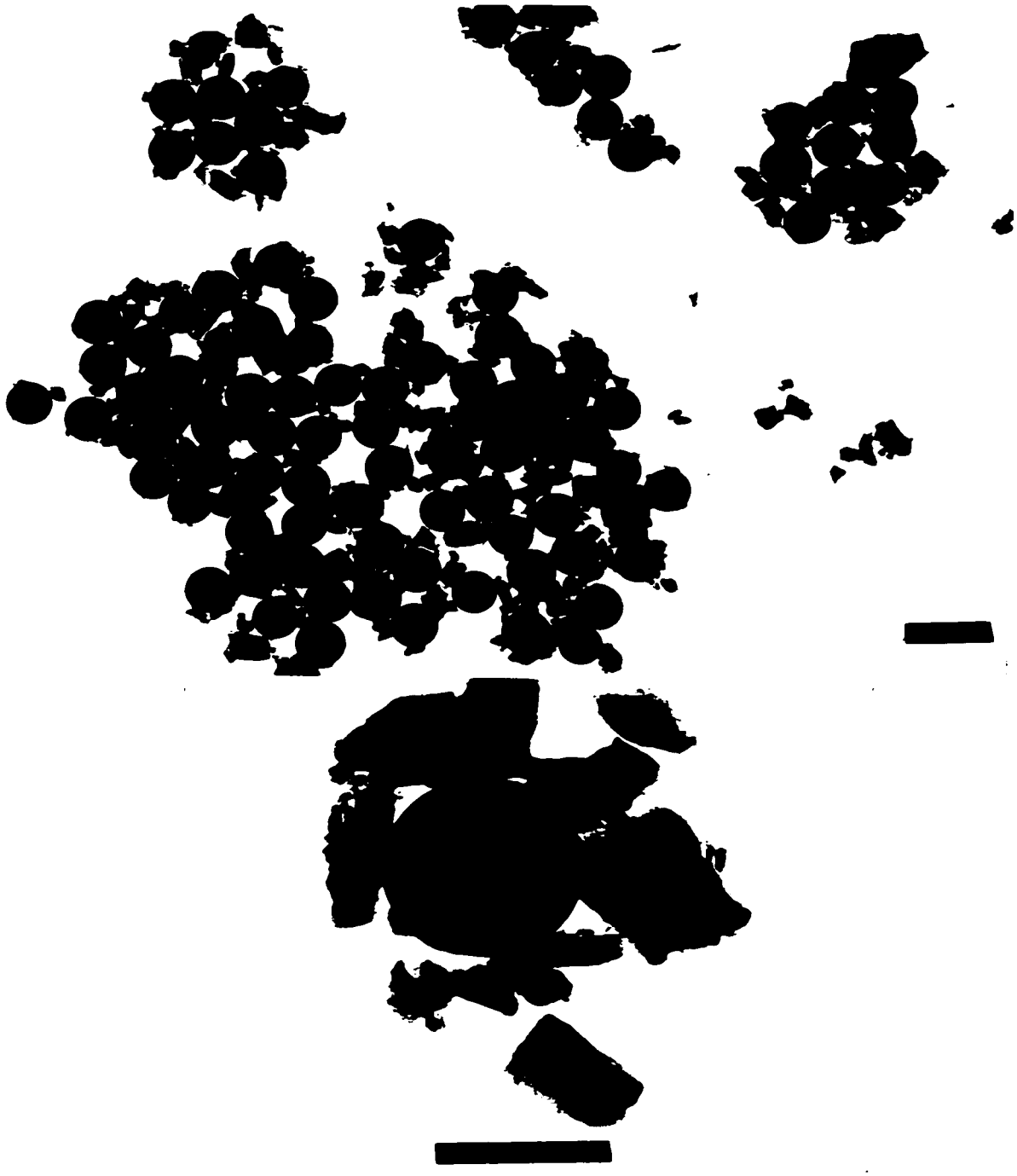

Figure 6.34 TEM micrograph showing achievement of predominantly heterocoagulation between magnesia and silica at operational pH 8.73 with composition of 10 vol% magnesia (Bar = 1 μm in (A) and 0.5 μm in (B)).

VI-4 The Surface Chemistry and Rheology of Ionically-stabilized Alumina Suspensions in Polar Organic Media

VI-4.1 Introduction

Colloidal suspension rheology is strongly influenced by the surface chemistry, concentration, size distribution and shape of the suspended particles, as well as the chemical nature of the solvents. The surface chemistry control is an effective method of rheological property modification, that results in control of the range and magnitude of the interparticle forces. The latter can change the viscosity and yield stress by several orders of magnitude. The parameter often used to characterize the surface properties of the colloids is the zeta potential for ionically stabilized suspensions. Hunter (1981) proposed the extrapolated Bingham yield stress should decrease proportionally with the square of the zeta potential.

The ionic strength of the suspension also alters the interparticle interaction. This section describes how the surface chemistry and interparticle forces were manipulated via the ionic strength of polar organic suspensions. Alumina powder was used to model the rheological properties of oxides in polar organic solvents without dispersants. The interrelations between ionic strength, stability, solid-loading and rheological properties are established.

VI-4.2 The Dissociation of Electrolytes

Figure 6.35 shows the equivalent conductance, Λ, for LiCl in EtOH and DMSO as a function of electrolyte concentration. The equivalent conductivity decreased with electrolyte concentration. The effect was most dramatic in EtOH and less so in DMSO. This is typical for weak electrolytes and is indicative of ion-pair formation (Robinson and Stokes, 1959). According to the Eigen-Denison-Ramsey-Fuoss (EDRF) ion-pair formation model (Gordon, 1975), it is assumed that ions are only associated when they touch. An expression for the association constant for;

$$C^+ + A^- \overset{K_{assoc}}{\Longleftrightarrow} C^+A^-$$

can be written:

$$K_{assoc} = \frac{4\pi N a_o^3}{3000} e^b \quad (6.2)$$

where N is the Avagadro number, a_o the center-to-center distance of the ions in contact and

$$b = |z_C z_A| e^2/a_o \varepsilon_r kT \quad (6.3)$$

A handy form of this equation at 25°C, is;

$$pK_{assoc} = 2.598 - 3 \log a_o (Å) - b/2.303 \quad (6.4)$$

$$\text{where} \quad b = 560.43 |z_C z_A|/a_o(Å)\varepsilon_r \quad (6.5)$$

which assumes a_o = 5 Å, T = 25°C and the association constants (K_{assoc}) for LiCl are 3.3 in DMSO and 32 in EtOH, respectively.

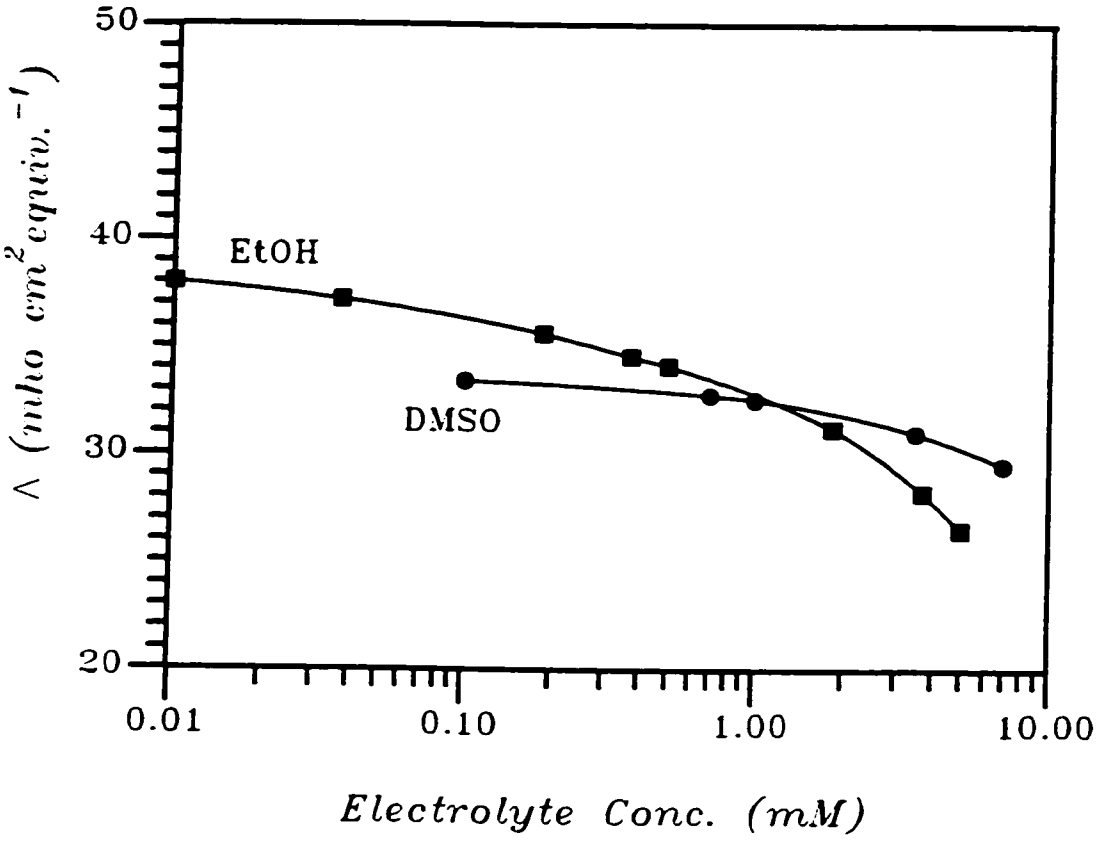

Figure 6.35 Equivalent conductance as a function of LiCl electrolyte concentration in EtOH and DMSO.

The conductivity data were analyzed using the Ostwald dilution law (Eq. 2.67). The Ostwald dilution law plots for LiCl in EtOH and DMSO are shown in Figure 6.36. The intercept gives Λ_o = 36.6 mho cm^2 equiv.$^{-1}$ for EtOH and 33.3 mho cm^2 equiv.$^{-1}$ for DMSO, respectively.

The degree of dissociation of LiCl in EtOH and DMSO was estimated from the conductivity measurements (Eq. 2.64) and Table 6.13 lists the concentrations of dissociated ions, C_i, calculated for the former and latter.

Also shown in Table 6.13 are the κa values for LiCl in EtOH and DMSO, corrected for ion-pair formation.

Table 6.13

Comparison of the Total Concentration of Electrolyte (LiCl) in EtOH and DMSO, C_o, with the Concentration of the Dissociated Electrolyte, C_i, Estimated from the Conductivity Data. Also Shown Are the Corresponding Estimated κ^{-1} and κa Values

EtOH				DMSO			
C_o (mM)	C_i (mM)	κ^{-1} (nm)	κa	C_o (mM)	C_i (mM)	κ^{-1} (nm)	κa
0.050	0.050	23.9	4.60	0.10	0.10	23.0	4.87
0.20	0.19	12.3	8.95	1.0	0.98	7.35	15.0
0.50	0.46	7.89	14.0	3.5	3.26	4.03	27.3
2.0	1.69	4.12	26.7	7.0	6.21	2.92	37.6
5.0	3.60	2.82	38.9				

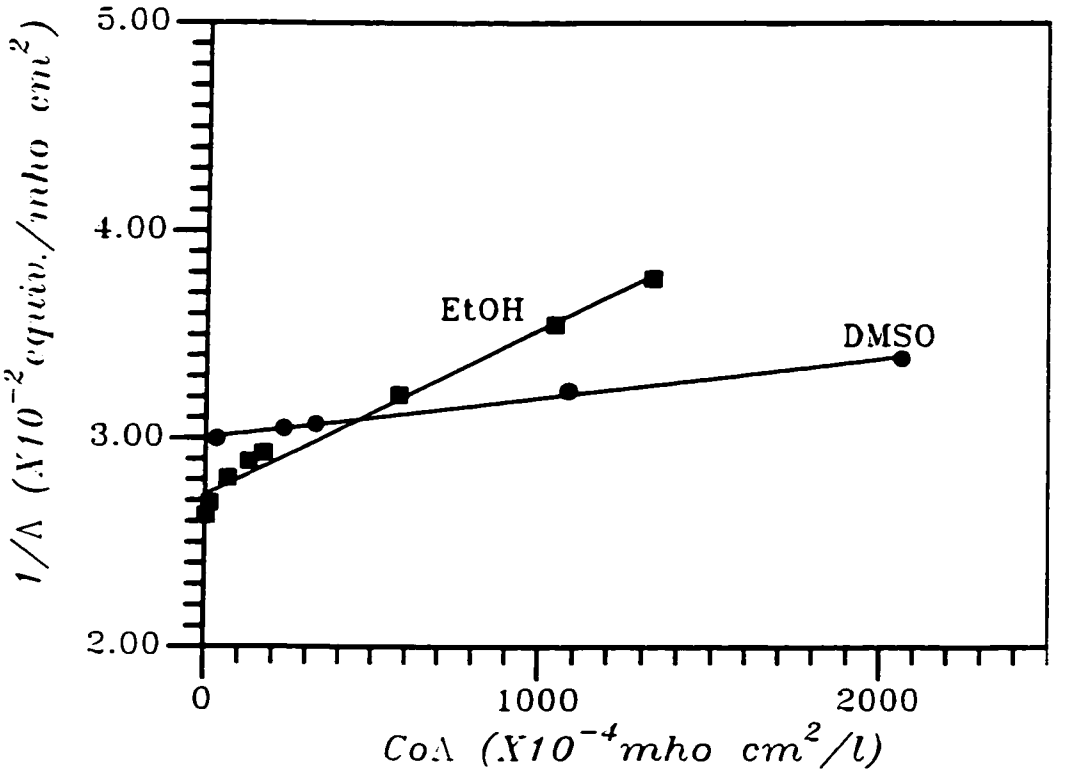

Figure 6.36 Ostwald dilution law plots for LiCl in EtOH and DMSO.

VI-4.3 The Electrokinetic Behaviour

The electrophoretic mobilities of alumina particles in EtOH and DMSO solutions containing LiCl are shown in Figure 6.37 as a function of electrolyte concentration. The mobility decreases with increasing LiCl concentration. The LiCl addition has less effect on the electrophoretic mobility of alumina in DMSO.

The low dielectric constant of organic liquids limit the dissociation of surface groups and additional mechanisms must be suggested to understand the charge developed on the suspended alumina particles.

The mechanism of charging in EtOH, a protic organic liquid, should be similar to water, i.e., proton transfer. This mechanism is based on the particle (P) in solvent (S) functioning as a proton donor or acceptor. The sign of the charge will depend on the direction of transfer (Lyklema, 1968), i.e.;

$$PH_2^+ + S^- \rightleftharpoons PH + SH \rightleftharpoons P^- + SH_2^+$$

where PH and SH are the surface groups on the particle and the solvent molecule, respectively. The relative acid-base character of the solid surface and the liquid determines the sign of the charge. The predominant form of the species on the partially hydrated alumina surfaces should be AlOH. These act as basic sites relative to EtOH. Therefore, the charging of alumina particles in EtOH could be attributed to acid-base reactions occuring at the interface in three steps similar to those proposed by Fowkes (1987) via a dynamic adsorption-dissociation-desorption process, i.e.;

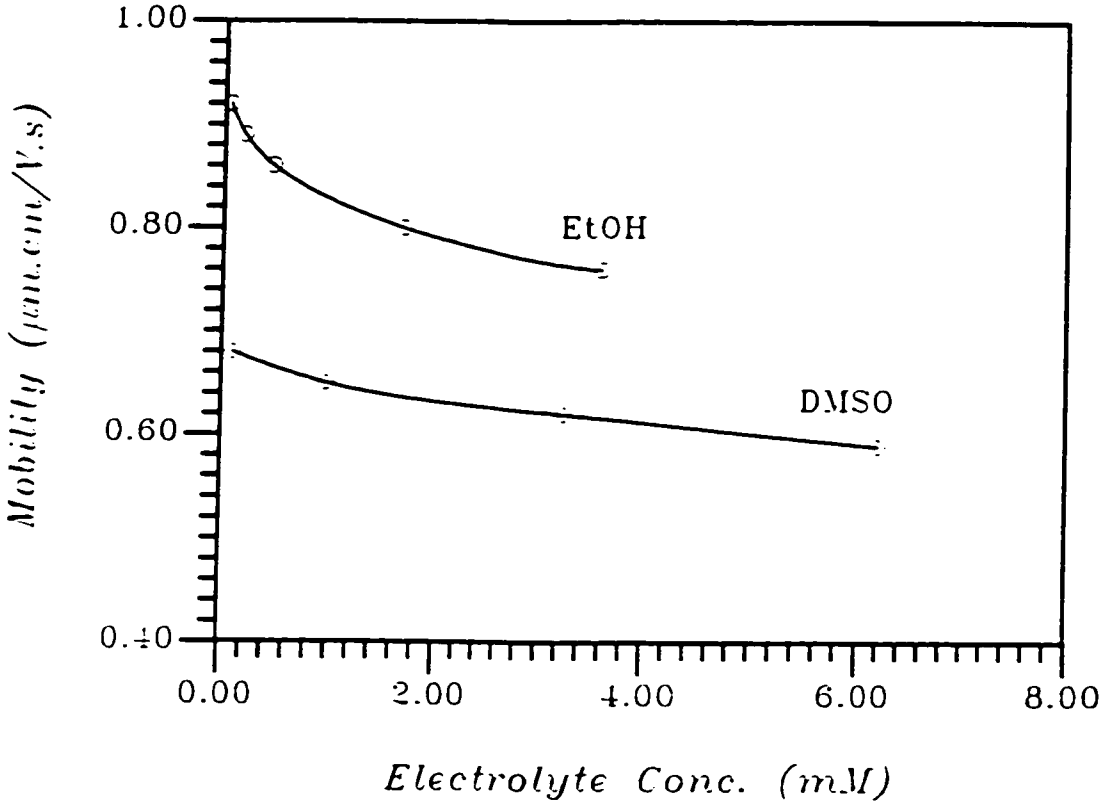

Figure 6.37 The variation of electrophoretic mobility for colloidal alumina in EtOH and DMSO as a function of LiCl concentration. (LiCl concentrations shown in graph are the concentrations of dissociated ions listed in Table 6.13).

1) adsorption of EtOH molecules in undissociated form on the basic surface sites of the alumina particles;
2) dissociation of the adsorbed EtOH molecules by proton transfer to the basic surface sites (AlOH), i.e.;

$$AlOH + C_2H_5OH = AlOH_2^+ + C_2H_5O^-$$

and 3) desorption of the $C_2H_5O^-$ anions into the solution thus leaving the alumina particles positively charged. Besides this proton transfer, the adsorption of water onto the particle surface renders it more positive (Lyklema, 1968).

The acid-base theory can also be applied to aprotic organic solvents such as DMSO. Lyklema (1968) proposed that the protons and hydroxyl ions, originating from the water impurity in the dispersions, act as the potential-determining ions and the relative acidity of both solvent and particle determine the sign of the charge on the latter. The surface charging mechanism, for alumina particles dispersed in DMSO, is;

$$AlOH + (CH_3)_2SO + H^+ + OH^- = AlOH_2^+ + (CH_3)_2SO + OH^-$$

VI-4.4 The Total Interaction between Alumina Particle Pairs

DLVO theory suggests the interaction between colloidal particles be governed by the ionic repulsion and the London-van der Waals attraction forces. Thus, there should be a point where the sum of repulsion and attraction is large enough to form a kinetic barrier if irreversible coagulation is to be avoided.

DLVO theory was used to calculate the total interaction potential energies and forces for pairs of identical alumina particles in EtOH and DMSO with LiCl addition. (A_{131} for alumina in EtOH and DMSO was approximated as 3.81 X 10^{-20} J and 1.99 X 10^{-20} J, using Eq. 2.49 and the data from Table 4.2).

The concentration of ionic species in the suspensions (κ) and the particle surface potentials (ζ) are required to calculate the ionic repulsion. The volume-fraction-dependent Debye screening parameter, κ_o, for concentrated suspensions is determined via the mean-field method of Russel and Benzing (1981), i.e.;

$$\kappa_o^2 = 2\frac{e^2 z^2 n_o}{\varepsilon_o \varepsilon_r kT}\frac{1+R(1+R^2)^{1/2}+R^2}{(1+R^2)^{1/2}+R} \qquad (6.6)$$

Here R = 3/2 ($q/eazn_o$)$\varphi/(1-\varphi)$, is a measure of the ratio of counterions to excess electrolyte in the fluid and q is the surface charge density.

When R<<1,

$$\kappa_o^2 \approx \frac{2e^2 z^2 n_o}{\varepsilon_o \ \varepsilon_r kT} = \kappa^2$$

When R>>1, however, i.e.; at finite concentrations with little or no excess electrolyte, then;

$$\kappa_o^2 \approx 3\frac{ezq}{\varepsilon_o \varepsilon_r akT}\frac{\varphi}{1-\varphi}$$

This equation indicates the counterions are entirely responsible for shielding the surface charge.

The relevant zeta potentials and density of the diffuse layer charge (σ_d) for dilute suspensions were calculated via a computer program (WinMobil, Department of Mathematics, University of Melbourne, Australia) based on the expressions derived by O'Brien and White (1978). The surface charge density ($q = - \sigma_d$) was estimated as - 10^{-4} C m^{-2} for the presently studied range of electrolyte concentration. The ratio of counterions to excess electrolyte in the fluid, R, was thus estimated as - 0.01 << 1 for a = 0.12 μm, φ = 0.1 and n_o = 6 X 10^{22} $1/m^3$ (C_i = 10^{-4} M). Thus, for the semi-dilute suspensions in this study, the volume-fraction-dependent Debye screening parameter (κ_o), can be replaced by the conventional Debye length (κ).

Zeta potentials were calculated from the electrophoretic mobilities given in Figure 6.37 and the results are given in Figure 6.38. The total interaction energies (Eqs 2.40 and 2.44) and forces (Eqs 2.42 and 2.45) versus distance between the particles are shown in Figures 6.39 and 6.40. The results demonstrate considerable repulsive barriers develop. To stabilize colloidal systems, a repulsive barrier of 15 kT is required and Figures 6.39 and 6.40 demonstrate this condition is met for the systems studied, by controlling the electrolyte concentration. Table 6.14 summarises the repulsive energy barrier, maximum repulsive force and pressure for the systems studied. This data indicates that all suspensions should be stable against flocculation except the one in EtOH at C_i of 3.60 mM. The sensitivity of the stability of alumina in EtOH, to small concentrations of LiCl is higher than in DMSO.

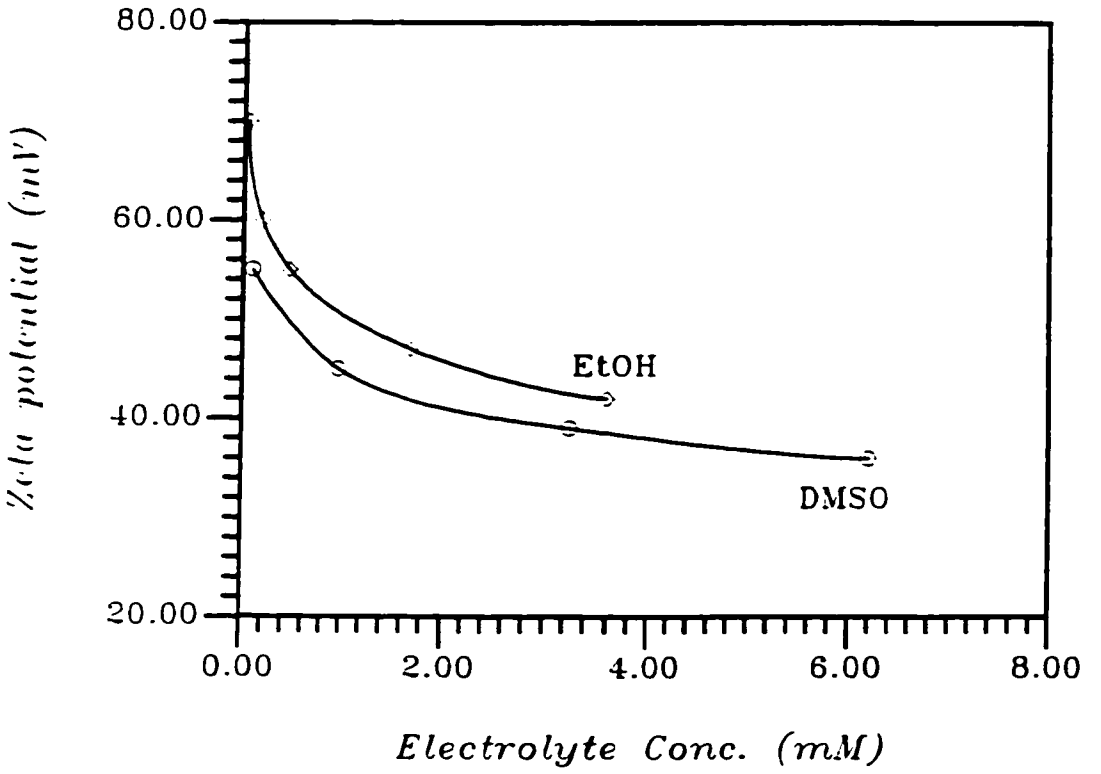

Figure 6.38 The variation of zeta potential of colloidal alumina in EtOH and DMSO as a function of LiCl concentration. (LiCl concentrations shown in graph are the concentrations of dissociated ions listed in Table 6.13).

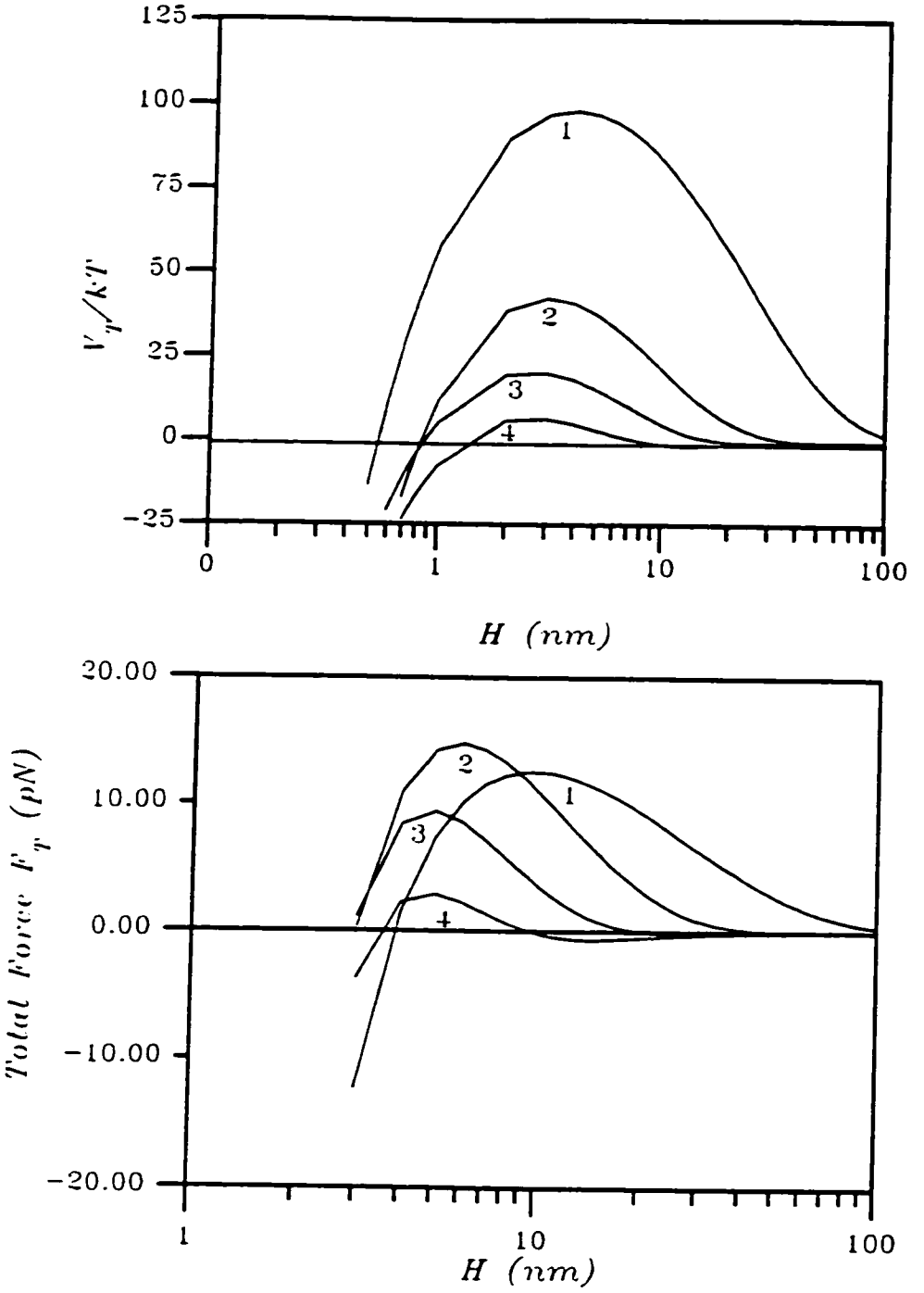

Figure 6. 39 Total interaction energies (a) and forces (b) as a function of particle separation for a pair of alumina particles in EtOH with additions of LiCl (line 1: C_i = 0.05 mM, ζ = 70 mV; line 2: C_i = 0.46 mM, ζ = 55 mV; line 3: C_i = 1.69 mM, ζ = 47 mV; line 4: C_i = 3.60 mM, ζ = 42 mV).

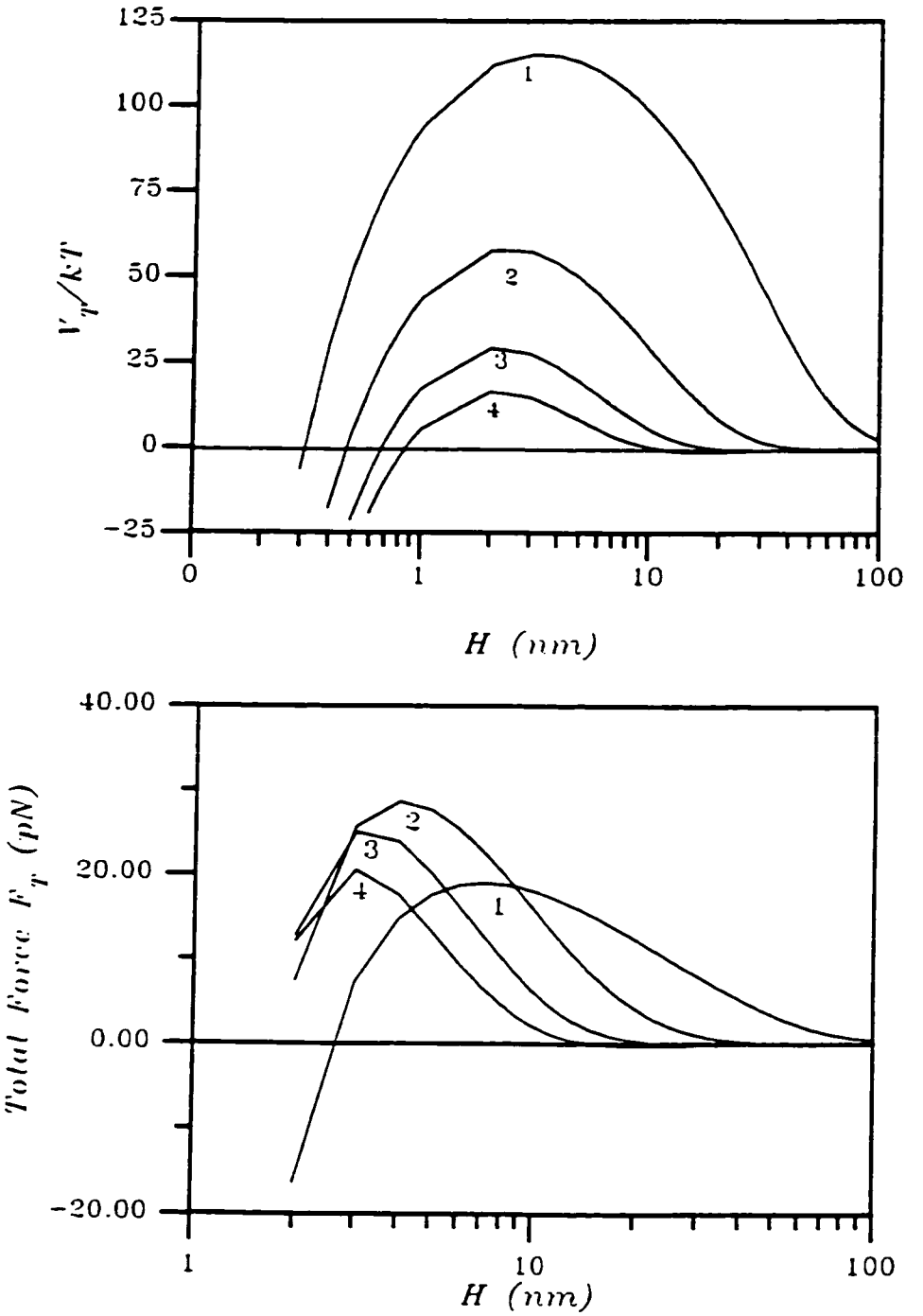

Figure 6.40 Total interaction energies (a) and forces (b) as a function of particle separation for a pair of alumina particles in DMSO, with additions of LiCl (line 1: C_i = 0.10 mM, ζ = 55 mV; line 2: C_i = 0.98 mM, ζ = 45 mV; line 3: C_i = 3.26 mM, ζ = 39 mV; line 4: C_i = 6.21 mM, ζ = 36 mV).

Similar observations have been reported for goethite (α-FeOOH) in acetone-water mixtures wherein the sensitivity of the organosols to additions of $LiNO_3$, increased as the dielectric permittivity decreased (De Rooy et al, 1980). This is not unexpected as lower dielectric permittivity implies stronger electrostatic interaction between the surface charge and the counterions.

Table 6.14

Total DLVO Interaction Energy, Force and Pressure for Two Alumina Particles at Different LiCl Concentrations in EtOH and DMSO

	C_i (mM)	V_T (max) (kT)	F_T (max)* (pN)	A (eff.) ($x10^{15}$ m^2)	P_T(max)* (kN/m^2)
EtOH	0.05	98.0	12.5	8.3	1.5
	0.46	42.4	14.8	2.7	5.4
	1.69	20.2	9.4	1.5	6.3
	3.60	6.5			
DMSO	0.1	115.2	19.0	7.9	2.4
	0.98	57.7	28.6	2.6	11.2
	3.26	29.2	25.0	1.4	18.1
	6.21	16.4	20.6	1.0	20.6

* F_T(max) and P_T(max) were calculated when V_T(max) > 15 kT.

A suspension is termed stable if the dispersed particles do not coagulate but remain as discrete, single particles. Particle size measurements were conducted on alumina particles in EtOH and DMSO at various LiCl concentrations. Plots of the geometric equivalent, surface-average of the surface equivalent diameter, $_G\langle D_s \rangle_{32}$, as a function of electrolyte concentration are shown in Figure 6.41. No significant particle agglomeration is observed up to 1.7 mM in EtOH and 6.21 mM in DMSO. These observations are in good agreement with theoretical predictions.

VI-4.5 The Rheology of the Alumina Suspensions in EtOH and DMSO

The viscosity of alumina particles dispersed in EtOH and DMSO vs. shear rate at various concentrations of LiCl are shown in Figure 6.42.

The viscosity decreases with increasing salt concentration via suppression of the secondary electroviscous effect (Krieger and Eguiluz, 1976). Both primary and secondary electroviscous mechanisms, for semi-dilute suspensions, are active but the latter is more important due to the greater probability of particle interaction.

The decrease of viscosity with increasing electrolyte concentration is explained in terms of the effective particle radius including the thickness of the electrical double layers (Brodnyan and Kelley, 1965). The effective volume is determined by the volume of the particles plus the volume of the double layer. The latter prevents particles approaching. Increasing the electrolyte concentration

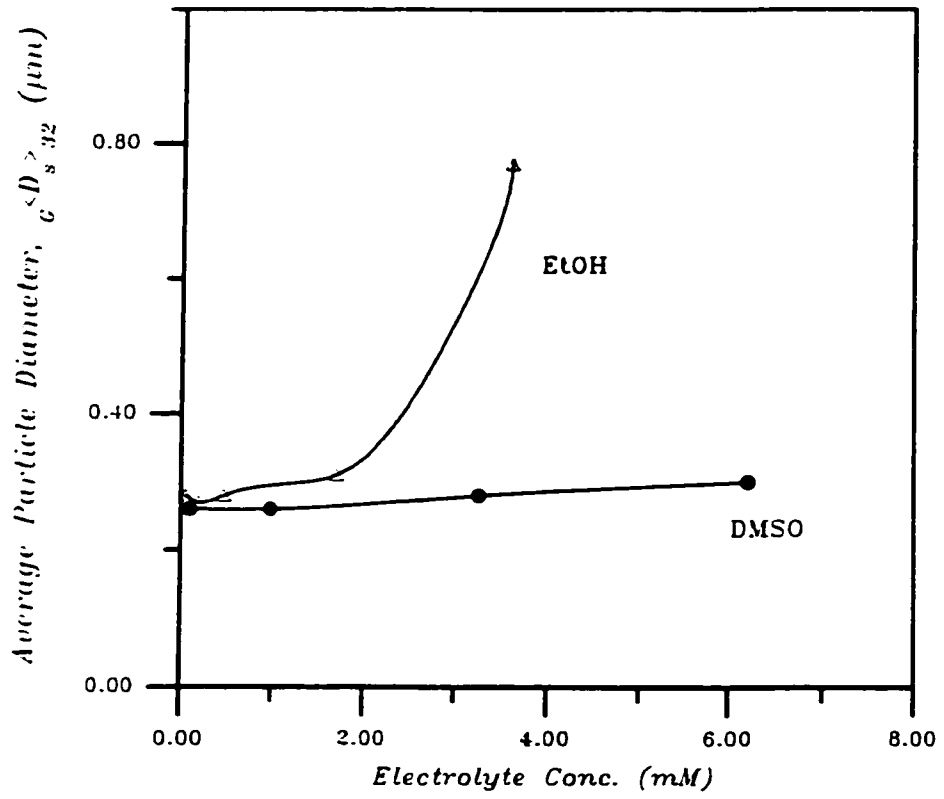

Figure 6.41 Average particle diameter as a function of LiCl concentration.

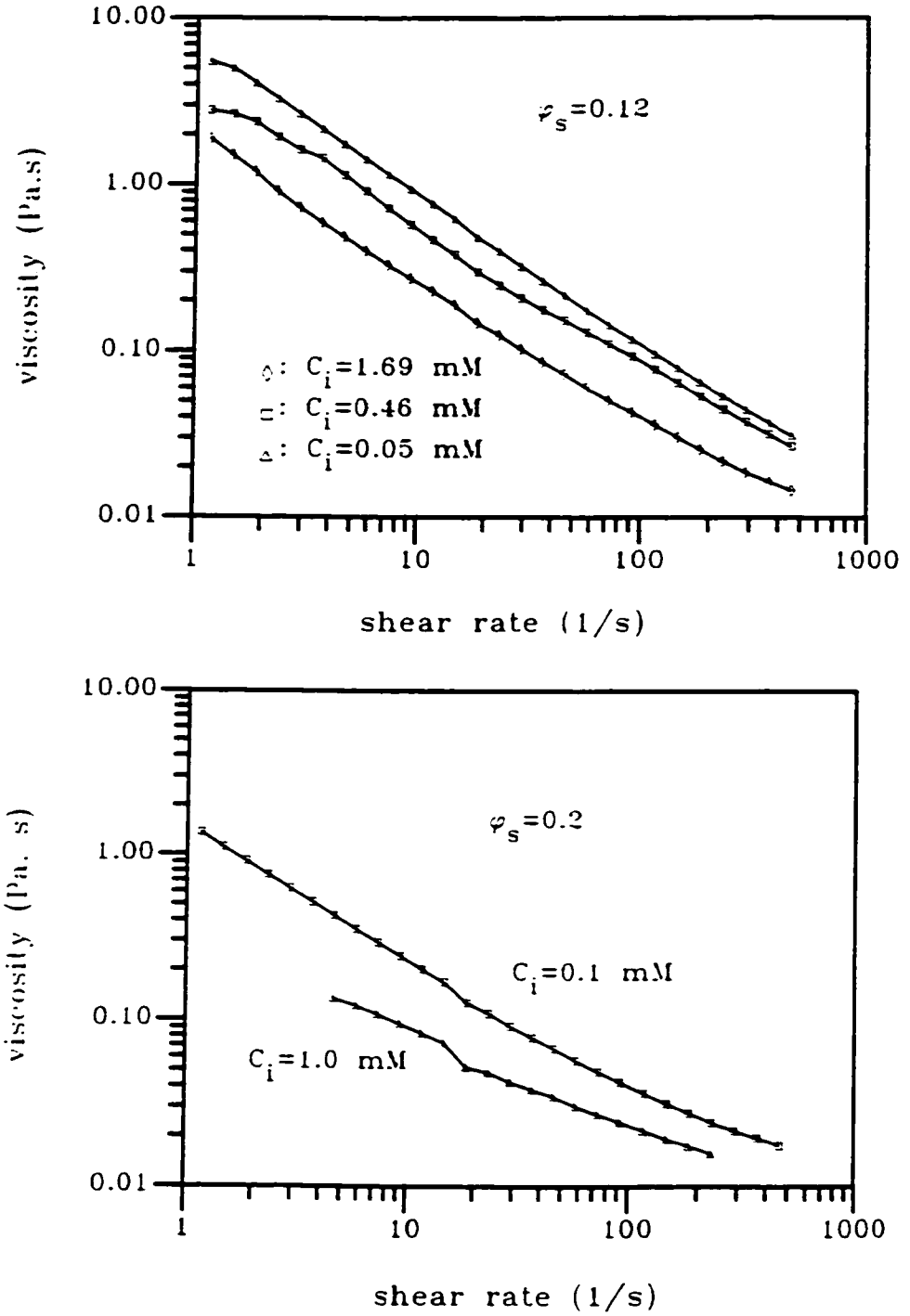

Figure 6.42 Viscosity versus shear rate of suspensions containing alumina powder dispersed in EtOH (a) and DMSO (b) as a function of LiCl concentration.

decreases the extent of the double layer and results in a decrease of the effective volume fraction of the particles.

To increase the actual volume fraction of the particles, whilst maintaining a fluid suspension, the double layers must be compressed, i.e., their effective volume fraction be reduced so $\varphi_{eff} \sim \varphi_s$. Clearly, if colloid stability is to be maintained, the electrolyte concentration should not exceed the critical coagulation concentration (CCC).

The observed shear thinning shown in Figure 6.42 is also explained by the secondary electroviscous effect. As the particles pass one another, their double layers overlap and they are displaced in a direction perpendicular to the lines of liquid flow thus increasing the energy dissipated. The total displacement will be less the more rapidly particles pass. This explains the decrease of viscosity with increasing shear rate (Brodnyan and Kelley, 1965).

Eq.2.41 shows the ionic repulsion (at a given separation distance κH, in Debye length) depends on the product of the dielectric constant and the square of the zeta potential. Thus the zeta potential in EtOH ($\varepsilon_r = 24.3$) must be 1.4 times that in DMSO ($\varepsilon_r = 45.0$) to produce the same repulsion. To meet this condition, zeta potentials of 39 mV in DMSO ($C_i = 3.26$ mM) and 55 mV in EtOH ($C_i = 0.46$ mM) were taken from Figure 6.38. The effect of the solvent on the relative viscosity of the alumina suspensions at same ionic repulsion is shown in Figure 6.43. The solvent has a marked influence on the relative viscosity, e.g.; at $\eta_r = 50$, the solid

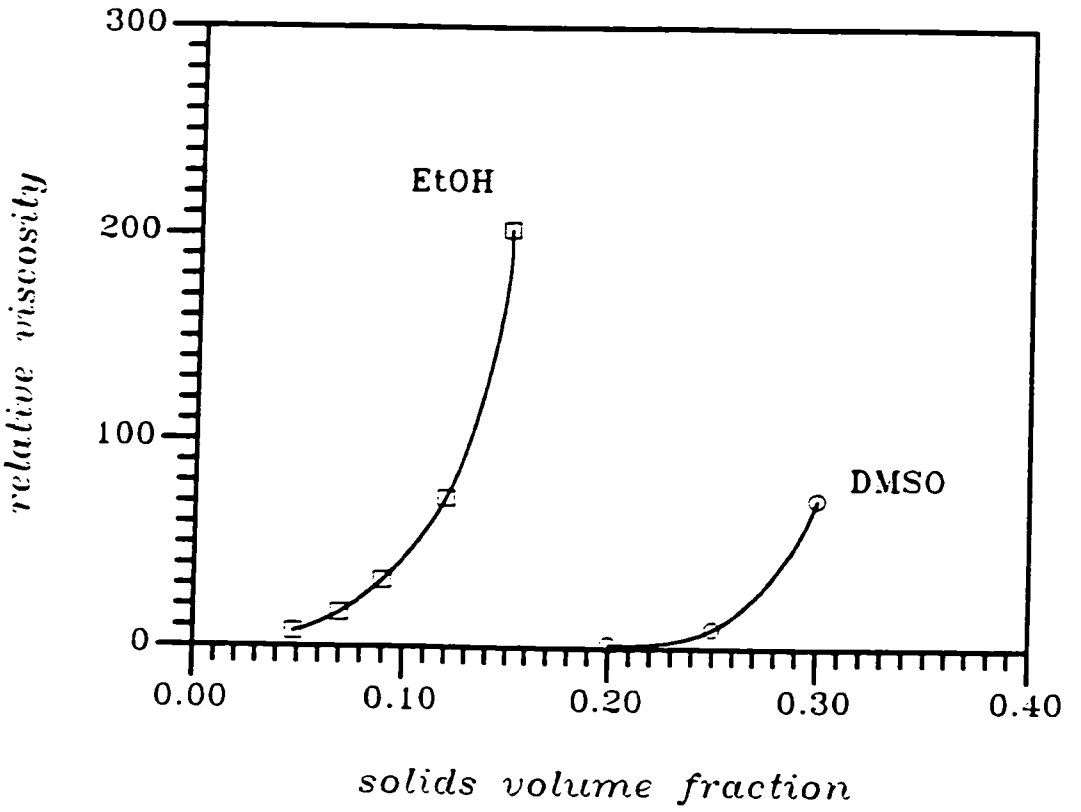

Figure 6.43 The relative viscosity of alumina in EtOH and DMSO suspensions as a function of the volume fraction of solids (at same ionic repulsion, shear rate D = 116 s^{-1}).

volume fraction (φ_s) increased from 0.11 in EtOH to 0.29 in DMSO. The enhancement of solid loading achieved in DMSO is due to the reduced excluded volume, i.e., κ^{-1} ~ 4 nm in comparison with κ^{-1} ~ 8 nm in EtOH (from Table 6.13). Therefore, at the same magnitude of ionic repulsion, the rheological properties of the suspension relate directly to the Debye length which characterises the range of the ionic interparticle repulsion. Thus the colloidal processing of ceramics would be best achieved in DMSO.

The shear stress was found to be lower for alumina particles dispersed in EtOH, whilst the shear rate was being stepped up, relative to being stepped down for increasing solid volume fraction (the equilibration time was 50 s at each shear rate) (Figure 6.44a). Similar behaviour was observed for alumina particles dispersed in DMSO (Figure 6.44b). This behaviour is due to the shear-induced flocculation. Warren (1975) found that the aggregation of ultrafine particles occurred at high shear speeds. The rate and the extent of aggregation increases with suspension concentration as a consequence of the high collision rate between particles. Therefore, in the present study, the hysteresis observed at high volume fractions of alumina reflects the increase of the size of the flow unit as the result of the extensive flocculation that occurs at high shear rates.

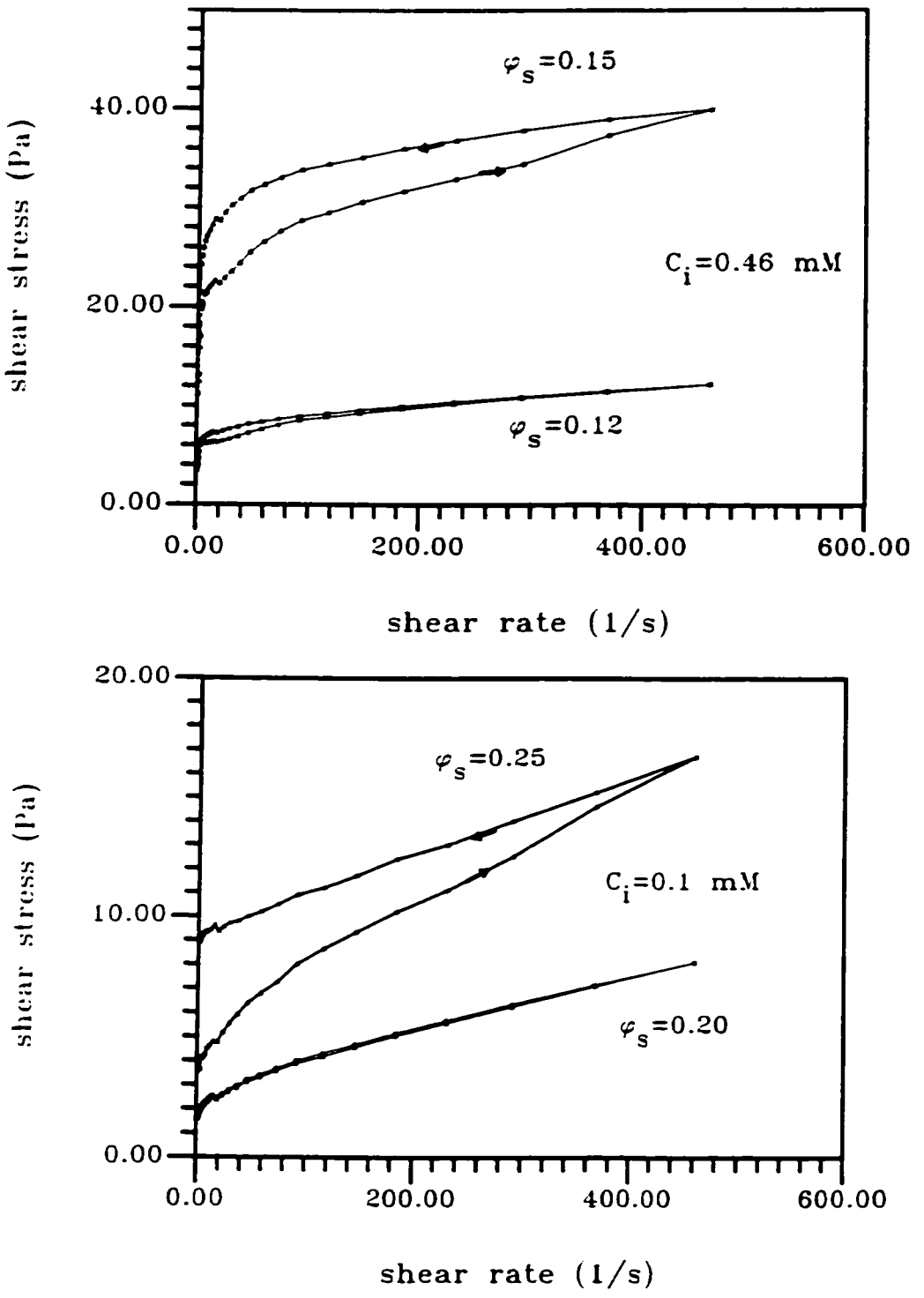

Figure 6.44 Flow properties of alumina in (a) EtOH and (b) DMSO suspensions. Arrows indicate the direction in which the shear rate was changed. The equilibration time was 50 s at each shear rate.

CHAPTER VII

CONCLUSIONS

When oxide powders are dispersed in EtOH, (a protic polar non-aqueous solvent), an acidity-dependent, electrical charge is induced on the particle surfaces. The charging mechanism for this case is the adsorption of protons or hydroxyls onto the surface sites of the oxide particles (MOH).

The acidity of ethanolic solutions can be determined via ion-transfer functions. The operational-pH-meter readings in ethanolic solution are converted to pa_H (referred to the aqueous standard state).

Electrophoretic mobility results identify the isoelectric points of oxide particles in EtOH and these can be used to characterize the surface acidity of oxide particles in EtOH.

It was found that high surface charge (zeta potential) and certain levels of ionic concentration in the solution can be achieved at the same time by addition of a simple acid or base.

DLVO theory was used to generate curves of the total interaction energy and forces vs. particle separation along the line joining spherical particle centres. The results predict that, for oxide particles dispersed in EtOH, ionic stabilization

can be achieved by controlling the acidity of suspensions. In the case where the zeta potential is high but the ionic strength low and a low repulsive force results, the ionic stability of oxide particles in EtOH can be better controlled by the combination of potential-determining-ions and indifferent-electrolyte to optimize the values of repulsive potential and repulsive force (pressure). It was also found that the colloidal stability of oxide particles in ethanol solutions is sensitive to salt addition and there is a range of electrolyte concentration that leads to a repulsive force high enough to stabilize the oxide, non-aqueous suspensions.

The experimentally determined stability ratios indicate a close correlation with the stability predicted by DLVO theory. This result shows that oxide particles can be charge-stabilized as in aqueous suspensions.

The viscosity and flow curves for oxide/ethanol suspensions are acidity dependent. The flow curves for the suspensions followed the Casson model in the range of shear rates investigated. The Casson yield value, τ_c, was used to evaluate the stability of the suspensions.

Maximum τ_c is observed at particular operational pH values in Al_2O_3/EtOH and MgO/EtOH systems. These maxima should occur at the iso-electric point (IEP) where the zeta-potential of the particles is zero but the iso-electric points (IEPs) for alumina and magnesia in ethanol, as determined by electrophoretic light scattering in dilute suspensions, disagree with the operational pH values for maximum Casson yield values.

Dynamic electrophoretic mobility was measured by electrokinetic sonic analysis (ESA) for > 1 vol% alumina and magnesia in ethanol. The IEP values obtained agreed with the operational-pH values for maximum Casson yield values. It was found that the IEP of alumina and magnesia shifts to higher operational-pH values on increasing the solid concentration whilst both dilute and concentrated aqueous suspensions of alumina, give the same isoelectric point.

The maximum Casson yield value was not observed at the iso-electric point in SiO_2/EtOH suspensions. This indicates that SiO_2/EtOH suspensions are stable near the IEP in spite of the low zeta potential and consequent low repulsive energy barrier thereat. This observation does not agree with the stability predictions of the DLVO theory and suggests the colloidal stability of silica in ethanol is not explained exclusively by ionic stability as per the DLVO theory. It would appear that a thin, steric barrier of a silicic-acid-gel network exists at the silica particle surfaces and this explains the rheological results for SiO_2 in ethanol.

Heterocoagulation can be brought about if the two particles types are stable over significantly-differing, acidity regimes. The essential part of this process is the adjustment of surface charges on the particles of each component. This can be done by appropriately adjusting the acidity of the suspensions.

Results indicate the critical importance of the relative colloidal stability of different particulate species in determining the morphology of the binary system.

It was demonstrated that, a variety of different heterocoagulate morphologies can be obtained by manipulation of the relative colloidal stability of the components,.

The surface chemistry and rheological properties of ionically stabilized, semi-dilute alumina suspensions in EtOH and DMSO are strongly influenced by ionic strength.

It was found that, over the range of particle volume fraction and ionic strength studied, the screening parameter, κ, is determined mainly by the concentration of added electrolyte. It was also found that self-screening is insignificant. The particle interaction potential and force can thus be calculated from DLVO theory. The resulting calculations suggest interparticle interactions can be dominated by the ionic repulsion via control of the electrolyte concentration and the sensitivity of the stability of alumina in polar organic media to small concentrations of indifferent electrolyte, increases with decreasing media dielectric constant.

Rheological measurements show the viscosity of the Al_2O_3-EtOH and Al_2O_3-DMSO suspensions decreases with increasing salt concentration due to suppression of the second electroviscous effect. It was also found, the solvent has a marked influence on the Al_2O_3 suspension rheology.

REFERENCES

Abramson, H. A., Moyer, L. S. and Gorin, M. H. (1942). "Electrophoresis of Proteins," Reinhold, New York.

Albers, W., Overbeek, J. Th. G., J. Colloid Sci., (1959) **14**, 501

Barringer, E. A., Novich, B. E. and Ring, T. A. (1984). J. Colloid Interface Sci., **100**, 584.

Barouch, E. and Matijevic, E., Ring, T. A. and Finlan, J. M., (1978) J. Colloid Interface Sci., **67**, 1.

Barouch, E. and Matijevic, E. (1985), J. Colloid Interface Sci., **105**, 505.

Barouch, E. and Matijevic, E. (1987). Chem. Eng. Commun., **55**, 29.

Bates, R. G., Paabo, M. and Robinson, R. A. (1963). J. Phys. Chem., **67**, 1833.

Bates, R. G. (1973). "Determination of pH, Theory and Practice," Wiley, New York.

Bell, S. H. and Crowl, V. T. (1973). In "Dispersion of Powders in Liquids", Ed. G. D. Parfitt, 2nd ed., p. 267, Wiley, New York.

Bergstrom, L., (1994), "Rheology of Concentrated Suspensions"; pp.193-228 in "Surface and Colloid Chemistry in Advanced Ceramic Processing". Edited by Pugh, R. J. and Bergstrom, L. Marcel Dekker, New York.

Bergstrom, L., Meurk, A., Arwin, H., and Rowcliffe, D. J., (1996) J. Am. Ceram. Soc., **79**, 339.

Bergstrom, L., (1997), Adv. Coll. Interface Sci., **70**, 125.

Bockris, J. O'M. and Reedy, A. K. N. (1970). "Modern Electrochemistry," Vol.1, p. 450, 265, Plenum Press, New York.

Brodnyan, J. G. and Kelley, E. L. (1965), J. Colloid Sci., **20**, 7.

Brown, D. R. and Salt, F. W., (1965), J. Appl. Chem., **15**, 40.

Cannon, D. W. and Mann, R. V., (1988), CMS Application Note 350.

Casson, N., (1959), pp. 84-104 in "Rheology of Disperse Systems", Edited by Mill, C. C., Pergamon Press, London, U.K.

Chan, D. Y. C., Pashley, R. M. and White, L. R., (1980) J. Colloid Interface Sci., **77**, 283.

Chan, B. K. C., Chan, D. Y. C., (1983) J. Colloid Interface Sci., **92**, 281.

Chapman, L. (1913). Philos. Mag. (6), 25: 475.

Chou, C. C. and Senna, M. (1987) Am. Ceram. Soc. Bull., **66**, 1129.

Chou, K. S. and Lee, L. J. (1989). J. Am. Ceram. Soc., **72**, 1622.

Conway, B. E. and Dobry-Duclaux, A. (1960). "Rheology: Theory and Application," vol. 3, F. R. Eirich, Ed., Academic Press, New York, ch. 3.

Darby, R., (1986), "Hydrodynamics of Slurries and Suspensions", pp. 49-65 in "Encyclopedia of Fluid Mechanics", Vol. 5, "Slurry Flow Technology". Edited by Cheremisinoff, N. P., Gulf Publishing, Houston.

De Rooy, N., de Bruyn, P. L. and Overbeek, J. Th. G. (1980). J. Colloid Interface. Sci., **75**, 542.

Debye, P. J. (1933). Chem. Phys., **1**, 13.

Derjaguin, B. V. and Landau, L. D. (1941). Acta Physicochim, URSS, **14**, 633.

Derjaguin, B. V., (1954) Discuss. Faraday Soc., **18**, 85.

Devereux, O. F. and De. Bruyn, P. L., (1963) "Interaction of Plane-Parallel Double Layers", MIT Press, Cambridge.

Ducker, W. A., Senden, T. J. and Pashley, R. M., (1991), Nature, **353**, 239.

Dukhin, S. S. and Deryaguin, B. V. (1974). in "Surface and Colloid Science", E. Matijevic ed., Vol. 7, pp. 52-75, John Wiley, New York.

Dynys, F. and Halloran, J. W., (1983), J. Am. Ceram. Soc., **9**, 655.

Dzyaloshinskii, E., Lifshitz, E. M. and Pitaevskii, L. P. (1960). Sov. Phys. JETP, **10**, 161.

Elimelech, E. M., (1991), J. Colloid Interface Sci., **146**, 337.

Feat, G. R. and Levine, S. (1976). J. Colloid Interface Sci. **54**, 34.

Firth, B. A. and Hunter, R. J., (1976), J. Colloid Interface Sci., **57**, 248.

Fowkes, F. M., Jinnai, H., Mostafa, M. A., Anderson, F. W. and Moore, R. J. (1982). Ch. 15 in "Colloids and Surfaces in Reprographic Technology". Eds. Hair, M. and Croucher, M.D., Am. Chem. Soc. Symposium Series 200.

Fowkes, F.M. and Push, R.J. (1984). ACS Symp. Ser. 240, American Chemical Society, Washington, DC, 331-354

Fowkes, F. M., (1987) pp.411-21 in Advances in Ceramics, Vol. 21, Ceramic Powder Science. Edited by Messing, G. L., Mazdiyasni, K. S., McCauley, J. W., and Harber, R. A., American Ceramic Society, Westerville, OH.

Frens, G. and Overbeek, J. Th. G. (1972). J. Colloid Interface Sci., **38**, 376.

Gordon, J. E., (1975), "The Organic Chemistry of Electrolyte Solutions", John Wiley & Sons, New York, pp.372.

Gouy, L. (1910). J. Phy. (4),9: 457; (1917). Ann. Phys. (9), 7: 129.

Grabbe, A. and Horn, R. G., (1993), J. Colloid Interface Sci., **157**, 375.

Grahame, D. C. (1947). Chem. Rev., **41**, 441.

Gregory, J. (1975). J. Colloid Interface Sci., **51**, 44.

Gregory, J. (1981). J. Colloid Interface Sci., **83**, 138.

Hamaker, H. C. (1937). Physica, **4**, 1058.

Harding, D. R., (1972) J. Colloid Interface Sci., **40**, 164.

Healy, T. W., Wiese, G. R., Yates, D. E. and Kavanagh, B. V., (1973) J. Colloid Interface Sci., **42**, 647.

Henry, D. C. (1931). Proc. Roy. Soc., (London), **Ser. A. 133,** 106.

Hiemenz, P. C., (1986), "Principles of Colloid and Surface Chemistry", Marcel Dekker, New York, pp. 207-17, pp. 753-57, pp. 659-65.

Hirata, Y, Otsubo, Y and Arimura, Y, (1995), J. Ceram. Soc. Japan, **103**, 782-85.

Hogg, R., Healy, T. W., and Fuerstenau, D. W., (1966), Trans. Faraday Soc., **62**, 1638.

Hough, D. B. and White, L. R., (1980), Adv. Colloid Interface Sci., **14**, 3.

Hunter, R. J. (1981). "Zeta potential in Colloid Science", Academic Press, New York.

Iler, R. K., (1979), "The chemistry of Silica", Wiley, New York.

Israelachvili, J. N. and Tabor, D. (1972). Proc. R. Soc. London, **A331**, 19.

Israelachvili, J. N. (1985). "Intermolecular and Surface Forces", Academic Press, New York.

Jang, H. M. and Moon, J. H. (1990). J. Mater. Res., **5**, 615.

Ketelson, H. A., Pelton, R. H. and Brook, M. A., (1996), Langmuir, **12**, 1134.

Kitahara, A., Karasawa, S. and Yamada, H. (1967). J. Colloid Interface Sci., **25**, 490.

Kitahara, A. (1973). Progr. Org. Coatings, **2**, 81.

Kitahara, A. (1984). Non-aqueous systems, Ch. 5 in Surfactant Science Series, Vol. 15: "Electrical phenomena at interfaces. Fundamentals, measurements and applications". Eds. Kitahara, A. and Watanabe, A.

Komagata, S. (1933). Researches Electrotech. Lab. Tokyo. Comm. No.348.

Kosmulski, M. and Matijevic, E. (1992) Langmuir, **8**, 1060.

Krieger, I. M. and Eguiluz, M. (1976) Trans. Soc. Rheol., **20**, 29.

Lange, F. F., (1989), J. Am. Ceram. Soc., **72**, 3.

Lee, B. I. and Rives, J. P. (1991). Colloids Surface, **56**, 25.

Leong, Y. K., Boger, D. V. and Parris, D., (1991), J. Rheol., **35**, 149.

Lifshitz, E. M. (1956). Sov. Phys. JETP, **2**, 73.

Lyklema, J., (1968), Adv. Colloid Interface Sci., **2**, 65-114.

Lyklema, J., (1977), J. Colloid Interface Sci., **58**, 242.

Lyklema, J. and de Wit, J. N. (1978). Colloid and Polymer Sci., **256**, 1110.

Lyklema, J., (1983), in "Adsorption from solution at the solid/liquid interface", Academic Press, New York, pp.223.

Marlow, B. J., Fairhurst, D. and Pendse, H. P. (1988). Langmuir, **4**, 611.

Matijevic, E., and Kitazawa, Y., (1983) Colloid and Polymer Sci., **261**, 527.

Meagher, L., (1992), J. Colloid Interface Sci., **152**, 293.

Moelwyn-Hughes, E. A., (1957), "Physical Chemistry", Pergamon Press, New York, p.819.

Moloney, V. M. B., Parris, D. and Edirisinghe, M. J. (1995). J. Am. Ceram. Soc., **78**, 3225.

Muly, E. C. and Frock, H. N. (1980). Opt. Eng., **19**, 861.

Napper, D. H. (1983). "Polymeric Stabilization of Colloidal Dispersions", Academic Press, New York.

Nikumbh, A. K., Schmidt, H., Martin, K., Porz, F. and Thummler, F., (1990), J. Mater. Sci., **25**, 15.

O'Brien, R. W. and White, L. R. (1978). J. Chem. Soc. Faraday II. **74**, 1607.

O'Brien, R. W. (1988). J. Fluid Mech., **190**, 71.

O'Brien, R. W., Midmore, B. R., Lamb, A. and Hunter, R. J. (1990). Faraday Disc. Chem. Soc., **90**, 301.

Oja, T., Petersen, G. L. and Cannon, D. W. (1985). US Patent #4,497,208.

Overbeek, J. Th. G., (1986), p. 431 in Colloid and Interface Science, Vol. I, Academic Press, New York.

Overbeek, J. Th. G., (1988), J. Chem. Soc., Faraday Trans. 1, **84**, 3079.

Parfitt, G.D. and Peacock, J. (1978). pp. 163-226 in Surface and Colloid Science, Vol. 10. Edited by Matijevic, E., Plenum, New York.

Parish, M. V., Garcia, R. R. and Bowen, H. K. (1985). J. Mater. Sci., **20**, 996.

Parks, G. A. (1965). Chem. Rew., **65**, 177.

Pelton, R., Miller, P., McPhee, W. and Rajaram, S., (1993) Colloids and Surface, **80**, 181.

Popovych, O. and Tomkins, R. P.T. (1981). "Non-aqueous Solution Chemistry", Chs. 5 and 6, Wiley, New York.

Pugh, R. J., (1994) " Dispersion and Stability of Ceramic Powders in Liquids"; pp.127-30 in "Surface and Colloid Chemistry in Advanced Ceramic Processing". Edited by Pugh, R. J. and Bergstrom, L. Marcel Dekker, New York.

Rajagopalan, R. and Kim, J. S., (1986), J. Colloid Interface Sci., **83**, 428.

Robinson, R. A. and Stokes, R. H., (1959), "Electrolyte Solutions", Butterworths Scientific, London, pp. 392.

Russel, W. B. and Benzing, D. W., (1981). J. Colloid Interface. Sci., **83**, 178.

Russel, W. B., Saville, D. A. and Schowalter, W. R. (1989). "Colloidal Dispersions", p. 456, Cambridge Univ. Press, New York.

Sacks, M. D. and Khadilkar, C. S. (1983). J. Am. Ceram. Soc., **66**, 488.

Sarkar, P., Huang, X. and Nicholson, P. S. (1992). J. Am. Ceram. Soc., **75**, 2907.

Sarkar, P., Huang, X. and Nicholson, P. S. (1993). Ceram. Eng. Sci. Proc. **14**, 707.

Sarkar, P., Prakash, O., Wang, G. and Nicholson, P. S. (1994). Ceram. Eng. Sci. Proc. **15**, 1019.

Sarkar, P., Datta, S. and Nicholson, P. S. (1997). Composites Part B **28B**, 49.

Sasaki, S. and Maeda, H., (1994) J. Colloid Interface Sci., **167**, 146.

Stern, O. (1924). Z. Elektrochem., **30**, 508.

Tadros, Th. F., (1980). Adv. Colloid Interface Sci., **12**, 141.

Tadros, Th. F. and Lyklema, J., (1968), J. Electroanal. Chem., **17**, 267.

Tamura, H., Matijevic, E., Meites, L., (1983), J. Colloid Interface Sci., **92**, 303.

Tanabe, K., (1970) "Solid Acids and Bases", Academic Press, New York, p. 48.

Timasheff, S. N., (1966) J. Colloid Interface Sci., **21**, 489.

Usui, S. and Hachisu, S. (1984). Interaction of electrical double layers and colloid stability, Ch. 3 in Surfactant Science Series, Vol. 15: "Electrical phenomena at interfaces. Fundamentals, measurements and applications". Eds. Kitahara, A. and Watanabe, A..

Van der Hoeven, Ph. C. and Lyklema, J. (1992). Adv. Colloid Interface Sci., **42**, 205-277.

Van Mil, P. J. J. M., Crommelin, D. J. A., Wiersema, P. H., (1984) J. Colloid Interface Sci., **98**, 61-71.

Verwey, J. W. and Overbeek, J. Th. G. (1948). "Theory of the Stability of Lyophobic Colloids", Elsevier, Amsterdam.

Vigil, G., Zhenghe, X., Steinberg, S. and Israelachvili, J., (1994) J. Colloid Interface Sci., **165**, 367.

Walbridge, D. S. (1975). in Barrett, K. E. (Ed.), "Dispersion Polymerization on Organic Media", Wiley-Interscience, New York, p.45.

Ware, B. R. (1974). Adv. Colloid Interface Sci., **4**, 1.

Warren, L. J., (1975). J. Colloid Interface Sci., **50**, 307.

Weast, R. C., (Ed.) (1990) "Handbook of Chemistry and Physics", 71st ed. CRC Press.

Wiersema, P. H., Loeb, A. L. and Overbeek, J. Th. G. (1966). J. Colloid Interface Sci., **22**, 78.

Wiese, G. R. and Healy, T. W. (1975). J. Colloid Interface Sci., **51**, 427.

Woods, D. R. (1983). "Colloids, Surfaces and Unit Operations", McMaster University, Hamilton, Ontario.

APPENDIX

ERROR ANALYSIS IN DOPPLER ELECTROPHORETIC LIGHT SCATTERING MEASUREMENT

In this study, electrophoretic mobility measurement in dilute suspensions was made using a Coulter DELSA (Doppler Electrophoretic Light Scattering Analyzer) 440.

A major source of error in measuring the electrophoretic mobility is due to "electro-osmosis". The presence of electrically charged, dissociated silanol groups on the surface of silica electrophoresis cells used in the apparatus causes electro-osmotic flow of liquid in the presence of an electric field. Komagata (1933) solved the electro-osmotic flow profile for a rectangular cell, such as that in the DELSA 440 systems, neglecting end effect, to give an equation for the velocity of the liquid as a function of position across the cell.

$$V_{os}(y) = V_w\left(1 - \frac{3(1 - y^2/h^2)}{2 - (384/\pi^5 K)}\right) \qquad (A1)$$

where K is the ratio of the major to minor cross-sectional dimensions (3.18 for the Coulter cell), y is the distance from the cell to the measurement location, $V_{os}(y)$ is the osmotic velocity at position y divided by the electric field strength, V_w is the

electro-osmotic velocity next to the wall (assumed to be constant) divided by the electric field strength, and h is the distance from the cell centre to either wall (500 μm for the Coulter cell). This equation predicts a parabolic flow profile with two planes of zero flow (usually called stationary levels) between the two walls.

The apparent mobility of a charged particle, U_{meas} (y), measured at position y, is the summation of the electro-osmotic flow and the electrophoretic mobility U_E;

$$U_{meas}(y) = V_{os}(y) + U_E \qquad (A2)$$

The measurement position can be transformed to give a variable x:

$$x = 1 - (y^2 / h^2) \qquad (A3)$$

Substitution of Eqs. A2 and A3 into Eq. A1 gives

$$U_{meas}(y) = U_E + V_w Z \qquad (A4)$$

where

$$Z = 1 - \left(\frac{3x}{2 - (384/\pi^5 K)}\right) \qquad (A5)$$

There are two methods of circumventing the effect of electro-osmosis. A common method is to measure the mobilities at the stationary layer. However, there are two possible problems with such measurements. The first is with particles that sediment appreciably over the time scale of a measurement. In this case, the sedimented, charged particles coat the bottom channel wall and change its potential. As a result, a parabolic flow profile in the channel is skewed and the stationary layer is no longer in the position determined before. The

second problem is that the flow profile of the particles (i.e., the change in measured mobility vertically across the channel) is such that the velocity gradient at the stationary layer is large. This means that a small error in positioning can cause a substantial error in value of electrophoretic mobility.

Another method to circumvent electro-osmosis is to measure the mobility at points across the channel to determine the actual flow profile. Pelton (1993) develop a procedure for improving electrophoresis data from Coulter DELSA :

(1) Determine the cell wall positions by the procedure recommended in the instrument manual.

(2) Collect apparent mobility data at locations across the cell.

(3) Construct the Komagata plot (Equation A4). Based on Eq. A4, plotting $U_{meas}(y)$, the measured mobility, vs. Z, the measurement position, gives a straight line.

This procedure was followed in this study for electrophoretic mobility measurement in dilute suspensions. Figure A1 shows the example of apparent mobility, $U_{meas}(y)$, (a) as a function of cell position and the fitted parabola (indicated by the solid line in the figure) and (b) as a function of Z, the dimensionless measurement position (the solid line is the least-squares fitted line). The true mobility, U_E, can be found at Z=0, corresponding to the stationary level.

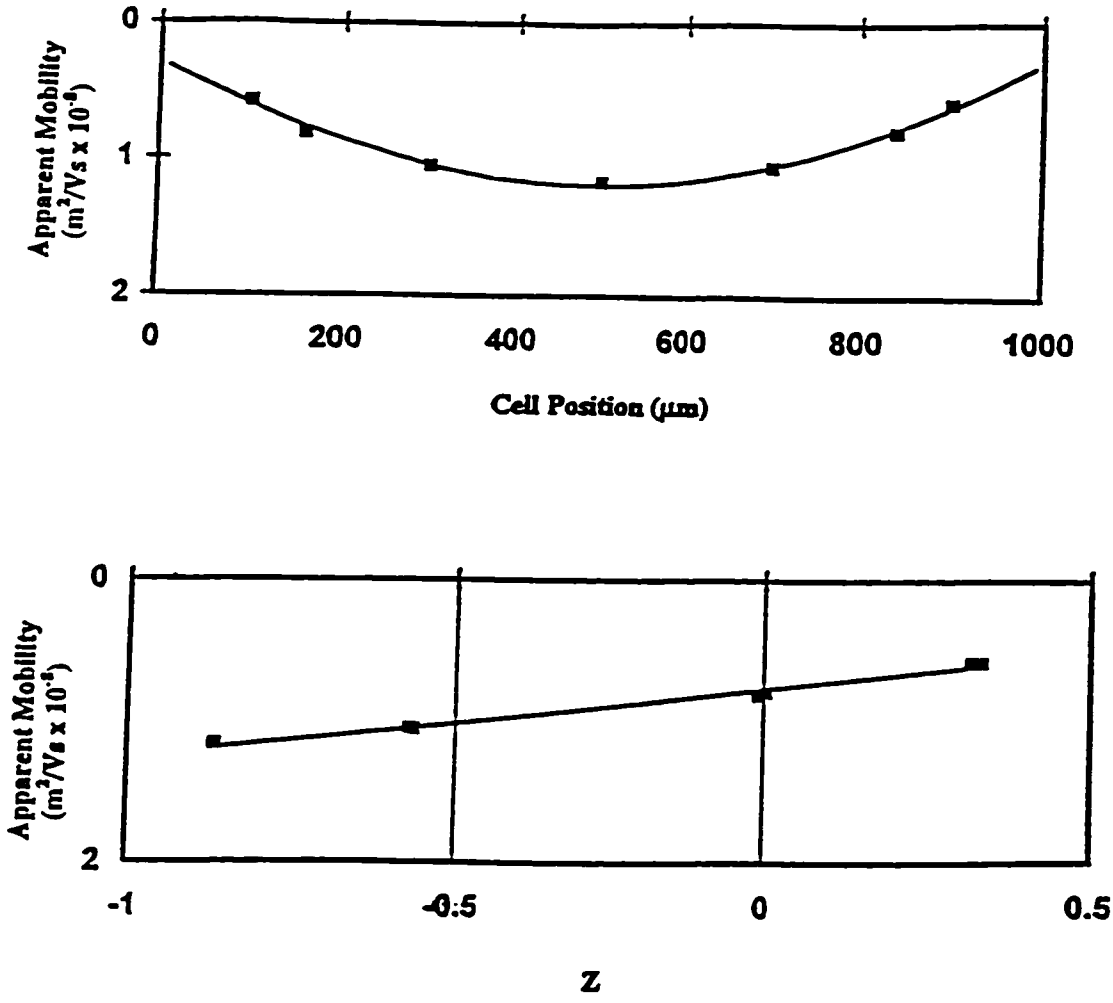

Figure A1 Apparent mobility as a function of (a) cell position and the fitted parabola (b) Z, the dimensionless measurement position.